Titre: Title:	Pultrusion of Natural Fiber-Reinforced Composites Injection molding assisted
Auteur: Author:	Nawaf Alsinani
Date:	2022
Type:	Mémoire ou thèse / Dissertation or Thesis
Référence: Citation:	Alsinani, N. (2022). Pultrusion of Natural Fiber-Reinforced Composites Injection molding assisted [Thèse de doctorat, Polytechnique Montréal]. PolyPublie. https://publications.polymtl.ca/10422/

POLYTECHNIQUE MONTRÉAL

affiliée à l'Université de Montréal

Pultrusion of Natural Fiber-Reinforced Composites Injection Molding Assisted

NAWAF ALSINANI

Département de génie mécanique

Thèse présentée en vue de l'obtention du diplôme de *Philosophiae Doctor*

Génie mécanique

Juin 2022

POLYTECHNIQUE MONTRÉAL

affiliée à l'Université de Montréal

Cette thèse intitulée :

Pultrusion of Natural Fiber-Reinforced Composites Injection Molding Assisted

Présentée par **Nawaf ALSINANI**

en vue de l'obtention du diplôme de *Philosophiae Doctor*

a été dûment acceptée par le jury d'examen constitué de :

Aurelian VADEAN, président

Louis LABERGE LEBEL, membre et directeur de recherche

Bruno BLAIS, membre

Ali YOUSEFPOUR, membre externe

DEDICATION

To my beloved family and to everyone who helped me reached this point

AKNOWLEGMENTS

First and foremost, I would to express my deep gratitude to my philosopher and mentor Professor Louis Laberge Label. My genuine and heartfelt thanks and appreciation to this magnificent supervisor for providing me with the guidance and counsel I need to succeed in the PhD and life in general over the last six years. Prof. Laberge Lebel has been the greatest influence in mapping my PhD journey, advising on my research topic, finding the resources I need, being available and replying to my questions and emails. My supervisor is the best philosopher in my area of research interest and the richness of his professional experience has made the study even more interesting and enriching.

Additionally, I would like to thank Professor Aurelian Vadean, Professor Bruno Blais and Professor Ali Yousefour for accepting to be part of my thesis committee.

I would like also to thank Danielle Szydlowski, the hidden soldier, for her experimental support in the lab and endless sessions of proof reading. Without her help and support, the quality of our published manuscripts and thesis would not be as great.

Moreover, I would to express my thanks to all ACFSlab and LAPOM members for their support, including Felix Lapointe, Felix Lesard, Mohammed Ghaedsharaf, Maissaloun El-jakl, Pablo Chaves, Vincent Rohart, Natalia Cardona Vásquez, Vincent Fortier, Christophe Absi, Cristian Talos, Pascal Assi, Marc Gordan, Boris Burgarella, Chrstian Charles and Josee Laviolette.

Finally, I would like to also thank Bombardier Aerospace, Pultrusion Technique, Saudi Arabia’s Saline Water Conversion Corporation and Ministry of Education, NSERC and Prima Quebec for financing this research project.

RÉSUMÉ

Les imperfections de la finition de la surface ainsi que la déconsolidation thermique sont des problèmes courants dans la Pultrusion des Composites Thermoplastiques (PCT). Ces problèmes sont généralement dus à une exécution erronée du processus de refroidissement. L'industrie automobile s'efforce avec enthousiasme d'accroître l'utilisation des matériels composites à base de fibres naturelles et de cellulose, tels que les thermoplastiques à fibres longues (TFL). La PCT est une technique de fabrication qui peut être utilisée pour produire des granulés TFL renforcés de fibres naturelles. Cependant, le niveau de maturité de cette technique ne répond pas encore aux exigences de vitesse de production élevée qui correspondent au volume de fabrication important de l'industrie automobile. L'objectif principal de cette thèse est de produire des granulés TFL renforcés de lin PP pour des applications automobiles en utilisant la PCT.

Le premier objectif est de développer un système de refroidissement capable de contrôler avec précision le profil de température de refroidissement du pultrudé. Des pultrudats de Carbone/Polyéthylèneimine (C/PEI) (amorphe) et de C/Polyétheréthercétone (C/PEEK) (semi-cristallin) ont été produits et retraités pour mesurer les forces d'adhésion pendant le processus de refroidissement. Des moindres forces de traction ont été observées, et la déconsolidation a été évitée lorsque les pultrudés ont été rapidement refroidis en dessous de la température de transition vitreuse (T_g). Pour le polymère amorphe (C/PEI), on a atteint un état de surface (Ra) de 0,72 lors du refroidissement à un température de $T_g/2$. Pour le polymère semi-cristallin (C/PEEK), la qualité de finition de surface la plus impressionnante a été atteinte à une température de refroidissement de 243°C. On soupçonne que cette température de refroidissement a induit une cristallisation rapide.

Le deuxième objectif était d'appliquer notre processus de PCT multi-moules récemment développé avec une étape de refroidissement pour produire des granulés renforcés de fibres de lin (TFL). Après avoir produit ces granulés TLF, nous avons étudié l'impact de leur teneur en vide sur les propriétés mécaniques des composants moulés par injection. Nous avons constaté que la fraction de vide du TFL avait un impact significatif sur la qualité de granulation du TFL et sur les propriétés mécaniques des composants moulés par injection. Les granulés de lin/ Polypropylène (lin/PP) qui avaient des fractions de vide allant jusqu'à 8%, ont été moulés par injection sans aucun

problème. Pour les granulés de lin/PP ayant des fractions de vide de 15%, le processus de granulation de ces pultrudés à haute teneur en vide a été très dommageable, ce qui a donné des granulés éclatés avec des fibres sèches et détachées. Une intervention manuelle était nécessaire pour faire couler les granulés TFL et les fibres sèches de lin dans la machine à injecter. Enfin, la qualité et la taille de l'imprégnation TFL n'ont pas eu d'impact sur les résistances maximales à la traction des composants moulés par injection.

Le troisième objectif à présenter est à l'effet des vitesses de tirage élevées sur les morphologies des pultrudés dans un procédé de PCT. Trois vitesses de traction, entre 50 et 1000 mm/minute, ont été sélectionnées pour étudier l'effet de la variation des vitesses de traction. À l'aide d'un modèle, la pression du polymère dans les moules de pultrusion a été calculée pour chaque vitesse de pultrusion. Les images microscopiques ont montré une reconfiguration des tiges pultrudées à une vitesse de traction plus élevée qui a produit de plus grandes zones non-imprégnées et riches en polymère. La résistance à la traction la plus élevée a été obtenue par les pultrudés produits à 50 mm/minute. La résistance à la traction a chutée de près de 20% lorsque la vitesse de traction a été augmentée à 1000 mm/minute. La reconfiguration de la tige pultrudée, attribuable à la fonte progressive des fibres de polymères qui compactent les fils de lin, serait responsable de la baisse de la qualité de l'imprégnation et des propriétés mécaniques.

Cette étude ouvre la porte à l'utilisation des composites thermoplastiques pultrudés dans de nombreux domaines, y compris la production de granulés TFL renforcés de lin de haute qualité. Le système de refroidissement développé a été utilisé pour fabriquer des granulés TFL renforcés de lin, ce qui a permis d'obtenir des pièces injectées en lin/PP dont le module a augmenté de 2,5 fois par rapport au module du PP pur, et des résistances aux chocs supérieures à 10,5 pour les coupons injectés avec une teneur en lin de 25 %. Ces résultats sont incomparables a ceux examinée dans la littérature. Nous avons pu augmenter les vitesses de tirage à 1 m/minute afin de rendre la production de TFL par PCT adaptée aux applications industrielles. Nos résultats démontrent une solution pratique pour l'adoption de matériaux alternatifs respectueux de l'environnement

ABSTRACT

Surface finish irregularities and deconsolidation are common issues in ThermoPlastic Composites (TPC) pultrusion. These issues normally happen due to inappropriate execution of the cooling process. The auto industry is enthusiastically trying to increase their use of natural fibers cellulose-based composites such as long fiber thermoplastics (LFT). TPC pultrusion is a manufacturing technique which can be used to produce natural-fiber-reinforced LFT pellets. Yet, this technique's maturity level does not meet the high production speed requirements that fit the automotive industry's high manufacturing volume. This dissertation's main objective is to produce Flax/Polypropylene (Flax/PP) LFT pellets for automotive applications using TPC pultrusion.

The first objective is to develop a cooling system which is capable to accurately control the pultrudate's cooling temperature profile. Carbon/Polyethylenimine (C/PEI) (Amorphous) and C/Polyether ether ketone (C/PEEK) (Semi-crystalline) pultrudates were produced and reprocessed to measure the adhesion forces throughout the cooling process. Lesser pulling forces were observed, and deconsolidation was evaded when the pultrudates were rapidly cooled below the polymers' glass transition temperature (T_g). For the amorphous polymer (C/PEI) attained a surface finish (Ra) of 0.72 when cooling at $T_g/2$. For the semi-crystalline polymer (C/PEEK) attained finest surface finish quality at a cooling temperature of 243°C. It is anticipated that this cooling temperature induced fast crystallization.

The second objective was to apply our recently developed multi-die thermoplastic pultrusion process with cooling stage to produce Flax fiber-reinforced (LFT) pellets. After producing those LFT pellets, we studied the impact of their void contents on the mechanical properties of the injection molded components. The LFT's void fraction was found to have a significant impact on the LFT pelletizing quality and on the mechanical properties of the injection-molded components. Flax/PP pellets which had void fractions up to 8%, were injection-molded without any issue. For Flax/PP pellets which had void fractions of 15%, the pelletizing process of these high-void pultrudates was very damaging, resulting in shattered pellets with detached dry fibers. Manual intervention was required to make the LFT pellets and dry Flax fibers sink in the injection molding machine. Finally, the LFT impregnation quality and size did not have any impact on the maximum tensile strengths of the injection-molded components.

The third objective to present to the effect of high pulling speeds on the morphologies of pultrudates in a TPC pultrusion process. Three pulling speeds, between 50 and 1000 mm/minute, were selected to study the effect of varying the pulling speeds. Using a model, the polymer pressure in the pultrusion dies was calculated for respective pultrusion pulling speed. The microscopic images showed a reconfiguration of the pultruded rods a higher pulling speed that led to greater unimpregnated and polymer rich areas. The highest tensile strength was achieved by the pultrudates produced at 50 mm/minute. The tensile strength dropped by almost 20% when the pulling speed was increased to 1000 mm/minute. The pultruded rod's reconfiguration, attributed to the progressive melting of the PP fibers exerting high compaction pressure on Flax yarns, is thought to be responsible for the decline in impregnation quality and mechanical strength.

This study opens the door for the utilization of pultruded thermoplastics in numerous fields including producing high quality Flax-reinforced LFT pellets production. The developed cooling system was used to make Flax reinforced LFT pellets resulted in Flax/PP injected parts having modulus increase of 2.5 times the modulus of Pure PP, and impact strengths above 10.5 kJ/m^2 for coupons injected with 25 wt% Flax content. Those results are unmatched in the literature reviewed. We were able to raise the pulling speeds to 1 m/minute in order to make the production of LFT using TPC pultrusion more suited for industrial applications. Our results demonstrate a practical solution towards adopting environmental-friendly material alternatives.

TABLE OF CONTENTS

LIST OF TABLES

LIST OF FIGURES

LIST OF SYMBOLS AND ABBREVIATIONS

Ra	Arithmetical mean height
K_z	Backflow impregnation Kozney
$\phi_{Die,i}$	Deconsolidated diameter of the pultrudate
$\phi_{Die,i-1}$	Deconsolidated diameter of the pultrudate of the previous die
$\Delta v_{f,i-1}$	Deconsolidation fiber volume content variation
ρ	Density
DSC	Differential scanning calorimetry
L_{eff}	Effective die length
R_f	Filling ratio
SFT	Short fibre-reinforced thermoplastic
$v_{f,\infty}$	Final fiber volume fraction
f	Flax yarn fineness
R_0	Flax yarn radius
T_g	Glass transition temperature
Tex	Grams per 1,000 metres of yarn
H_m	Heat of fusion
H_c	Heat of fusion of cold-crystallization
HDPE	High density polyethylene
$v_{f,i}$	Initial fiber volume fraction
TGA	Thermogravimetric analyses
TPC	Thermoplastic composites
TSC	Thermoset composites

T_m	Melting point temperature
LFT	Long fibre-reinforced thermoplastic
N_γ	Number of yarns bobbined together
PEEK	Polyetheretherketone
PEI	Polyethylenimine
PP	Polypropylene
PLA	Polylactic acid
PMMA	Polymethylmethacrylate
P	Pressure
F	Pulling force
K_r	Radial impregnation Kozney
SEM	Scanning electron microscope
W_F	Weight fraction
$\overline{N_Y}$	Total number of Flax yarns
α	Yarn compaction factor

LIST OF APPENDICES

CHAPTER 1 INTRODUCTION

Inorganic fillers in polymeric composites are widely used in the automotive industry [1]. Nevertheless, production and disposal of these materials have a negative impact on the environment. Due to growing environmental awareness, new environmental rules and laws have been introduced to help decrease the inorganic waste issue [2]. These new environmental regulations are exerting a great pressure on automotive industry to replace these fillers with biodegradable alternatives. The U.S Department of Energy`s Vehicle Technologies Office (VTO) have mandated to develop automotive Lightweight Materials (LM) to ensure energy security through renewables. VTO determined that the replacement of inorganic fibers with organic alternatives will make lighter parts to be used while at the same time increase the percentage of renewables within the vehicle [3]. As a result, the automotive industry is actively trying expand the use of producing natural-fiber-reinforced composites through the use of natural-fiber-reinforced long fiber thermoplastic (LFT) pellets [4].

Thermoplastic composites (TPC) pultrusion is a candidate manufacturing technique that could be used to produce natural-fiber-reinforced LFT. Figure 1.1 shows a thermoplastic pultrusion process. The pultrusion apparatus typically includes a preheater, heating die(s), a cooling die, a pulling system and a pelletizer. However, this technique's maturity level does not meet the high production speed requirements that fit the automotive industry's high manufacturing volume. Surface finish deficiencies and deconsolidation are common issues in (TPC) pultrusion. These issues normally happen due to inappropriate execution of the cooling process. In contrast to thermoset composites, thermoplastic pultrudates must go through a cooling process while being under pressure between mold surfaces. If this does not occur, the pultrudates will deconsolidate to become a structure with high void content, resulting in pultrudates with low mechanical strength. "Sloughing" is another negative phenomena that is caused by high metal-polymer adhesion forces in pultrusion [5]. Fragments stick to the surface and then tear off from the pultrudate after the adhesion forces become higher than the pultrudate's strength. These broken pieces drive into the pultrudate's surface, resulting in rough surface finish quality. Although few studies were done on sloughing in TPC pultrusion, this topic has been thoroughly surveyed for thermoset composites pultrusion (TSC pultrusion) in recent years [5-7].

Several scholarly works conducted experiments using TPC pultrusion; however, these works were done at processing speeds similar or below the speed of commercial thermoset pultrusion [8, 9]. The main reasons for the low speed problem are related to the difficulties associated with processing thermoplastic polymers as they have very high melt viscosities compared to thermoset. Viscous drag is heavily linked to the polymer's viscosity. The fiber breakage is linked to pressure buildup in a die. High pressure buildup will lead to fiber breakage. Thus, increasing pulling speed in TPC pultrusion can result in fiber breakage, increasing void contents and high pulling forces.

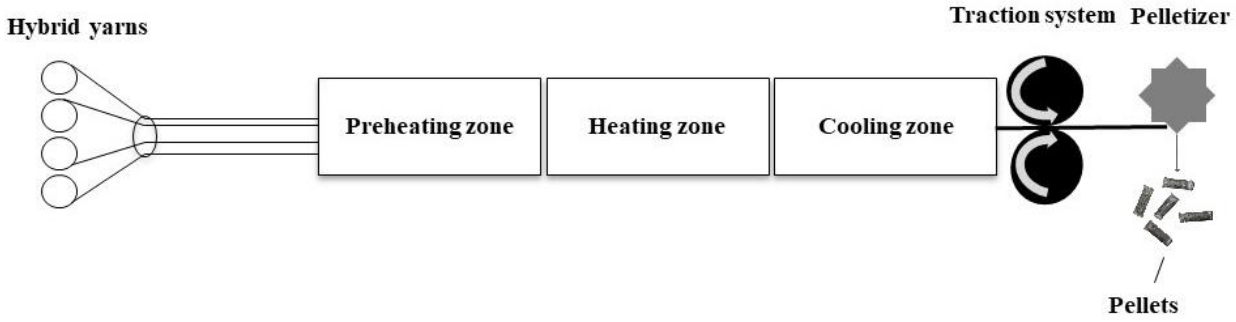

Figure 1.1: A thermoplastic pultrusion process. The pultrusion apparatus typically includes a preheater, heating die(s), a cooling die, a pulling system and a pelletizer.

This research project proposal's main objective is to develop a high quality and low-cost manufacturing method to produce Flax/polypropylene (Flax/PP) reinforced injection mouldable. First, an enhanced cooling die system is developed to improve pultruded beam surface finish in pultruded beams. Second, an evaluation is done on the effect of LFT pellet consolidation on the mechanical properties of injected components. Third, the pultrusion speeds then is increased to 1 m/min.

1.1 Dissertation structure

The dissertation contains eight Chapters. After presenting a literature review in Chapter 2, the problem is described in Chapter 3 including descriptions of research objectives. The main achievements of the research are described in detail in Chapters 4, 5, and 6. Chapter 4 presents the effect of cooling temperature on deconsolidation and pulling forces in a TPC pultrusion process.

Chapter 5 presents the effect of Flax/PP pellets' morphology on the mechanical properties of injection-molded parts. Chapter 6 presents the effect of high pulling speeds on the morphologies of pultrudates in a TPC pultrusion process. Chapter 7 provides a general discussion of this research's achievements. Chapter 8 presents a conclusion, discusses the limitations, and offers recommendations for future work.

CHAPTER 2 LITRATURE REVIEW

In this chapter, the studies related to the field of this thesis are concisely studied. The literature in pultrusion of bio-composite injection molding pellets are briefly surveyed in Section 2.1. Furthermore, we explicitly review the literature on cooling in TPC pultrusion in Section 2.2. High speed pultrusion of thermoplastic composites are then surveyed in Section 2.3.

2.1 Production of Bio-composite Injection Molding Pellets

The automotive industry is one of the front-runners in finding applications for organic fibers. They are becoming more popular due to their low environmental impact; these fibers are light and can be harvested. Due to its high cellulose content (64%) and low lignin content [10]. Flax fibers are one of the favorite choices amid natural fibers for industrial uses. In comparison to other bio-fibers, Flax fibers can be processed at higher temperatures thanks to its high cellulose content [10]. Degradation happens when cellulose reaches temperatures between 250-350°C, while lignin starts to degrade when the temperature approaches 160°C. In addition, Flax fibers have the highest modulus of elasticity values among natural fibers [11]. Therefore, composite materials that are Flax-reinforced are an excellent substitute for glass-reinforced composite materials. The automotive industry often uses PP as the polymer in their applications [12]. There are many reasons for this including its great mechanical properties, high impact strength, dimensional stability, low density and its excellent process-ability [13]. In addition to these great qualities, PP's cost is reasonably low and its T_m is below the degradation temperature of natural fibers [14]. Using (LFT) glass fiber-reinforced PP pellets was proven to improve impact and fatigue [13]. Typically, a twin-screw extruder is used to produce short fiber thermoplastics (SFT) Glass/PP by melt-mixing the matrix and chopped fibers in the extruder. Yet. this process causes damage to the fiber due the high shear stresses during processing [15].

TPC pultrusion is a manufacturing technique in which the raw materials can be used in different forms to make composite materials with the same cross-section continuously. Figure 1.1 shows a typical TPC pultrusion process. The pultrusion apparatus typically includes a preheater, heating die(s), a cooling die, a pulling system and a saw/pelletizer. There are several pultrusion processes and they can be divided into two different categories: reactive and non-reactive TPC pultrusion

processes. The reactive process is not available for PP polymer, thus it will not be considered in this research project [16]. Table 2.1 shows TPC pultrusion precursors for natural fiber-reinforced composites. The advantages and disadvantages of each process are included in the table. First, injection pultrusion (IP) is a process which entails pulling fibers from rolls into an impregnation die. However, achieving impregnation using IP is challenging. IP requires special polymers that have low viscosities in order to achieve full impregnation [17]. Thus, using IP to produce natural fiber-reinforced LFT may yield LFT with high void contents which might lead to having low mechanical properties.

Table 2.1: TPC pultrusion precursors for natural fiber-reinforced composites. The advantages and disadvantages of each process are included in the table.

Process name	Precursors	Advantage	Disadvantage	Ref
Injection pultrusion	Polymer pellets and dry fibers	Low cost	Low impregnation	[17]
Blended-precursor pultrusion	Pre-pregs	Possible high speed	Expensive raw material. Does not allow textile operations	[18]
	Commingled hybrid	Moderate cost. High conformability. Reduced inter-yarn friction	Low speeds	[10]
	Powder impregnated	Low impregnation distance	High inter-yarn friction	[19]
	Parallel hybrid	Low cost	Low speed Long impregnation distance	[9]

Another form of non-reactive precursors is the blended-precursors. Figure 2.1 shows commonly-used blended-precursors for TPC pultrusion. Blended-precursors pultrusion consists of fibers and matrix (in the form of fiber, powder or tape) that are pulled together through multiple heated tapered dies. The prepreg form is basically a tape which contains pre-impregnated fibers. Pultrusion using prepregs requires a relatively small amount of impregnation pressure to produce

fully impregnated beams since the fibers are already fully impregnated. Therefore, pultrusion using pregregs can be done effortlessly in high speeds. Flax/PP Prepregs made are usually produced in lab scale quantity. These prepregs were used before to manufacture composites using automated fiber placement [18]. The same prepreg kind can also be used for TPC pultrusion. The commingled yarns consist of the reinforcement and polymer which are blended mechanically. This blend allows better mixing by reducing the impregnation distance. Powder impregnated yarns contain reinforcement fibers that are blended with thermoplastic powder. To conclude, using parallel hybrid seems to be the lowest cost option compared to the other non-reactive precursors. Parallel hybrid yarns do not require any mechanical or chemical mixing steps before using them for the pultrusion. Since no mixing is done before pultrusion, parallel hybrid yarns may require more residence time in the heating/pultrusion die to achieve proper impregnation level. Yet, the low manufacturing cost provides a major advantage for using parallel hybrid yarns in thermoplastic pultrusion.

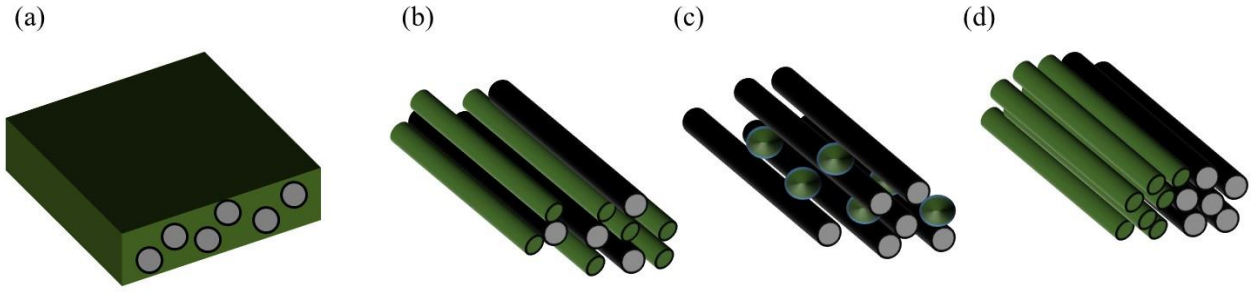

Figure 2.1: several types of hybrid yarns used for blended-precursor. (a) Pre-consolidated, (b) Commingled, (c) Powder impregnated and (d) Parallel yarns.

2.1.1 Pultrusion of natural fiber composites

Van de Velde et al. [20] pultruded Flax/PP commingled yarns. The TPC pultrusion settings, for instance, pulling speeds and set temperatures were not reported. Later, Angelov et al. [10] were able to improve the mechanical properties of pultruded Flax/PP compared to the work done by Van de Velde et al. [20]. Yet, the authors did not share any data for void content of the produced pultruded rods [10]. Void content data provides more information on the impregnation quality

during pulrusion. Nakai et al. [21] pultruded jute spun yarn/PLA tubular braided composite. They fixed the production speed at 18 mm/min and used two different filling ratios of 1% and 20% to generate pressure at die cavity. The lowest void content was around 10%.

Reinforcement fibers can come in different fiber sizes. These sizes have a strong influence on the final impregnation quality of the pultruded beams. Oswald et al. [10] tested three different yarn sizes (200, 400 and 1000 tex) to pultrude Flax and poly-lactic-acid (Flax/PLA). Higher impregnation level was achieved when smaller yarn sizes were used. Image analysis showed that for lower fiber finess, the fiber spatial distribution was more homogenous and void content was reduced to be as low as 2.5%. Kim et al. [22] determined that fiber yarn fineness was the most dominant factor in influencing the impregnation quality. Fibers with smaller yarn fineness (Tex number) achieved higher impregnation quality. Later, Alsinani et al. [8] produced Flax/PP LFT using the pultrusion of parallel hybrid yarns using 200 tex fibers. The average void content reported in the LFT`s was around 3.5%. Thus, these results indicate that smaller yarn sizes could result in a higher impregnation level.

2.2 Cooling in thermoplastic pultrusion

Post-impregnation challenges in TPC pultrusion such as the surface finish defects are very common [15]. In contrast to thermoset composites, thermoplastic pultrudates must go through a cooling process while being under pressure between mold surfaces. If this does not happen, the pultrudates will deconsolidate to become a porous structure, resulting in pultrudates with low mechanical strength [25]. Figure 2.2 shows a deconsolidated thermoplastic pultrudate. The pultrudate’s shape looks irregular as well. Deconsolidation due to improper execution of the cooling process.

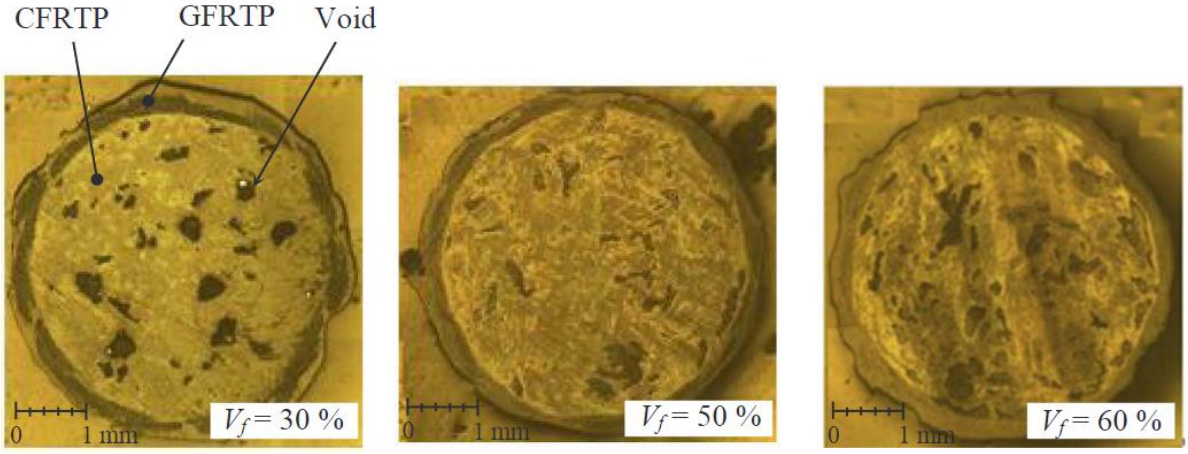

Figure 2.2: An example of deconsolidated thermoplastic pultrudate [23].

Throughout the cooling process, the behavior of a thermoplastic polymer is based upon its molecular arrangement, which can be either amorphous such Polyetherimide (PEI) or semi-crystalline such PP. When cooling an amorphous polymer from the melt phase, the polymer chains start to get arranged into a random molecular structure. Furthermore, a share of the semi-crystalline polymer chains arranges into crystals while they themselves are dispersed in a arbitrarily arranged chains phase. The crystalline potion's percentage within a semi-crystalline structure is heavily influenced by many factors including the cooling conditions and thermal history, and may change from one semi-crystalline polymer to another. Yet, the semi-crystalline portion has a major influence on the polymer's mechanical properties [24].

Two important characteristic temperatures related to thermoplastic polymers stand out: first, the glass transition temperature (T_g) and second, the melting temperature (T_m). T_g can be associated with both amorphous and semi-crystalline polymers. Below T_g temperature, the polymers' randomly arranged chains are frozen and cannot move relative to each other [24]. Once the polymer is heated to T_g, the randomly arranged polymer chains receive sufficient thermal energy to rotate. This leads to a dramatic reduction in their stiffness. The other characteristic temperature, T_m, can only be associated with semi-crystalline polymers. Once a semi-crystalline polymer is heated to around T_m, the crystalline arrangement of the polymer chains becomes weak. A semi-crystalline polymer becomes less stiff at T_g , followed by a significant drop in stiffness

around T_m [24]. Due to its stiff crystalline phase, the semi-crystalline polymer holds some of its stiffness between T_g and T_m.

2.2.1 Thermoplastic polymer adhesion with metal

The amorphous phase of a thermoplastic polymer undergoes a transformation from a glassy to a viscous flow state when the polymer is heated over T_g. This transformation impacts the microscale adhesion behavior between the thermoplastic polymers and metal surfaces. The polymer adhesion with a surface can change when there is a change in temperature [25]. "Sloughing" is a damaging phenomena that is caused by high metal-polymer adhesion forces in [5]. In TPC pultrusion, adhesion forces between the polymer and die surface change during the cooling process as the temperature change between the processing temperature (T_p) and T_g. Therefore, the sloughing occurs when the pultrudate's temperature is between T_p and T_g. Fragments stick to the surface and then tear off from the pultrudate after the adhesion forces become higher than the pultrudate's strength. These broken pieces drive onto the pultrudate's surface, resulting in rough surface finish quality.

Although very few studies were conducted on sloughing in TPC pultrusion, the topic has been comprehensively studied for thermoset composites pultrusion (TSC pultrusion) in the latest decades [5]. Batch et al. [5], for example, suggested a few instructions to lessen the likelihood of sloughing, such as polishing the die surface and increasing fiber volume fraction. They observed that any cracks or roughness in the die surface can add to the chances of sloughing. Furthermore, increasing the fiber volume fraction, thus providing more fibers for the polymer next to the die wall, decreased the chances of sloughing [5]. Yet, Batch et al. [5] did not recommend using any specific coating technique for the die surfaces. Sloughing can also cause a massive increase in pulling force leading to major fiber damage. Another typical method to prevent sloughing in TSC pultrusion comprises of attaining a rapid transition during curing or gelation phase [6]. In TSC pultrusion, it was observed that the longer the polymer stays in a gel-like phase, the higher the likelihood of sloughing occurring.

2.3 High speed pultrusion of thermoplastic composites

Several scholarly works conducted several successful TPC pultrusion experiments using parallel hybrid yarns; however, these works were done for simple cross sections, and at processing speeds similar or below the speed of commercial thermoset pultrusion [8, 9]. The main reasons for the low-speed problem are related to the difficulties associated with processing thermoplastic matrices as they have very high melt viscosities compared to thermoset. The major contributor to the pulling force is the high viscous drag generated between the fibers and the polymer. Viscous drag is heavily linked to the polymer's viscosity. Viscosity decreases as the polymer is heated. Thus, increasing temperature can decrease the pulling force [26]. Devlin et al. [27] pultruded using Glass/Nylon-12 (Glass/Pa-12) and C/PEEK prepregs. They varied the production speed to study the varying speed's effect on the impregnation quality. The impregnation quality was characterized by inter-laminar shear stress (ILSS) tests. Running at high speeds made ILSS fall off considerably. For both polymer systems, the ILSS went down when the production speed was raised from 300 mm/min to 1000 mm/min.

Lowering the pulling forces can help increase the speed. Kamble [28] tested the effect of die temperature on pulling force with commingled glass/PP by changing temperature between 199 ºC to 216 ºC and keeping and line speed constant at 0.38 m/min. The pulling force increased gradually when the temperature was increased then gradually the temperature decreased. The increase in temperature made the viscosity of the polymer to decrease. As a result, the pulling forces became less dominant since the resin started to flow freely. Lowering the pulling forces can help increase the production speeds. Thus, this can be done by increasing the processing temperature as much as possible while avoiding degradation of the fiber and the polymer. There were several attempts to increase the pultrusion speeds and they all involved adding a preheating unit – content or contactless to raise the temperature of polymer to a temperature close to processing temperature.

The high melt viscosity of thermoplastic polymer makes it extremely difficult for the melt polymer to fully impregnate the reinforcement. The high viscous forces impede achieving higher production speeds. Therefore, a preheating unit is utilized to raise the temperature of the resin fibers to a temperature close to its melting temperature in order to ensure that the temperature of the resin reaches the process temperature inside of the hot die. The preheater lowers the residence time

required for the composite mixture to remain inside the hot die(s) allowing for more room to increase production speed without jeopardizing the mechanical properties of the final product. However, it is very important to note that the preheater should not heat the resin above its melting temperature upon entrance of the prehreater. Otherwise, the resin fibers will just become too weak to enter the heating die with the reinforcement fibers due to the lack of friction between the reinforcement and resin fibers. As a result, more resin will be wasted in the form of backflow at the entrance of the first die. The wasted polymer can result in lowering backflow pressure inside the heating die lowering the final impregnation quality in pultruded beams. To avoid PP dripping at the inlet of heating die, Kamble suggested setting the preheater temperature at 149 ℃ (lower than T_m: 165℃ of PP). Novo et al. [29] observed that higher preheating temperature led to deteriorating flexural properties for carbon/PP towpregs. The reason for these low mechanical properties was that higher preheater temperatures that are very close to melting temperatures were used. In addition, this work did not report any values for impregnation level. Carlsson et al. [30] conducted pultrusion experimental work using glass fibers reinforced polypropylene (glass/PP) prepregs. A decrease in beam flexural modulus was also observed when the preheater temperature was increased from 155 ℃ to 175 ℃, a temperature which is above the melting point of polypropylene (165 ℃). It seems that higher preheating temperature may ruin mechanical properties. Therefore, the preheating temperature should be set at a temperature below melting temperature.

Betchtold et al. [31] used contact pins for the pre-heating section of the pultrusion process and introduced a new modeling approach of the preheating unit of the thermoplastic braid-trusion process with a contact preheating system. The application of contact heating pins allowed the pultruded samples to achieve higher profile qualities and they were produced at a production speed three times faster. The shear strength also improved by around 50% compared to samples pultruded without contact pins. This improvement in mechanical properties suggests a good impregnation quality. Bates et al. [32] used contact pins in the pultrusion process using commingled Glass/PP roving. Yet, the pins were incorporated in the hot die. This indicates that the contact preheater was acting as a consolidation unit. The contact preheater was set to temperature above the melting temperature. Results of pultruded products with contact pins showed significant improvements in the consolidation which were characterized by flexural strength and scanning electron microscopy

analysis. Angelov et al. [10] used pultrusion to process Flax/PP commingled fibers and used a non-contact preheater to improve impregnation, however the maximum pulling speed was 360 mm/min. The beams' images showed dry fibers on the surface which indicate very low impregnation levels. Increasing the temperature might help reduce drag forces during pultrusion. Yet, Angelov et al. [10] suggested using a non-contact preheater is more suitable when pultruding with natural fibers. They argued that contact preheaters can too aggressive on fragile reinforcement fibers such as natural fibers.

Oswald et al. [33] used two heating dies to improve impregnation quality. The exit diameter of the first heating die was almost 10% larger than the exit diameter of the second die. A reduction of void content from 12% to 4% was observed when two subsequent heating dies were used. The use of the multi-die system also allowed an increase in pultrusion speed to 350 mm/min compared to the maximum speed of 50 mm/min that was achieved with a single-die pultrusion system. Later, Lapointe et al. [34] used a four-die pultrusion system to pultrude C/PEEK hybrid yarns rods. With this pultrusion system, the lowest void content achieved was 1.7% [34]. The maximum speed attained with the four-die system was 100 mm/min. They observed that the use of multiple heating dies allows an increase in the residency time. These results hint that using a multi-dies may increase the chances to achieving higher speeds in TPC pultrusion.

2.4 Identification of problems

The literature survey showed the followings:

Surface finish irregularities and deconsolidation are problems that are connected to the cooling process. Yet, the experimental and modeling work done on TPC pultrusion in literature has always been more focused on the heating sections and overlooked the importance of the cooling section. First, according to the literature surveyed, the two ways to conduct cooling in TPC pultrusion generate several problems such as sloughing, deconsolidation and high frictional forces. Therefore, there is a need to develop an efficient cooling system to improve pultruded beams.

Second, LFT pellets are preferred for injection molding and they are typically produced using a TPC thermoplastic pultrusion. Well-impregnated Flax/PP LFT can be produced using hybrid yarns using TPC pultrusion [8]. However, it is not clear if the void content in the Flax/PP LFT has

any effect on the injected components. Among the literature surveyed, few works discussed the influence of the LFT pellets' morphology on the injection molded components [15]. It is important to note that having a low void content requirement in LFT pellets might limit the range of the pulling speed of TPC pultrusion which might lead to restricting the usage of LFT pellets in industrialised applications. Therefore, it is vital to quantify the LFT pellets' void content that would not jeopardize the mechanical properties of the final injected parts.

Third, Pultrusion of thermoplastic is a high shear stress and high temperature process. Natural fibers are low strength fibers that degrade at relatively low temperatures. At high pultrusion speeds, natural fibers could break. Pultrusion of natural fibers-reinforced thermoplastics suffered from low production speeds. The low production speeds prevent the commercialization of natural fibers reinforced thermoplastic pultrusion. There is no available research that reported successfully pultruding natural fibers at high speeds (1 m/min).). The highest Flax/PP pulling speed was 0.36 m/minute and it was achieved by Angelov et al. [10]. Also, to put things into perspective, the typical LFT pellets production speed using a twin-screw extruder is around 9 kg/hr [35, 36]. Producing Flax/PP at 1 m/minute in pultrusion will result in an output of 1.3 kg/hr (50% fiber volume fraction). Yet, achieving 1 m/minute production speed for Flax/PP LFT pellets will be a significant step in the right direction towards making the pultrusion close to twin-screw extruder production rate on top of other benefits of using pultrusion to produce LFT pellets.

CHAPTER 3 RESEARCH OBJECTIVES AND COHERENCE OF ARTICLES

3.1 Research objectives

The goal of the project is to develop a high quality and low-cost manufacturing method to produce Flax/PP injection moldable at a high production speed that can be utilized in an industrial setting. According to the literature surveyed, the pulling speed that is going to be achieved in this research is going the highest pulling speed of Flax/PP pultrudates. This will help applicable sustainable industries get closer to their required industrial pulling speed.

According to the literature reviewed and the problems identified at Section 2.2, three specific objectives need to be achieved to reach this goal:

1. **Develop an enhanced cooling die system to improve pultruded beams' surface finish and to reduce sloughing**

2. **Determine the effect of LFT pellet consolidation on mechanical properties of the injected components**

3. **Accelerate the pultrusion production speed to 1 m/min**

3.2 Coherence between the objectives and articles

The specific objectives were achieved and presented in three chapters; Chapter 4, 5, and 6 are presented here in the form of published (Chapter 4 and 5) and submitted (Chapter 6) peer-reviewed journal articles. These chapters cover the main objectives mentioned in section 3.2.

Chapter 4 presents the first article [37] entitled "Effect of cooling temperature on deconsolidation and pulling forces in a thermoplastic pultrusion process" Published in *Composites Part B: Engineering* (2021 Impact Factor: 9.078). This article satisfies the first objective. Due to the novelty of this objective and its vast potential industrial applications, notably in the aerospace and automotive industries, a patent for one of our cooling designs is pending approval by the US patent office entitiled "Pultrusion system with cooling stage and method therefor" (WO patent number: WO2020237381A1). A conference paper [38] entitled " Thermoplastic pultrusion's

cooling temperature effects on pulling forces and deconsolidation" was also published in SPE Automotive Composites Conference & Exhibition (SPE ACCE) 2019 proceedings about the newly developed cooling system. This efficient cooling system was developed to be to precisely control the pultrudate's cooling temperature profile. Lower pulling forces were observed, and deconsolidation was avoided when the pultrudates were rapidly cooled below T_g. The developed cooling system established in this article will be used in the next two chapters to produce Flax reinforced LFT pellets and evaluation the effect of LFT pellet consolidation on mechanical properties of the injected components and to accelerate the pultrusion pulling speed to 1 m/minute.

Chapter 5 presents the second article [4] entitled "Effect of Flax/PP pellets' morphology on the mechanical properties of injection-molded parts" Published in *Journal of Thermoplastic Composite Materials* (2021 Impact Factor: 3.330). This article evaluates the consolidation quality and length variation effects of Flax/polypropylene (Flax/PP) pellets on the mechanical properties of injection molded final products. Pultrudates of were produced using a multi-die pultrusion system. Pultrusion settings were varied to be able to produce four different void content points. Results showed that well consolidated pultrudates were more resilient to the cutting process such that the pellets remained structurally intact after the cutting. The pellets that came from the low-void-content pultrudates were combined with pure PP pellets and went smoothly throughout the hopper into the injection molding machine screw. Flax/PP Pellets with high void content lost integrity during the cutting process, thus exposing dry Flax fibers. In the hopper, these detached fibers from the pellets could not be processed uniformly. Mechanical properties were also heavily affected by pellets' void contents and lengths. In addition, a conference paper entitled "Effect of Flax/PP pellets' morphology on the mechanical properties of injection-molded parts" was published in SPE ACCE 2018 proceedings showing preliminary results on producing low-void Flax/PP pellets using TPC pultrusion.

Chapter 6 presents the third article [39] entitled "Effect of high pulling speeds on the morphologies of pultrudates in a thermoplastic pultrusion process" submitted to *Journal of Thermoplastic Composite Materials* (2021 Impact Factor: 3.330). The third objective was achieved using this article. Three distant pulling speeds, between 50 and 1000 mm/minute, were selected to study the effect of varying the pulling speeds. Using a model, the polymer pressure in the pultrusion

dies was calculated for respective pultrusion pulling speed. The microscopic images showed a reconfiguration of the pultruded rods a higher pulling speed that led to greater unimpregnated and polymer rich areas. The highest tensile strength was achieved by the pultrudates produced at 50 mm/minute. The tensile strength dropped by almost 20% when the pulling speed was increased to 1000 mm/minute. The pultruded rod's reconfiguration, attributed to the progressive melting of the PP fibers exerting high compaction pressure on Flax yarns, is thought to be responsible for the decline in impregnation quality and mechanical strength.

CHAPTER 4 ARTICLE 1: EFFECT OF COOLING TEMPERATURE ON DECONSOLIDATION AND PULLING FORCES IN A THERMOPLASTIC PULTRUSION PROCESS

Nawaf Alsinani, Mohammad Ghaedsharaf and Louis Laberge Lebel*

*LLL@polymtl.ca.

Advanced Composite and Fiber Structure laboratory (ACFSlab), Research Center for High Performance Polymer and Composite Systems (CREPEC), Department of Mechanical Engineering, Polytechnique Montréal, 2900 boul. Édouard-Montpetit, Campus of the University of Montreal, Montreal, H3T 1J4, Canada

This article was published in Composites Part B: Engineering

Publication date: April 27, 2021

Abstract

Surface finish deficiencies and thermal deconsolidation are common problems in thermoplastic composites pultrusion (TPC pultrusion). These problems occur in general as a result of the improper execution of the cooling process. We have developed an efficient cooling system that is able to precisely control the pultrudate's cooling temperature profile. The aim of this study is to investigate the impact that changing the cooling die temperature profile will have on the thermal deconsolidation behavior and pulling forces in a TPC pultrusion process. C/PEI (Amorphous) and C/PEEK (Semi-crystalline) pultruded rods were pultruded and reprocessed to quantify the adhesion forces during the cooling process. The selected cooling temperatures were in relation to the glass transition and melting temperature, (Tg) and (Tm) respectively. The cooling profiles were characterized by inserting a follow-on thermocouple. Deconsolidation and surface finish quality were assessed through the use of microscopy and by measuring the surface roughness. Lower pulling forces were experienced, and deconsolidation was avoided when the pultrudates were quickly cooled below Tg. For the amorphous PEI polymer, a surface finish (Ra) of 0.72 μm was achieved when cooling at 100 °C below Tg. The best surface finish (Ra = 0.56 μm) for C/PEEK was achieved at a cooling temperature of 243 °C. It is suspected that this cooling temperature promoted fast crystallization. The cooling system was then used during steady-state pultrusion experiments producing 10 m of C/PEI and C/PEEK fully consolidated rods having surface finish

Ra value lower than 0.8 μm. The developed cooling system will create significant new opportunities for the usage of pultruded thermoplastic composites in many fields, including additive manufacturing and composite joining.

Keywords: Pultrusion, Cooling, Deconsolidation, Thermoplastic

4.1 Introduction

While the manufacturing technique of thermoplastic composites (TPC) pultrusion was first developed in the 1990s, it has recently gained popularity [10, 16, 17, 20-22, 26, 27, 30, 31, 40-52]. The multi-die pultrusion was developed to overcome the impregnation challenges associated with the TPC pultrusion [34, 53]. During the multi-die pultrusion process, yarn precursors that contain the polymer and reinforcement fibers are wound onto bobbins that are placed in a creel. The creel holds the bobbins and allows the adjustment of the yarns' tensions. The polymer and reinforcement fibers are then pulled together through a cascade of dies that are heated to liquify the polymer fibers. In order to completely impregnate the reinforcement fibers, the yarns that enter the dies contain a surplus of polymer fibers. This surplus polymer, therefore, creates a backflow that helps raise the impregnation pressure [54]. At this stage, the impregnated fibers can be referred to as the pultrudate. This pultrudate then enters the cooling die to begin the solidification process; this process is also intended to prevent any thermal deconsolidation. The pulling speed is controlled by a traction system. The multi-die system is capable of producing impregnated composite rods via utilizing several materials including Flax/PLA [52], Flax/PP [8], C/PA [50], C/PEI [55], C/PEEK [34]. A multi-die pultrusion system was implemented into additive manufacturing technology and was successful to bring down the void content in the printed extrudates by over 80% [53]. These results suggest the high potential of multi-die pultrusion technology to overcome impregnation challenges.

Nevertheless, post-impregnation challenges persist, namely the surface finish defects that commonly result from TPC pultrusion [10]. Contrary to thermoset composites, thermoplastic pultrudates must undergo a cooling process while being constrained between mold surfaces. If this does not occur, the pultrudates will deconsolidate in a porous structure, resulting in composite materials with low mechanical properties [53]. During the cooling process, the behavior of a

thermoplastic polymer is dependent on its molecular arrangement, which can be either amorphous (*e.g.*, Polyetherimide, PEI) or semi-crystalline (*e.g.*, Polyetheretherketone, PEEK). When cooling an amorphous polymer from the melt, the polymer chains are arranged in a random molecular structure. Contrastingly, a portion of the semi-crystalline polymer chains arrange in crystals while they themselves are dispersed in a randomly arranged chains phase. The percentage of crystalline content within a semi-crystalline structure depends upon the thermal history and cooling conditions, and can vary from one semi-crystalline polymer to another; the size of this percentage has a significant influence on the polymer's mechanical properties [56, 57].

Among the several characteristic temperatures related to thermoplastic polymers, two important ones stand out: firstly, the glass transition temperature (T_g) and secondly, the melting temperature (T_m). The T_g can be found in both amorphous and semi-crystalline polymers. Below T_g, the polymers' randomly arranged chains (i.e., not within crystals) are frozen and cannot move with respect to one another [58]. When the polymer is heated to T_g, the same randomly arranged polymer chains receive enough thermal energy to rotate and extend, leading to a dramatic decrease in their stiffness. The other characteristic temperature, T_m, is only present in semi-crystalline polymers. When a semi-crystalline polymer is heated to T_m, the crystalline arrangement of the polymer chains is lost. A semi-crystalline polymer experiences a slight decline in stiffness at T_g , followed by a dramatic drop in rigidity around T_m [58]. Due to its rigid crystalline phase, the semi-crystalline polymer retains some of its stiffness above T_g.

The amorphous phase of a thermoplastic polymer evolves from a glassy state to a viscous flow state when the thermoplastic is heated above T_g, thereby influencing the microscale adhesion behavior between the thermoplastic polymers with metals. It was observed that polymer adhesion with a surface may vary when there is a change in temperature [25, 59-61]. For instance, PMMA, which is an amorphous polymer, is widely used as a polymer film for nanoimprint lithography (NIL). To make structures in NIL, a mold is pushed onto a deformable material, usually a heated polymer film such as PMMA, on a rigid substrate. The polymer film deforms according to the mold patterns. The patterns are then transferred onto the polymer film following the detachment of the mold. During the detachment process, it was observed that the adhesion and frictional forces can cause deformation and damages to the polymer. Later, Kim et al. [59] tested the effects of

temperature on both the adhesion and friction behavior of PMMA film, which had a T_g around 123 ℃. Their set-up included an atomic force microscope (AFM) and a fixed cantilever for measuring the adhesion and friction forces on PMMA film. As they carried out the heating process, they increased the temperature from 27 to 147 ℃ in steps of 25 ℃; they echoed this procedure in the cooling process, decreasing the temperature from 147 ℃ in steps of 25 ℃. After each temperature was reached, the polymer was kept for 5 minutes and then adhesion as well as friction tests were conducted. It was observed that PMMA film adhesion forces begin to increase at a temperature of 25 ℃ lower than the T_g of PMMA. In addition, the highest increase in adhesion and friction behaviors was observed at 25 ℃ higher than the T_g. At this temperature, the polymer PMMA film surface became adequately soft and the adhesion and friction behaviors changed.

Another damaging effect caused by high metal-polymer adhesion forces in pultrusion is the "sloughing" phenomenon [5]. In the event that the adhesion forces are higher than the pultrudate's strength, fragments stick to the die surface and tear off from the pultrudate. These broken pieces drive into the pultrudate's surface, resulting in irregular surface finish quality. While few studies were conducted on sloughing in TPC pultrusion, the topic has been extensively reviewed for thermoset composites pultrusion (TSC pultrusion) in recent decades [5-7]. Batch et al., for instance, recommended a few practices to reduce the chance of sloughing, including polishing the die surface, increasing fiber volume fraction, and adding lubricants [5]. They found that any roughness or cracks in the die surface contributed to the likelihood of sloughing. Moreover, increasing the fiber volume fraction, thereby providing more fibers for the polymer next to the die wall, lessened the likelihood of sloughing since the shear and tear surface strength of the pultrudate was augmented [5]. Not only does sloughing cause poor surface finish quality, but it also has the ability to cause a massive pulling force if left unchecked, leading to major fiber damage. Another common way to prevent sloughing in TSC pultrusion involves achieving a rapid transition during curing or gelation [6]. In TSC pultrusion, it was discovered that the longer the polymer stays in a gel-like state, the greater the probability of the occurrence of sloughing. This finding dictates the TSC pultrusion die design in three temperature zones. The middle zone, which is at high temperature, is used to gel the resin as fast as possible. This swift curing reduces the time the polymer spends in a gel-like state, thereby curtailing the potential bonding length.

Similarly, in TPC pultrusion, adhesion forces between the polymer and die walls vary during the cooling process as the temperature varies between the processing temperature (T_p) and T_g. Thus, for a TPC pultrusion process, the apparent sloughing critical distance (SCD) can be defined as the distance in the cooling die wherein the pultrudate's temperature is between T_p and T_g. Because the distribution of metal-polymer adhesion forces over a specific distance is not always clear with respect to temperature changes, the actual SCD can be different than the apparent SCD.

Exploiting the shrinkage phenomena during the cooling process in TPC pultrusion can assist in lowering the pulling forces. When a molten amorphous polymer is being cooled, it shrinks at a constant rate until its temperature reaches T_g[62]. However, a semi-crystalline hot molten polymer shrinks at a constant rate similar to the amorphous polymer until T_m is reached. From T_m and below, the semi-crystalline polymer begins arranging itself in compact crystals, which reduces the specific volume. The rate of shrinkage increases considerably during crystallization. When the crystallization content is stabilized, the rate of shrinkage stabilizes before T_g [62]. Below T_g, the semi-crystalline polymer continues to shrink; however, it does so at a relatively lower rate to the shrinkage rate that occurs above T_g.

According to the literature surveyed, there are two primary ways to conduct cooling in TP pultrusion: (1) when cooling and heating dies are combined in one embodiment; and (2), when the cooling and heating dies are separated with an air gap. In the first method, when the heating and cooling die are combined in one continuous embodiment, the cooling die section tends to thermally interfere with the heating section. The cooling section extracts heat from the heating section through the continuous tooling material. Powerful cooling techniques must therefore be used to reach a significant temperature gradient between the heating and the cooling sections. Accurate monitoring of the temperatures and high heating flux are needed to ensure that the polymer will not be cooled prior to impregnating the reinforcement fibers. These requisite high heating and cooling heat flows lower the energy-efficiency of the system. Due to the difficulties enumerated above, continuous heating and cooling dies result in a slow cooling profile along the die length; therefore, the actual SCD is long.

Table 4.1 summarizes the literature surveyed for the optimal conditions when using the

continuous embodiment set-up of cooling and heating dies. It is to be noted that in the surface finish quality column, the data was directly collected from researchers' written observations. A certain number of these studies did not report the surface quality in writing, but offered cross-section images instead. In these cases, the notes were reported based on the authors' interpretation of surface finish quality. The other studies provided no written observations or cross-section images. Ueda et al. [23], for instance, produced pultrudates using Glass and Carbon/PA commingled fibers. In their pultrusion arrangement, the heating and cooling functions were connected in one single continuous embodiment. The exit temperature was set at 270 °C, which was close to the process temperature of 290 °C. The exit temperature was additionally higher than the T_g of PA, which was at 215 °C. The microscopic images displayed a high void content and irregular surface finish from the thermal deconsolidation. Brack et al. [63] produced a MRI-image-artifact-free aneurysm clip using the pultrusion of C/PEEK commingled yarns. Yet, the microscopic images showed that the edges of the round cross-section images were irregular. This can be attributed to either a deconsolidated state or sloughing. However, since neither production speeds nor cooling temperatures were reported, the exact temperature profile is unknown to the authors. Laberge Lebel et al. [64] manufactured an L-shaped thermoplastic composite beam using a C/PolyAmide-66 (C/PA66) braid. Their pultrusion arrangement consisted of both cooling as well as heating dies in one continuous embodiment. The reported pultrusion speed was 21.4 mm/min and the heating die was set at 300 ℃. The cooling temperature was set at 270 ℃, which was above the melting point of PA66. Microscopic cross-sectional images of the pultruded L-shape showed voids in several locations, and the surface finish quality was reported to be rough, possibly a result of long actual SCD. Eichenhofer et al. [53] utilized a multi-die pultrusion system to process PA-12/Carbon commingled fibers for additive manufacturing. Their pultrusion set-up also consisted of both cooling and heating dies in one continuous embodiment. The reported pultrusion speed was 52.5 mm/min and the polymer temperature in the heating die was 221.39 ℃. The cooling temperature was not reported as being controlled. Microscopic images revealed that the pultrudate's cross-sections were irregular.

Table 4.1: Summary for the reported optimal conditions for the set-up of cooling and heating dies are one embodiment.

No.	Polymer /Fiber	Type of precursor	T_m (℃)	T_g (℃)	T_c (℃)	Speed (mm/min)	Polymer type	Surface quality	Ref.
1	C/PA		265	215	270	N/A			[40]
2	C/PEEK		343	143	150	N/A			[41]
3	C/PA-66	Commingled	220	60	270	21.4	Semi-crystalline	Irregular	[42]
4	C/PA-12		179	40	N/A	52.5			[25]

In order to avoid thermal interference, a second method has been devised, according to which the heating die as well as the cooling die can be separated by an air gap that provides a thermal barrier. With the air gap established, the pultrudate leaves the heating die at T_p; this leads to thermal deconsolidation. Then, the hot molten and the deconsolidated pultrudate comes into contact with the cold cooling die inlet. This quenches the composite to T_c. When T_c is set lower than T_g, solidification can occur at the cold cooling die inlet. For low process speeds, this solidification can occur before the material has entered the cooling die. Therefore, the pultrudate is cooled while having a larger diameter than the cooling die diameter. As previously mentioned, the polymer becomes solid and stiff at a temperature below T_g. Therefore, the solidification at a larger diameter causes the pulling forces to increase since a solid material is forced into a smaller hole. This generally results in damaging the pultrudate's surface.

Table 4.2 summarizes the literature surveyed for the reported optimal conditions when using the set-up of cooling and heating dies separated by an air gap. It should be noted that the specific length of the air-gap was never explicitly quantified by previous researchers; they simply reported that the air gap was "narrow." The examples shown in Table 4.2 were conducted under quite diverse conditions. In examples 1, 2 and 4, the pultrusion speed was low (below 100 mm/min) and the cooling temperature T_c was set higher than T_g. At these low pultrusion speeds, the pultrudate would likely deconsolidate in the gap between the heating and cooling die. The selection of a T_c higher than T_g prevented a premature solidification of the deconsolidated beam at the cooling die inlet, and would have complicated material entry therein. On the other hand, examples 5 and 6 in Table 4.2 show that when T_c was selected to be lower than T_g, a relatively higher pultrusion speed

was used. At moderate and high pultrusion speeds, it is suspected that the hot material at the heating die exit does not cool significantly in the gap, and that the hot molten pultrudate has less time to deconsolidate; additionally, it effectively heats the cooling die entrance. Therefore, the hot pultrudate might reconsolidate at the cooling die entrance without impacting the pulling forces. However, since the material must cool in contact with the cooling die surface to temperatures lower than T_g, the actual SCD is long. Therefore, the outcome would be higher pulling forces and potential sloughing, which would damage the pultrudate [65].Neither was the actual SCD for examples 5 and 6 in Table 4.2 mentioned, nor was the beam surface quality characterized by the researchers. For example 3, Wiedmer et al. [65] observed thermal deconsolidation and low surface finish quality at low speeds (90 mm/min), and recommended slightly opening the cooling die at low speeds via widening the diameter for reducing the thermal deconsolidation. However, at high speeds (280 mm/min), Wiedmer et al. [65] observed better surface finish quality, which, nevertheless, suffered from higher pulling forces. For all experiments using PP polymer (Examples 7 to 11), T_c was always set higher than T_g. Examples 9 and 11 reported the surface quality and had different outcomes. The above-reported results indicate that the polymer type, the type of precursor, the selected T_c and the pultrusion speed were highly linked variables in their influence on the surface finish quality. In fact, no system was able to provide an independent control on all the parameters that would influence the surface quality.

Table 4.2: Summary for the reported optimal conditions when the set-up of cooling and heating dies separated by an air gap was used.

No.	Polymer/ Fiber	Type of precursor	T_m (℃)	T_g (℃)	T_c (℃)	Speed (mm/min)	Polymer type	Surface quality	Ref.
1	Jute/PLA	Parallel hybrid	200	60	165	18		N/A	[17]
2	Flax/PLA	Parallel hybrid			130	50		Irregular	[50]
3	C/PA-12	Commingled	177	40	N/A	280		Good	[43]
4	C/PEEK	Commingled	343	143	150	50		Irregular	[24]
5		Pre-preg			100	120		N/A	[51]
6		Pre-preg			100	240	Semi-crystalline	N/A	[4]
7					60	30		N/A	[4]
8					80	1000		N/A	[12]
9	Glass/PP	Pre-preg	160	-20	60	120		Good (no cross-section images)	[7]
10					50	200		N/A	[22]
11	Flax/PP	Commingled			25	120		Rough, dry, Irregular	[15]

Thus, for improving the cooling process in TPC pultrusion, the basic requirements shall be: (i) avoid slow cooling (in order to prevent sloughing); (ii) avoid having an air gap to keep the pultrudate constrained between mold surfaces before reaching T_g (in order to prevent deconsolidation); and (iii) achieve an enhanced control over the cooling process of pultrudates for improving crystallization. In this study, we propose an efficient cooling die design in order to achieve pultrudates with outstanding surface finish quality at high consolidation levels. This cooling system was utilized for studying the effect of cooling temperature on the thermal history of the pultrudates. The thermal cooling profile was used to determine the apparent SCD values of the pultrudates using an amorphous and a semi-crystalline polymer. The effect of cooling temperatures on the crystallinity contents in the C/PEEK pultrudates was studied, and the effect of cooling temperature on the thermal deconsolidation, pulling forces and surface finish quality in

C/PEI, and C/PEEK pultrudates was reported. Finally, to validate the findings from reprocessing experiments, the cooling system was tested in two pultrusion experiments which achieved steady-state equilibrium and produced 10 m of each of the pultrudates, C/PEI and C/PEEK. The results of pulling forces and surface finish quality of the steady-state pultrusion experiments were reported and compared with the results of reprocessing experiments.

4.2 Methodology

4.2.1 Materials

Two commingled yarns (Concordia fibers) types of different material combinations were used for the manufacturing of the pultrudates in our experiment. For both yarns, the reinforcement was 12k carbon fiber yarns (AS4, Hexcel) with a density of 1.79 g/cm^3 and the fiber fineness consisted of 858 tex. The Carbon/Polymer ratio was 48%/52% in both cases. One yarn type blended the carbon fibers with PEI (Ultem 9011, Sabic) and the other with PEEK (151G, Victrex). Table 4.3 displays the properties of PEI and PEEK. It should be noted that the PEI and PEEK viscosities are presented for reference only as the shear rate used for the measurement of the reported values was higher than what would typically be used during pultrusion.

Table 4.3: Properties of PEEK and PEI.

Parameter	Unit	Value	Ref
PEI			
Melting point	°C	N/A	
Glass transition	°C	217	[52]
Solid density	g/cm^3	1.28	
Melt density	g/cm^3	1.21	[53]
Melt viscosity	Pa.s	[200, 500]	[54]
PEEK			
Melting point	°C	343	
Glass transition	°C	143	
Solid density	g/cm^3	1.30	[55]
Melt density	g/cm^3	1.18	[55]
Melt viscosity	Pa.s	[130, 300]	[55]

4.2.2 Pultrusion apparatus

Figure 4.1 presents the schematic for the pultrusion system used in this study. The pultrusion apparatus contained a creel, a guide, a preheater, four heating dies, a cooling die, a load-cell and a pulling system. The creel allowed for individual adjustment of each of the bobbins' tension. A three-Newton tension was applied to each bobbin. The preheater consisted of a metallic tube, 300 mm-long and 16.2 mm in diameter, wrapped with a strip heater. All four heating dies had a 31.75 mm conical cavity tapered at 5° relative to the horizontal axis followed by a straight 6.67 mm cylindrical cavity. The diameter of each die's cylindrical exit was 5.13, 5.00, 4.90 and 4.76 mm respectively. The white triangles in Figure 4.1 denote a thermocouple's location in the heating dies. Additionally, red circles represent the location of the heating cartridges whereas the blue circles represent the location of the air-cooling channels. A thin-walled tube protruded from the last pultrusion die toward the cooling die. Two different tube lengths were used for pultrusion of C/PEI and C/PEEK. The tubes' lengths that were exposed to the air were 8.4 and 27.6 mm for the pultrusion of C/PEI and C/PEEK respectively. The selection of these lengths is explained in Section 2.2.1. The tube was inserted into a 3 mm-deep hole at the cooling die's inlet. The fit between the tube and cooling die inlet's hole was a medium running fit (RC5). The thickness of the thin wall was 1.59 mm in order to reduce the thermal interference between the fourth heating die and the cooling die. In order to gain an enhanced control over the temperature, each bottom and top part of the cooling die was equipped with a heating cartridge as well as an air-cooling channel. The main elements of the system, from the preheater to the cooling die, were installed on sliding rails in order to measure the pulling forces by using a load-cell. The pultrusion speed was controlled by a puller throughout the process.

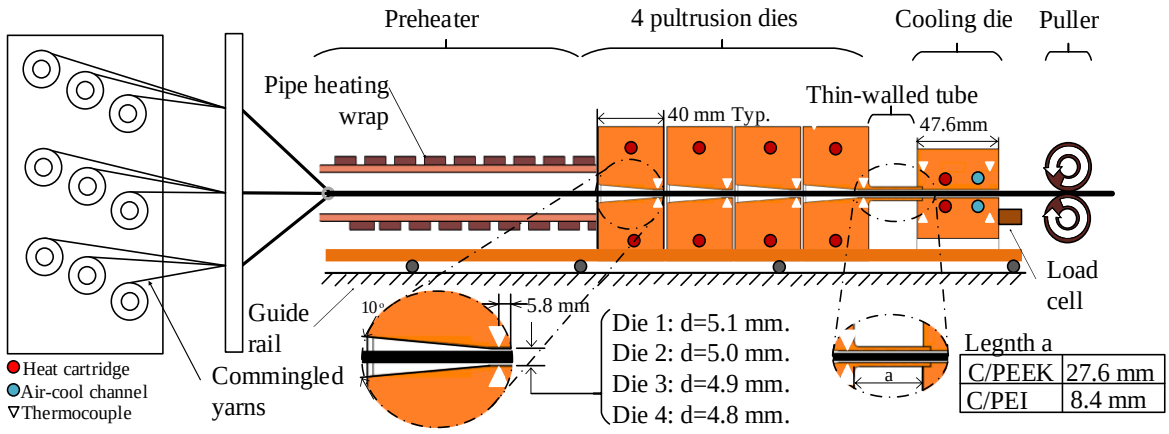

Figure 4.1: Schematic of the multi-die pultrusion system used in this study. The pultrusion system includes a creel, a pre-heater, four pultrusion dies, a thin-walled tube, a cooling die, a load-cell and a pulling system. The red and blue circles indicate the locations of the heating and cooling channels. The white triangles indicate the locations of the control thermocouples. (For interpretation of the references to colour in this figure legend, the reader is referred to the Web version of this article).

4.2.3 Selection of the thin-walled tube length

As stated in the introduction, since the cooling system is designed to prevent sloughing and consolidation while ensuring controlled crystallization, the thin-walled tube's length was intended to be short enough to limit the SCD, yet long enough to ensure that the pultrudate can cool below T_g before reaching the tube's end. The T_g of PEI is around 216℃ and its T_p is around 380 ℃. Additionally, the T_g of PEEK is around 143 ℃ and its T_p is around 400 ℃. Consequently, the C/PEI pultrudate must be cooled down by 164 °C ($T_p - T_g$) whereas C/PEEK pultrudate must be cooled down by 257 °C ($T_p - T_g$) before reaching the tube's end. Consequently, two thin-walled tube cooling die systems were required to support the difference in temperature gradients. Based on preliminary FEM results, which can be found in this paper's supplementary section, a short thin-walled tube of 8.4 m was selected for the cooling distance of C/PEI pultrusion, while a longer one (27.6 mm) was selected for C/PEEK pultrusion.

4.2.4 C/PEI and C/PEEK rod pultrusion

The pultrusion of both C/PEI and C/PEEK rods utilized 21 commingled yarns. The filling ratio

was calculated as the ratio of the area of total material (polymer and reinforcement fiber) divided by the die exit area. The polymer areas were calculated utilizing the polymer yarn size in tex count, which was then divided by the melt density of the polymers. The 21 bobbins produced a filling ratio of 93%, 98%, 102% and 106% in the first, second, third, and fourth heating dies respectively. The change in the die's exit area gradually increased the composite V_f to a nominal value of 56%. The pultrusion speed was 50 mm/min. For C/PEI, the heating dies were set at 380℃ and the cooling die temperature was set at 108℃. For the pultrusion of C/PEEK, all heating dies were set at 400 ℃. The cooling die temperature was set at 100 ℃.

4.2.5 Single-die reprocessing experiments

Figure 4.2 displays the schematic of the single-die pultrusion system that was used for testing the cooling die temperature effects on the pulling forces utilizing pre-consolidated pultrudates. This set-up was identical to the four-die pultrusion system with the exemption that it had only a single heating die. A 36-gage type J thermocouple was attached to the rod's tip cross-section center. The rod's center was melted using a digital soldering station (FX888D, Hakko) to insert and attach the thermocouple. The pre-consolidated rod was inserted in the system at room temperature. The thermocouple end was flushed with the preheater entrance and the puller gripped the other end. The preheater, the heating die, and cooling die were then heated to reach set temperatures. Table 4.4 displays the temperature set points and the production speed used for the single-die force measurement.

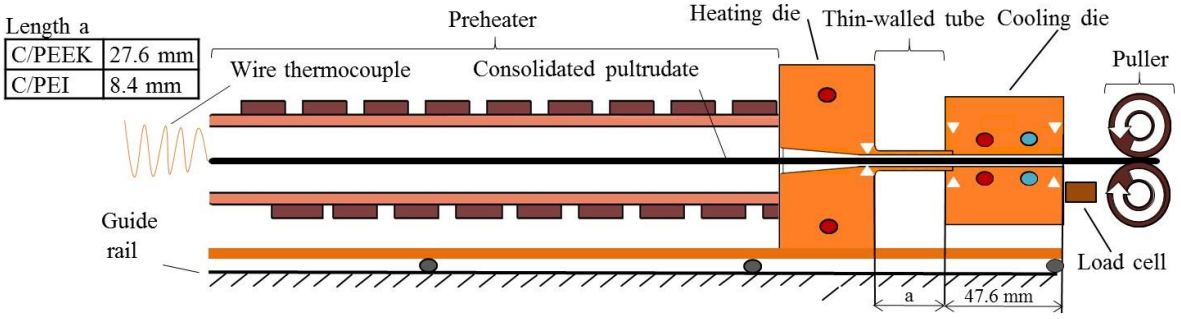

Figure 4.2: Schematic of the single-die system used to test the cooling die temperature effects on the pulling force. The set up contained a wire-thermocouple, a well-consolidated rod, a pre-heater, a heating die, a thin-walled tube, a cooling die, a load-cell and a puller.

Table 4.4: Pultrusion parameters using different cooling temperatures for the the single-die reprocessing as well as steady-state experiments.

Polymer and Sample name	Preheater ($°C$)	Heating die(s) ($°C$)	Cooling die ($°C$)	Pulling Speed (mm/min)
PEI	200	380		50
PEI-109			109	
PEI-216			216	
PEI-300			300	
PEI-Steady			109	
PEEK	300	400		
PEEK-100			100	
PEEK-143			143	
PEEK-243			243	
PEEK-343			343	
PEEK-370			370	
PEEK-Steady			243	

4.2.6 Characterization

Five cylindrical rod samples were cut using a precision saw. The cylindrical samples were then polished and analyzed under a microscope (Metallovert, Leitz). The void content was measured utilizing the standard ASTM D2734-09 method C. The degree of crystallinity (DOC) in the C/PEEK pultrudates was determined using differential scanning calorimetry (DSC) machine TA Instruments Q1000. The method used for calculating the DOC of the C/PEEK pultrudates was based on equation (1) [66].

$$\%DOC = \frac{\Delta H_m + \Delta H_C}{\Delta H_F (1 - W_f)} \times 100\% \qquad (1)$$

In equation (1), H_m is the heat of fusion, H_c is the heat of fusion of cold-crystallization, H_F is the heat of fusion of a 100% crystalline material, which was found from literature to be 122.5 J/g [67]. W_f Corresponds to the fiber weight fraction of the composite. The surface finish quality was quantified utilizing a surface roughness characterization machine (Surfcoder-SE700, Kosaka). Nine readings were taken from each sample for Ra roughness measurements. Those readings were positioned 45° apart from each other. The surface roughness characterization machine had 5

samples, each set at an evaluation length of 4.0 mm, a sample length of 0.8 mm and a pitch of 0.5 μm.

4.2.7 Steady-state pultrusion experiment

To validate the findings from the reprocessing experiments, two steady-state pultrusions were done using commingled tows. The multi-die pultrusion system shown in Figure 4.1 was used to produce 10 m of both C/PEI and C/PEEK pultrudates. The preheater's and heating dies' set temperatures had the same values as in section 2.3 and Table 4.4 except for the cooling die set points. The selected cooling temperatures were 109 and 243 ℃ for C/PEI and C/PEEK respectively. The pultrusion speed was 50 mm/min for a duration of approximately 3.4 hours for each experiment. The pultrusion force was recorded continuously throughout the experiment. The resulting pultrudates of the steady-state experiments were cut into 1 m length samples. Representative cross-section images were acquired as per the method described at Section 2.5. The surface finish quality was measured three times along the length of each 1 m sample as per the method described in Section 2.5.

4.3 Results and discussions

The results and discussions section provides the results of the single die reprocessing experiments. To summarize, C/PEI and C/PEEK pultrudates were produced using the four-die pultrusion system before being reprocessed by a single die system. The pultrudates were well-consolidated and the calculated void contents were below 2%. We will first demonstrate the thermal history of the SCD values of the reprocessed samples. Then we will discuss the crystallinity percentages in the reprocessed C/PEEK samples. The consolidation assessment subsection will examine the void content in all reprocessed samples and will be followed by a full discussion on the effects of cooling temperature on the pulling forces. We will also bring forward the shrinkage phenomena for consideration. The surface finish quality subsection will discuss the connection between the cooling temperature and surface finish quality in the reprocessed pultrudates. Finally, steady-state experiments results will be shown.

4.3.1 Thermal history of the reprocessed samples

Figure 4.3 (a) presents the temperature measurement during a PEI-109 experiment. PEI is an amorphous polymer with a T_g around 216 ℃. In this experiment, T_c was set at 109 ℃. From the temperature-position plot, the measured SCD was around 23 mm. The pultrudate also left the cooling die with a temperature below T_g, which prevented any potential deconsolidation upon exiting the cooling die. Figure 4.3 (b) presents the temperature measurement during a PEI-216 experiment. Here, the cooling temperature was set to the T_g of PEI. Hence, the pultrudate was cooled more slowly than the PEI-109. The measured SCD was around 43.3 mm. Yet, the pultrudate still left the cooling die with a temperature 10 degrees below T_g. The reason for the difference between the cooling die set point and the exit temperature of the rod may also be due to the location of the air cooling channels near the exit; these channels could have caused the pultrudates to cool down below the set point. Figure 4.3 (c) presents the temperature measurement during a PEI-300 experiment. Here, the cooling temperature was set to 300, and the measured SCD was longer than 61.8 mm, indicating that PEI-300 continued to be cooled down towards T_g beyond the cooling die's exit. Among all C/PEI experiments, the maximum recorded pultrudates' temperatures were 359.2 ℃, 363.4 ℃ and 377.5 ℃ for PEI-109, PEI-216 and PEI-300 respectively. These recorded temperatures were below the desired T_p. The data collected for the control thermocouples placed within the heating die (see triangles in Figure 4.1), measured a temperature equal to the desired T_p of 380 ℃. The difference between the rod and die temperature indicates that the cooling die extracted heat from the rod upstream of the cooling die's inlet while the rod was still inside the heating die. This phenomenon is attributed to the high axial thermal conductivity of the C/PEI pultrudate; it was also observed during the C/PEEK reprocessing experiments. These results indicate that the thermal contribution of the pultrudate is significant and should be included in any future thermal modelling of the pultrusion process.

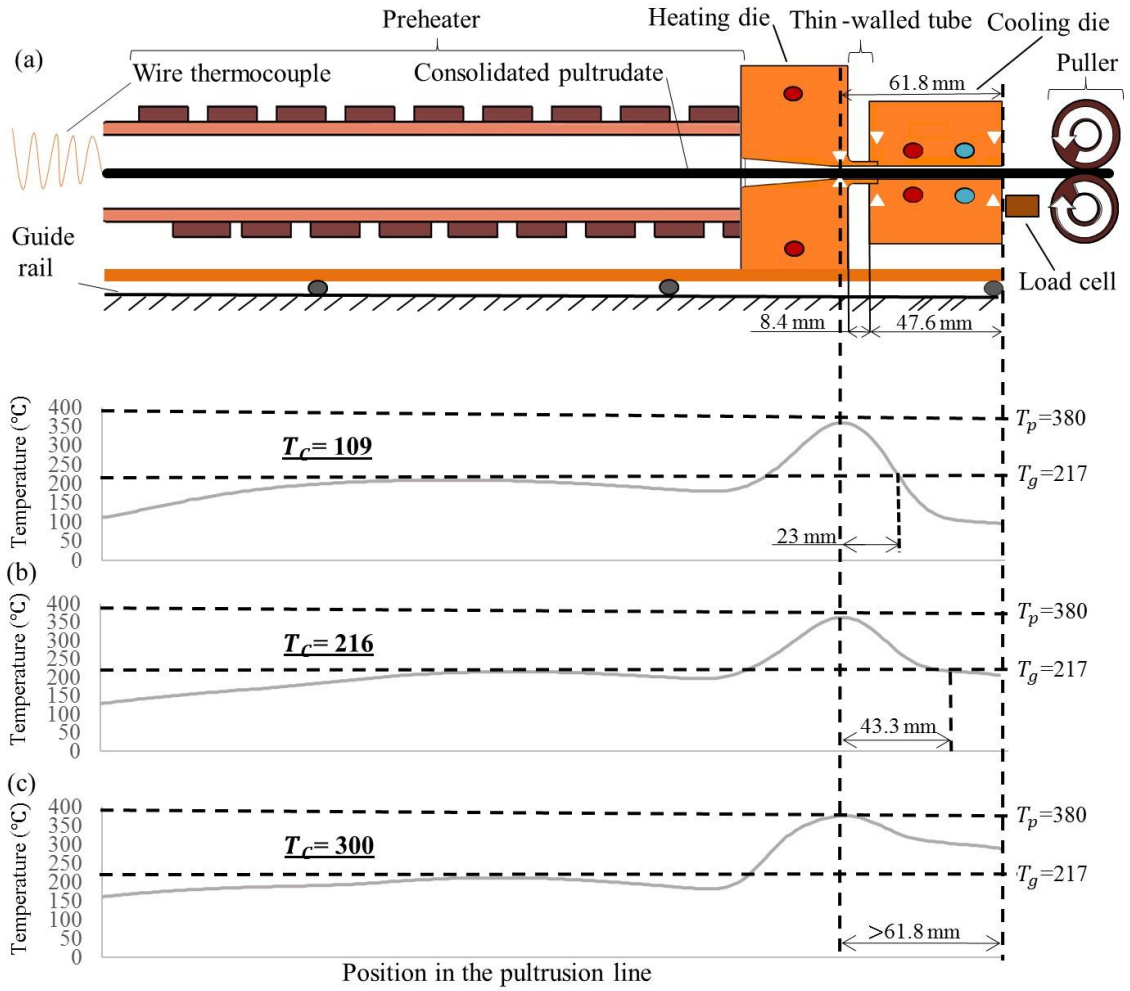

Figure 4.3: Temperature measurements with respect to the position of the wire thermocouple following the C/PEI pultrudate during the single-die reprocessing experiments with measured SCD (a) The measured SCD during the PEI-109 experiment was 23mm. (b) The measured SCD during the PEI-216 experiment was 43.3 mm. (c) The measured SCD during the PEI-300 experiment was longer than 61.8. Note that for all three graphs, the horizontal axis length was adjusted to fit the schematic of the single-die pultrusion system shown in a).

Figure 4.4 shows the temperature measurements taken by the wire-thermocouple in the single die reprocessing experiments during the C/PEEK experiments. Figure 4.4 (a) shows the temperature measurement during a PEEK-100 experiment. T_c was set at 100 ℃. From this temperature-position plot, the SCD was measured to be 46.7 mm. The rod also left the cooling die

at a temperature below T_g, which would prevent any potential deconsolidation upon exiting the cooling die. Figure 4.4 (b) shows the temperature measurement during a PEEK-143 experiment. In this experiment, the cooling temperature was set to the T_g of PEEK. Therefore, the pultrudate was cooled more slowly than the PEEK-100. The SCD was measured to be 65 mm. However, the pultrudate still left the cooling die with a temperature 10 degrees below T_g. As noted above, this same observation was made for the C/PEI samples, and the discrepancy was attributed to the location of the air cooling channels. Figure 4.4 (c), (d) and (e) show the temperature measurement during a PEEK-243, PEEK-343 and PEEK-370 experiments. The measured SCD was longer than 81 mm since the pultrudates left the cooling die before reaching T_g. This finding indicates that the pultrudates continued cooling downwards to T_g outside the cooling die.

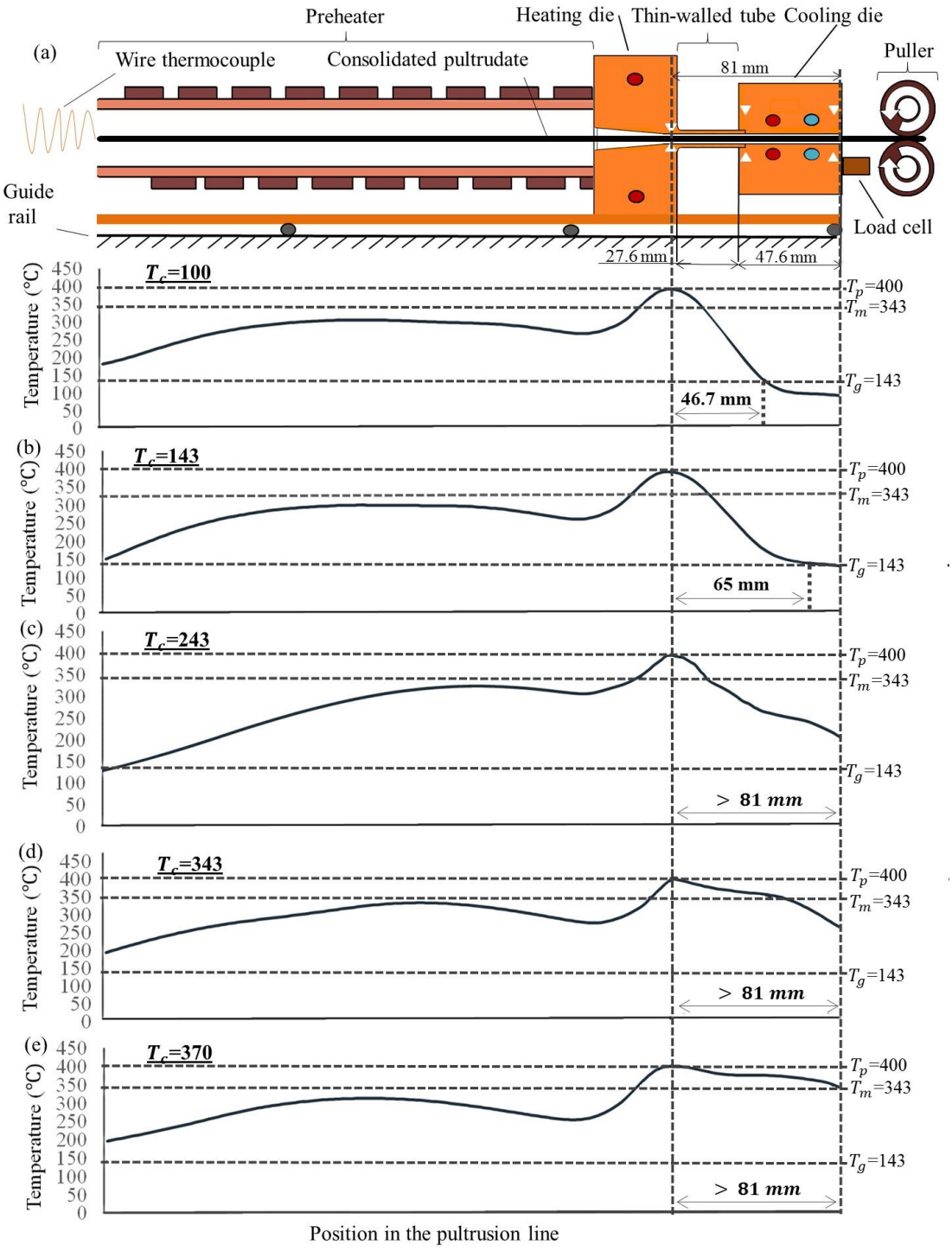

Figure 4.4: Temperature measurements with respect to the position of the wire thermocouple following the C/PEEK pultrudate during the single-die reprocessing experiments and measured SCD. (a) The measured SCD during the PEEK-100 experiment was 46.7mm. (b) The measured

SCD during the PEEK-143 experiment was 65 mm. (c)-(d)-(e) The measured SCDs during the PEEK-243, PEEK-343, and PEEK-370 experiments were all longer than 81. Note that for all four graphs, the horizontal axis length was adjusted to fit the schematic of the single-die pultrusion system shown in a).

4.3.2 Crystallization

Figure 4.5 (a) shows the percentage of crystallinity in the C/PEEK samples after the single-die reprocessing experiments, all of which appeared to have very similar crystallinity contents. PEEK-100 and PEEK-143 were the only samples that fully crystalized inside the cooling die; therefore, their temperature shifted from T_m to T_g before reaching the end of the cooling die (see Figure 4.4). The cooling rates for PEEK-100 and PEEK-143 were 370 ℃/min and 204 ℃/min respectively. These cooling rates were not significant enough to create a large difference in the degree of crystallinity in these samples. In fact, Gao et al. [29] tested the effect of cooling rates on the crystallinity contents in C/PEEK composites. Changing the cooling rate from 160 ℃/min to 600 ℃/min decreased the degree of crystallinity by 2% only. PEEK-243 and PEEK-343 were the only samples that were suspected to have crystallized partially inside the cooling die and then continued crystallization after leaving the cooling die. These two samples were quenched to room temperature after leaving the cooling die; however, their final crystallinity contents were still very similar to the other PEEK samples. PEEK-243 may have crystallized close to the maximum upon exiting the cooling. PEEK-370 was the only sample that crystallized completely after leaving the cooling die. Here also, quenching PEEK-370 that was in a fully viscous state to room temperature did not seem to affect the crystallinity content of the sample. It is likely that the quenching rates to room temperature for PEEK-343 and PEEK-370 were not high enough to be able to affect the crystallinity contents as PEEK based composites crystallize rapidly [29].

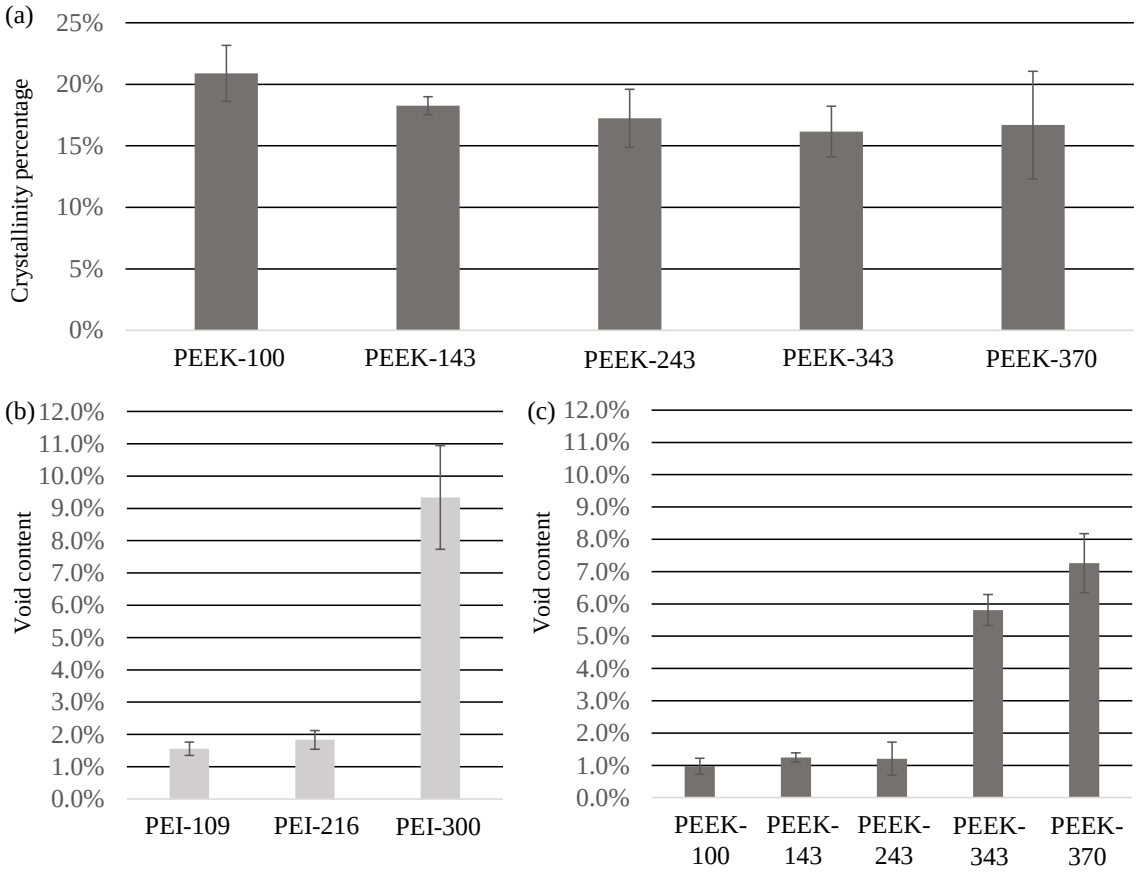

Figure 4.5: Characterization results for pultrudates obtained after the single-die reprocessing experiments: (a) The crystallinity contents in the C/PEEK samples are similar irrespective of the cooling temperature. (b) The void contents in the C/PEI samples. (c) The void contents in the C/PEEK samples. Void content significantly increased when the pultrudate exits the dies above T_g of 217°C for PEI and above T_m of 343°C for PEEK.

4.3.3 Consolidation Assessment

Figure 4.5 (b) and (c) show the comparative void content between the PEI and PEEK experiment results. All of the samples that were set at cooling temperatures less than their T_g had void contents below 2%. Contrastingly, the samples that were set at cooling temperatures above their T_g had significantly higher void contents. The high void contents are attributed to the thermal deconsolidation occurrence since the polymer at molten state could not retain the expansion of the rod upon exiting the cooling die. The only sample that was set at a cooling temperature above T_g

and still had a low void content was PEEK-243. This sample had a void content of 1.1% $\pm$0.4%. PEEK is known to crystallize rapidly at midpoint temperature between T_g and T_m, i.e., 243°C [68]. Therefore, the crystallization of the PEEK polymer most probably occurred during its passage through the thin-walled tube and cooling die, while the rod was still in contact with the die surface. Thus, the PEEK's crystalline phase provided enough rigidity to prevent thermal deconsolidation upon exiting the cooling die. Figure 4.6 (a) shows the microscopic image of PEI-109, which had the lowest cooling temperature among the C/PEI samples at roughly $T_g/2$. The cross-section image appears perfectly circular with insignificant void content. Figure 4.6 (b) presents the microscopic image of PEI-216, which was set at a cooling temperature close to T_g. The cross-section appears perfectly circular; black spots (small voids) are scattered at its top left of the center. Although voids were visible, the void content in this sample remained insignificant (below 2%). For PEI-216, the nearly perfect circular cross-section did not seem to be considerably affected by temperature increase to T_g. Figure 4.6 (c) presents the microscopic image of PEI-300, which had the highest cooling temperature relative to the other samples. Here, the microscopic image shows substantial irregularities along the outer surface of the cross-section; additional voids appear as black dots, possibly due to thermal deconsolidation. In fact, the thermal deconsolidation seems to considerably affect the roundness of the cross-section seen. These results indicate that an amorphous pultrudate will retain the cooling die shape as long as it leaves the cooling die with a temperature below T_g and is constrained between mold surfaces.

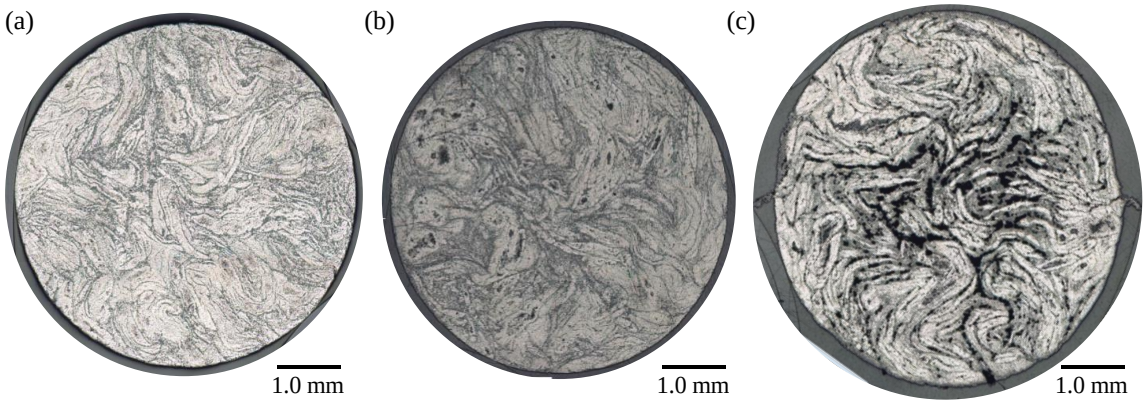

Figure 4.6: The microscopic photos of C/PEI pultrudates obtained after the single-die reprocessing experiments. (a) PEI-109. (b) PEI-216. (c) PEI-300.

Figure 4.7 consists of the microscopic image of the C/PEEK samples. Figure 4.7 (a) shows PEEK-100, which had the lowest cooling temperature among the C/PEEK samples. The microscopic image reveals a perfectly circular cross-section with insignificant void content. Figure 4.7 (b) shows the microscopic image of PEEK-143 which was set at around T_g. The microscopic image shows a circular cross-section where small voids appear as black spots scattered around its center. The nearly perfect circular cross-section does not seem to be significantly affected by the increasing cooling temperature to T_g. Also, both PEEK-100 and PEEK-143 cross-sections images show very few void contents, confirming the measured value below 2% (see Figure 4.5). Figure 4.7 (c) shows the microscopic image of PEEK-243, which was set at a cooling temperature between T_g and T_m. The microscopic image also shows a circular cross-section with insignificant voids. This is another indication that the PEEK polymer may have fully crystallized before leaving the cooling die, leaving the sample rigid enough to prevent any significant thermal deconsolidation. Figure 4.7 (d) and (e) show the microscopic image of PEEK-343 and PEEK-370, which were set at cooling temperatures close to T_m and higher. Their microscopic images reveal substantial irregularities along the outer surface of the cross-section with more voids scattered as black dots, possibly due to the thermal deconsolidation. Increasing the cooling temperature to T_m and above seems to significantly affect the roundness of the cross-sections. It is important to note that these samples did not fully crystalize upon leaving the cooling die; thus, they were not rigid enough to prevent the thermal deconsolidation which affected the roundness of their cross-sections.

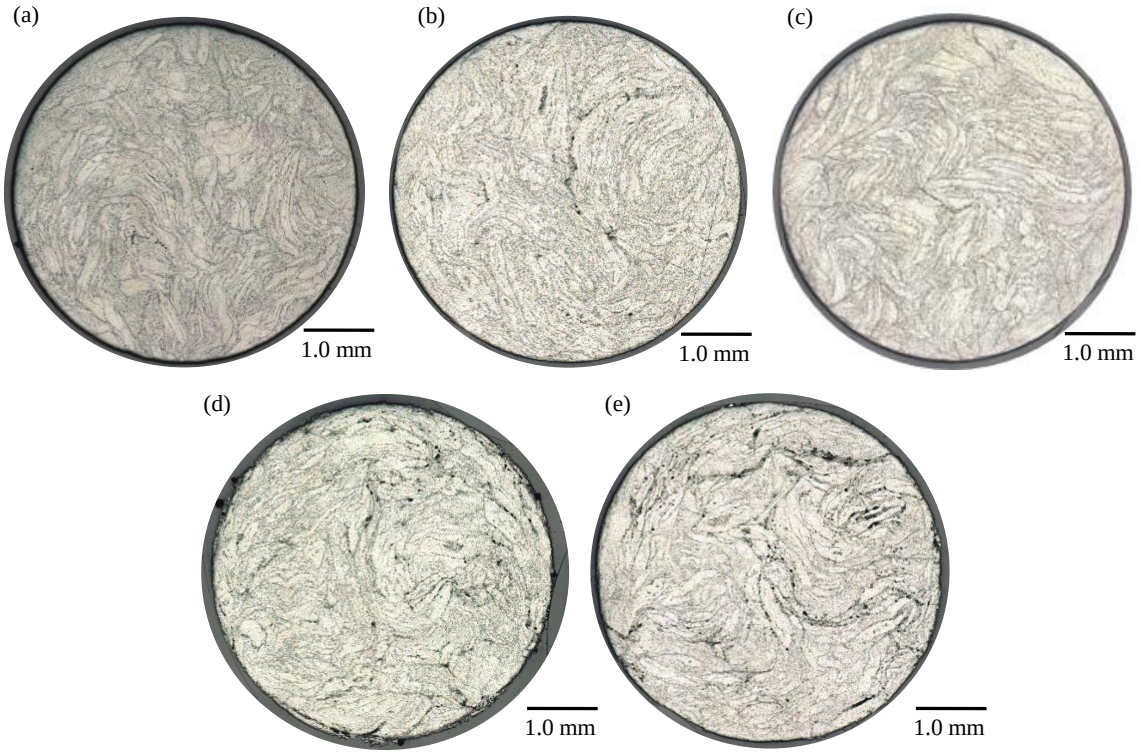

Figure 4.7: The microscopic photos of C/PEEK pultrudates obtained after the single-die reprocessing experiments. (a) PEEK-100. (b) PEEK-143. (c) PEEK-243. (d) PEEK-343. (e) PEEK-370.

4.3.4 Pulling force

Figure 4.8 (a) shows the cooling die temperature's effect on pulling forces. The results were taken from the time interval [100 to 400 seconds], which presented the steady-state interval for the reprocessed samples. PEI-109 exhibited the lowest pulling forces, which can be attributed to its low SCD being around 23 mm. PEI-216 exhibited significantly higher pulling forces: a result of the longer SCD generating longer metal-polymer adhesion. PEI-300 displayed very similar pulling forces to the PEI-216 at the beginning of the time interval. However, after a pultruded length of 200 mm, the pulling force reading began to diverge and displayed an increasing trend in pulling forces. During all PEI-300 experiments, sloughing caused some PEI impregnated carbon fibers to detach from the rod and stick to the cooling die surface. It was then perceived that carbon fibers started separating from the pultrudate. This is a typical sloughing incident. Consequently, the

increasing trend in the pulling forces was probably caused by the sloughing incident. Figure 4.8 presents the image of the cooling die's exit during PEI-300 experiment. The image illustrates carbon fibers detaching from the pultrudate upon exiting the cooling die. In this case, setting the cooling temperature 83 ℃ higher than T_g appeared to affect the pulling forces considerably for an amorphous pultrudate and caused sloughing. This observation justified the use of SCD to measure adhesion distance as it proves that high adhesion high adhesion does not only occur near T_g. Figure 4.8 (b) represents the cooling die temperature's effect on pulling forces during C/PEEK experiments. Again, the results were taken from the time interval [100 to 400 seconds]. PEEK-100 and PEEK-143 were the only samples that crystalized inside the cooling die; that is, their temperature went from T_m to T_g before reaching the end of the cooling die. PEEK polymer experiences a lower rate of shrinkage when the polymer is cooled under T_g [69, 70]. The crystallization induced shrinkage which occurred inside the cooling, and may have caused the contact lengths of PEEK-100 and PEEK-143 to become very similar. Thus, the two samples had nearly equal pulling forces. However, PEEK-243, PEEK-343 and PEEK-370, which had longer SCDs, exhibited significantly higher pulling forces. These samples partially or never crystallized inside the cooling die, and then concluded crystallization after leaving the cooling die. PEEK-243 may have fully crystallized before leaving the cooling die, but the amorphous component PEEK-243 may have been still adhesive. The crystallinity contents of the PEEK-243 were measured at approximately 26% and the rest was just an amorphous polymer. The pulling force analysis in this section for the C/PEI samples showed a significant decrease when the cooling temperature was lowered from T_g to $T_g/2$. Thus, the amorphous component of PEEK-243 may have contributed to keeping the pulling forces high. PEEK-343 and PEEK-370 were in the full viscous state before leaving the cooling die. Consequently, these samples needed high pulling forces to overcome the high metal-polymer adhesion forces.

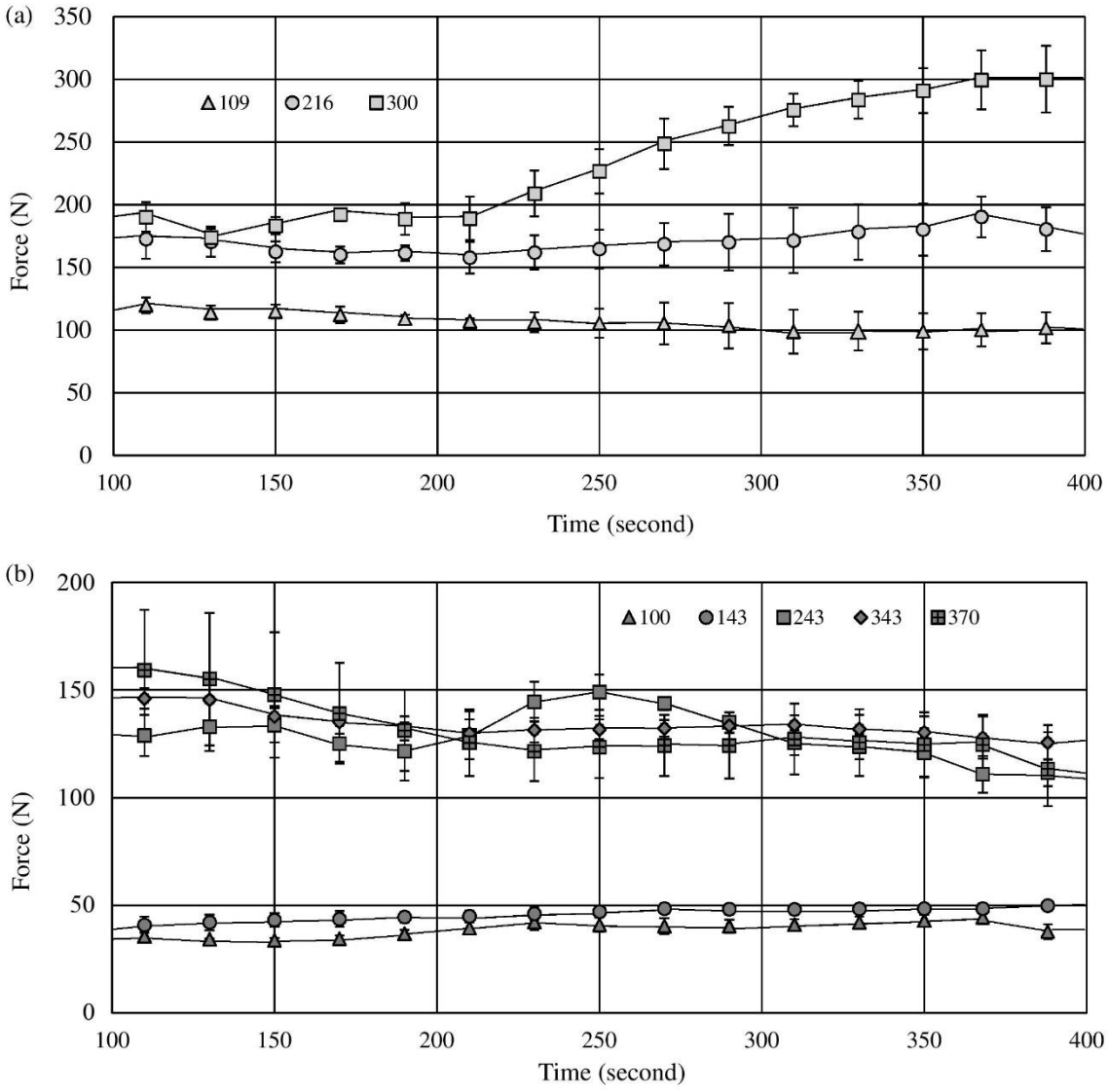

Figure 4.8: Cooling temperature's effect on pulling force for (a) C/PEI, and (b) C/PEEK, during the single-die reprocessing experiments. The force measured increases with increasing cooling temperature.

Figure 4.9 Image of the cooling die's exit during PEI-300 experiment. The image is displaying dry carbon fibers detaching from the pultruded material upon exiting the cooling die. This is a typical sloughing event.

4.3.5 Surface finish quality

Figure 4.10 (a) shows the effect of cooling die temperatures on surface finish quality for C/PEI. PEI-109 had Ra value of $0.72 \pm 0.09\ \mu m$. PEI-216 had a higher Ra value of $1.39 \pm 0.11\ \mu m$. Even though PEI-216 left the cooling die at a temperature below T_g, it had a lower surface finish quality than PEI-109. This decrease in surface finish quality can be attributed to having a longer SCD, which increased the direct contact and friction with the die surface. PEI-300 had the highest Ra value and highest error bar of $1.99 \pm 0.21\ \mu m$. Here, the low surface finish quality is attributed to the deconsolidated state of the pultrudate. Figure 4.10 (b) shows the effect of cooling die temperatures on surface finish quality for C/PEEK. PEEK-100 resulted in rods with Ra with $1.09 \pm 0.14\ \mu m$. PEEK-143 showed a similar Ra value of $1.11 \pm 0.17\ \mu m$. However, PEEK-243 showed the lowest Ra value with $0.56 \pm 0.06\ \mu m$. This value qualifies for the extremely fine finish category, i.e., Ra$<0.80\ \mu m$ [71]. PEEK-based composites crystallize as they are exposed to an environment where the temperature is between T_g and T_m [46]. Yet, Figure 5 (a) shows no significant difference in the crystallinity contents between the C/PEEK samples. PEEK-243 may have had higher crystallization rate than PEEK-343 and PEEK-370. PEEK-343 and PEEK-370 had nearly equal Ra values 2.60 ± 0.40 and μm $2.59 \pm 0.35\ \mu m$ respectively. The values were also

higher with larger error bars, and they were inferior to the other C/PEEK samples. These samples did not fully crystallize before leaving the cooling die, thus, leading to a deconsolidated state of the pultrudate.

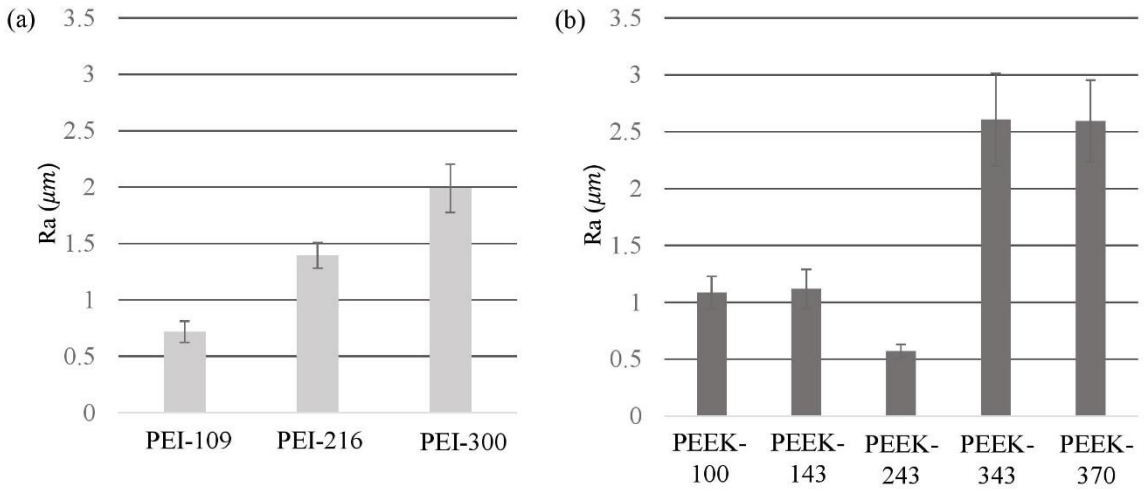

Figure 4.10: (a) Effect of cooling die temperatures on the surface finish quality (Ra) for pultrudates obtained after the single-die reprocessing experiments: (a) C/PEI. (b) C/PEEK. In general, lower cooling temperatures lead to better surface roughness. PEEK-243 outstanding surface quality is attributed to the high crystallisation rate at 243°C.

4.3.6 Steady-state pultrusion

The steady-state pultrusion experiments went without interruption for 10 m. A representative video of a steady-state pultrusion can be seen at https://youtu.be/nnMvdbEMNnU. Figure 4.11 (a) and (b) present the temperature measurements taken during the steady-state experiments of C/PEI (PEI-Steady) and C/PEEK (PEEK-Steady). Here, the cooling temperatures were set to 109℃ for PEI-steady and 243°C for PEEK-Steady experiments. These temperature set-points corresponded to the cooling temperatures which resulted in the lowest Ra value among the reprocessed samples (i.e., PEI-109 and PEEK-243). The temperature lines in Figure 4.11 indicate that the commingled tows reached the preheater temperature set-point of 200°C for C/PEI and 300˚C for C/PEEK before the first heating die's entrance. After entering the first heating die, the temperature continued to raise sharply towards the processing temperatures. Both samples reached the processing

temperature (380°C for C/PEI and 400°C for C/PEEK) by the time they reached the second die. By the end of the forth die, and entering in the cooling system, sharp drops in temperature were experienced. The measured SCDs of PEI-Steady and PEEK-Steady were 25.3 mm and above 81 mm, respectively. These values are close to the measured SCD values of the reprocessed sample PEI-109 and PEEK-243. This indicates that the steady-state experiments had similar temperature exposition histories after the forth die to PEI-109 and PEEK-243 reprocessing experiments.

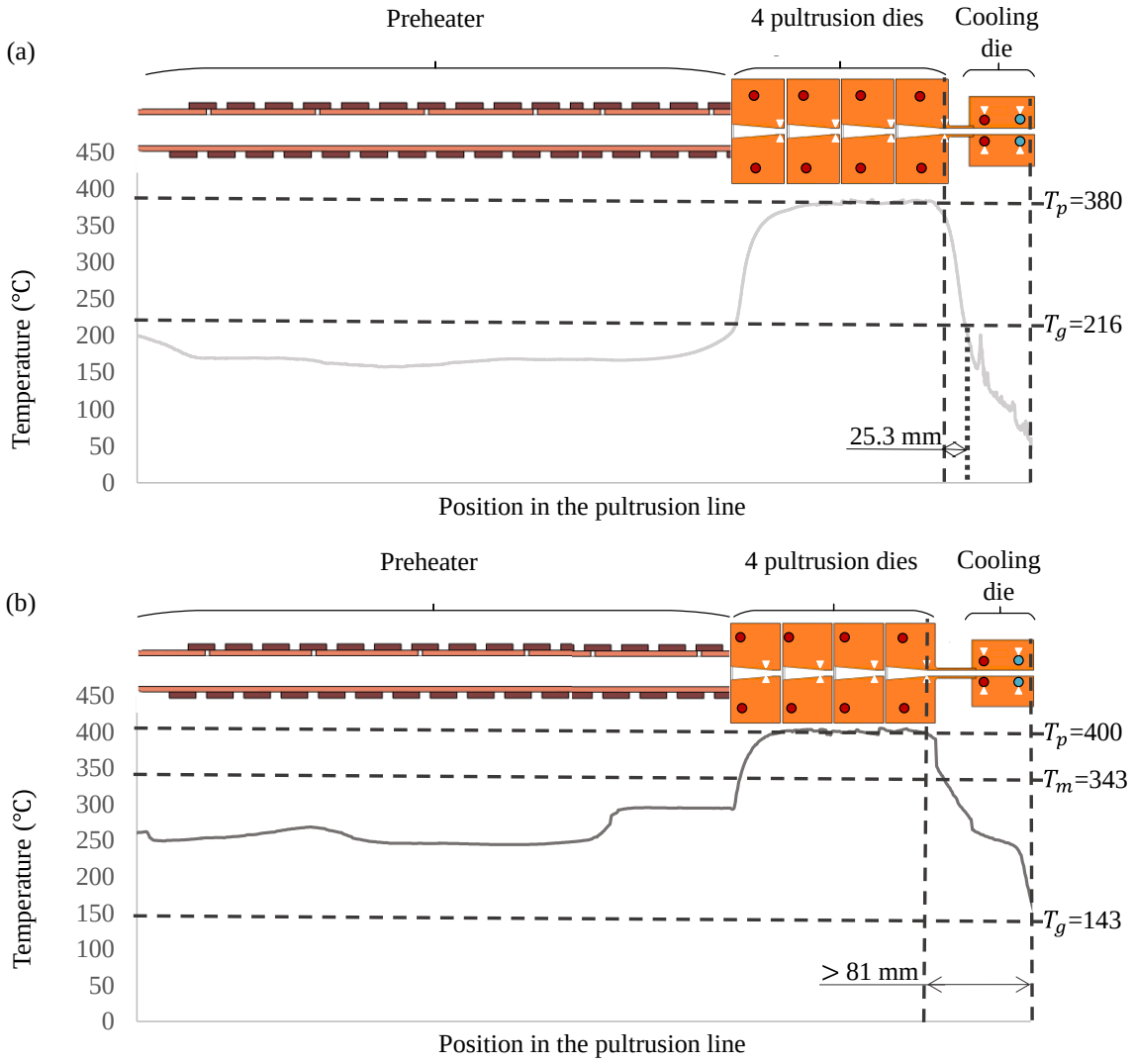

Figure 4.11: Temperature measurements taken during the steady-state pultrusion experiments. (a) The measured SCD of PEI-Steady was 25.3mm. (b) The measured SCDs of PEEK-Steady was above 81mm since the measure temperature was above $\boldsymbol{T_g}$ of 143°C at die exit. These values are similar to the SCDs of PEI-109 and PEEK-243 respectively.

Figure 4.12 shows the measured force (left axis) of the resulting 10 m pultrudates and the measured Ra (right axis) of PEI-Steady and PEEK-Steady samples. The force reading is shown as a continuous line with readings taken at every second. The measured forces appeared to be stable during the total duration of both experiments. This indicates that steady-state pultrusion conditions were reached. In addition, the measured forces were higher than the measured forces during the

single-die reprocessing experiments. The measured forces during PEI-Steady and PEEK-Steady averaged around 270 and 310 N respectively while the measured forces of PEI-109 and PEEK-243 both had values below 150 N. This is due to the direct processing of the commingled yarns in the steady-state experiments. This results in additional forces required to collimate the yarns from the creel to the entrance of the heating dies and to compact the fiber yarns into the dies' cavity [31]. The average Ra values of PEI-Steady and PEEK-Steady were 0.78 ±0.08 and 0.70 ±0.11 μm respectively. These values were slightly higher than the Ra values of PEI-109 and PEEK-243, 0.72 ± 0.11 and 0.56 ± 0.06 μm. However, these Ra values are considered equivalent when considering the standard deviation on the measurements.

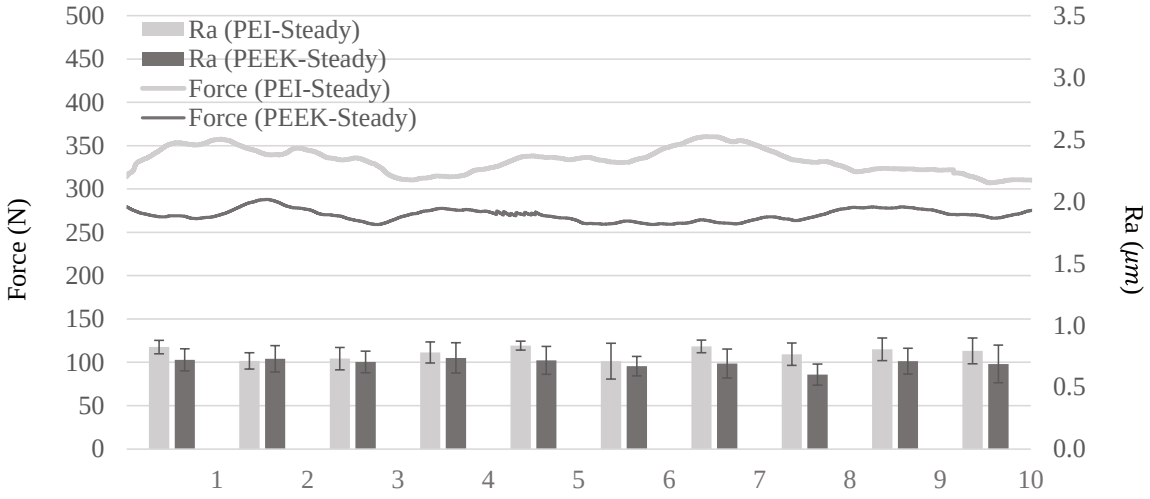

Figure 4.12: The measured force (Left axis) of the resulting 10 m pultrudates and the measured Ra of PEI-Steady and PEEK-Steady samples. The measured forces appeared to be stable throughout both PEI-Steady and PEEK-Steady experiments. The average Ra values of PEI-Steady and PEEK-Steady were 0.78 $\pm$0.08 and 0.70 $\pm$0.11 μm respectively.

Figure 4.13 presents the macroscopic photographs of a bundle of 1 m samples along with microscope images of the cross-sections of PEI-Steady and PEEK-Steady pultrudates. The macroscopic images (Figure 4.13 a),c) show a shiny appearance indicative of a high quality surface finish. The microscope images shown in Figure 4.13 b) and d) show fully impregnated pultrudates with circular cross sections. These findings indicate that the pultrudates produced in steady-state conditions achieved the same shape and consolidation quality as the single-die reprocessed

samples.

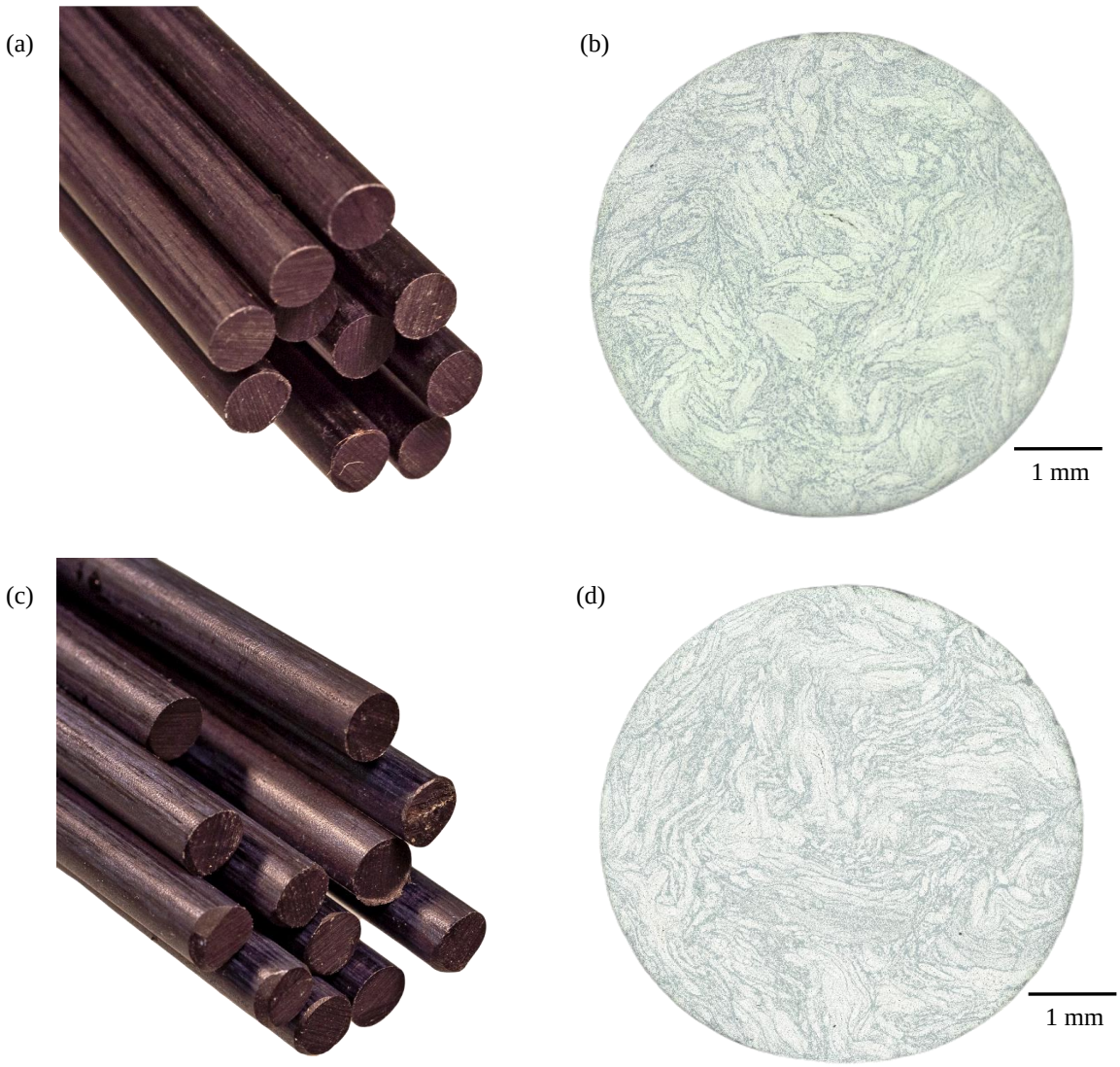

Figure 4.13: Macroscale photographs and cross-section microscope images of (a)-(b) PEI-Steady and (c)-(d) PEEK-Steady. Macroscale images show shiny pultrudates indicative of high-quality surface finish. Microscopic images are showing fully impregnated pultrudates having circular cross sections. PEI-Steady and PEEK-Steady achieved the same shape and consolidation quality as the reprocessed samples PEI-109 and PEEK-243, respectively.

4.4 Conclusion

This study introduced an efficient method to conduct cooling in TPC pultrusion. Pultrudates

were produced using the multi-die pultrusion system that was equipped with a proposed cooling system. The nominal void contents in the pultrudate were below 2%. The proposed cooling system was then used to study the effect of cooling temperatures on the thermal profile of the pultrudates. The cooling profiles resulted in different apparent sloughing at critical distances as well as different crystallization conditions for the semi-crystalline PEEK polymer. Microscopic images showed a direct correlation between the cooling temperature, the void content and the thermal deconsolidation. For C/PEI, thermal deconsolidation, a higher void content and a noticeable increase in pulling forces were observed when the cooling temperature was raised above T_g. Also, Ra results showed that rods with longer SCD had lower surface finish quality. PEI-109 resulted in rods with Ra value of $0.72 \pm 0.09\ \mu m$ whereas PEI-300 had the highest Ra number. For C/PEEK, the thermal deconsolidation and a higher void content were observed when cooling was set higher than T_m. In addition, a noticeable increase in pulling forces were observed when the cooling temperature was raised to$(\mathrm{T_g} + \mathrm{T_m})/2$ and above. Surface roughness (Ra) results showed that pultrudates with longer SCD had lower surface finish quality. However, PEEK-243 pultrudate had among the longest SCD while having the best surface finish quality (Ra = $0.56 \pm 0.06\ \mu m$) among all pultrudates, This is attributed to the selected cooling temperature of 243°C, which promoted fast crystallization of the PEEK polymer. To validate the findings from reprocessing experiments, two experiments were done in steady-state conditions using commingled tows. Pultrudates produced in steady-state conditions, PEI-Steady and PEEK-Steady, resulted in similar low Ra values and achieved the same shape and consolidation quality as the reprocessed samples PEI-109 and PEEK-243, respectively. Since the proposed cooling system was capable of controlling the temperature and producing rods with excellent surface-finish quality, this system will most definitely generate significant new opportunities for the use of thermoplastic pultrudates in many fields.

4.5 Acknowledgements

The authors would like to thank Felix Lessard, Bombardier Aerospace, Pultrusion Technique, Saudi Arabia's Saline Water Conversion Corporation and Ministry of Education (KSP12014087), NSERC (CRDPJ488387-15) and Prima Quebec (R10-009) for financing this research project.

CHAPTER 5 ARTICLE 2: EFFECT OF FLAX/PP PELLETS' MORPHOLOGY ON THE MECHANICAL PROPERTIES OF INJECTION-MOLDED PARTS

Nawaf Alsinani and Louis Laberge Lebel*

*LLL@polymtl.ca.

Advanced Composite and Fiber Structure laboratory (ACFSlab), Research Center for High Performance Polymer and Composite Systems (CREPEC), Department of Mechanical Engineering, Polytechnique Montréal, 2900 boul. Édouard-Montpetit, Campus of the University of Montreal, Montreal, H3T 1J4, Canada

This article was published in the Journal of Thermoplastic Composite Materials

Publication date: April 23, 2022

Abstract

Flax and polypropylene (PP) pultrudates of 4.76 mm in diameter were produced using a multi-die pultrusion system. The Flax content was 50 vol.%. Pultrusion conditions were varied to produce four porosity content between 4% and 22%. The pultrudates were pelletized into lengths of 6 and 15 mm, and injection-molded with pure PP to reduce the part Flax content to 25 wt.%. Results showed that well consolidated pultrudates, having porosities up to 8%, were more resilient to the pelletizing process such that the pellets remained structurally intact after the process. These pellets went smoothly through the hopper into the injection molding machine screw. Pellets with void content higher than 8% lost integrity during pelletizing leading to uniform mixing. Exposed fibers segregated from the polymer in the hopper leading to ununiform mixing. The highest mechanical properties improvement compared to pure PP was using 15 mm pellets that had a prorosity of 8%. The tensile modulus doubled at 4652 ± 113 MPa. The impact strength increased by almost five times at 10.5 ± 0.7 kJ/m^2. 15 mm pellets provided 1.7 times the impact strength of the 6 mm pellets. These improvement are attributed to low Flax fiber thermal degradation and improved fiber dispersion.

Keywords: Pultrusion; Flax; Thermoplastic; Long Fiber Thermoplastics; Injection

5.1 Introduction

Inorganic fibers and fillers such as glass fibers, talc and mica are widely used to reinforce the thermoplastic polymers in the in the automotive industry [1]. Yet, the production and disposal of such materials have an adverse impact on the environment. Due to rising environmental awareness, new environmental laws and regulations were introduced to help reduce the inorganic waste problem [2]. These new environmental laws and regulations are putting great pressure on automotive industry to replace some inorganic fillers with biodegradable alternatives. In fact, the U.S Department of Energy's Vehicle Technologies Office (VTO) introduced a multidimensional program to promote automotive Lightweight Materials (LM) to ensure energy security through renewables. VTO argued that the replacement of glass fibers with natural fibers will allow lighter parts to be used while increasing the percentage of renewables within the vehicle [72]. It is estimated that a 10% weight reduction could reduce fuel consumption by 6-8% [73] since lighter objects need less energy to get transported compared to heavier ones. Therefore, lighter materials provide an opportunity to improve vehicle fuel economy and mitigate greenhouse gas (GHG) emissions. In response, many auto-makers are increasing the use of natural fiber-reinforced composites. For example, Audi uses natural fiber-reinforced composites to produce boot liners, hat racks, seat backs, back door panels and spare tire-linings for their new cars. Like the automotive industry, many other industries such as medical and pharmaceutical, protective clothing, food packaging and hygiene clothing are finding more ways to utilize natural fiber reinforced composites for both structural and non-structural applications [74]. For example, Bcomp ltd. produces winter and summer sports equipment using only natural fiber-reinforced composites. GAF materials corp. uses natural fiber-reinforced PP to make composite deckings [74, 75].

Flax fibers are becoming more popular in industrial applications due to their low environmental impact and light weight. In comparison to other natural fibers, Flax fibers can be processed at higher temperatures due to its high cellulose content [10]. Natural fiber thermal degradation normally occurs when cellulose is exposed to a temperature range above 200°C. Lignin, on the other hand, starts to degrade when the temperature approaches 160°C. Flax fibers are made of low lignin content (2%) and comparatively high cellulose content (64%) [18]. This makes Flax more resistive to the thermal degradation compared to other natural fibers. In addition, Flax is also

preferred due to its higher tensile properties, which can be attributed to the high cellulose content as well. Flax fibers have the highest Young's modulus values amongst natural fibers, comparable to e-glass fibers [11]. Therefore, Flax-reinforced composites are a great choice for sustainable industrial applications.

There is normally very limited interaction between the hydrophilic fibers such as Flax fibers and hydrophobic matrices such as PP resulting in a reduced interfacial strength as well as increased moisture absorption. Different kinds of treatment can be used to improve the interaction including physical and chemical treatments [76, 77]. Of all chemical methods to improve the interaction in natural fiber composite, MAPP is recognized to be the most popular treatment. MAPP works by promoting better interfacial bonding through producing bonds between the fiber and the polymer. It has been proven to yield twice the strength as achieved when used with silane treatment [78].

Thermoplastic polymers have very high molten viscosity compared to thermoset polymers. This high viscosity makes it very difficult to impregnate fibers and mould the final part in a one-step process [79]. Thus, an intermediate form, in the form of bulk charge or pre-impregnated pellets, is introduced prior to the final part production which is normally done using compression or injection molding process. Fibre-reinforced thermoplastic composite materials are often categorized based on their fiber reinforcement lengths. For instance, long fibre-reinforced thermoplastics (LFT) are composite materials consisting of thermoplastic polymer and discontinuous reinforcement fibres whose length-to-diameter aspect ratio is larger than the critical aspect ratio above which fiber rupture is favored over fiber/matrix debonding [79]. LFTs offer superior mechanical properties compared to short fibre-reinforced thermoplastic (SFT) composites. LFT production has experienced fast growth in the last two decades. A market survey published in Jan 2017 projected that the LFT global market value will grow from USD 3.28 billion to USD 5.55 billion by 2022 [79]. Several thermoplastic polymers were utilized as LFT polymers including PP [80, 81], Polyamide 9 (PA6) [82],Polylactic acid (PLA) [83], Polymethylmethacrylate (PMMA) [84], and high density polyethylene (HDPE) [85].

The desire to reduce processing steps and shipping costs for LFT intermediate form resulted in the implementation of Direct LFT (D-LFT) in the 90's [79, 86]. The D-LFT works by combining the injection or compression molding station with an inline-compounding of fibers and polymers

[87, 88]. The polymer is fed into an extruder, often a twin screw extruder, where it is melted and mixed with fillers, pigments and additives in order to achieve a homogeneous molten mixture. It is then mixed with continuous fiber reinforcement strands. Glass fibers are typically used as reinforcements for such applications. This material is then extruded and cut into a charge, and then transferred to a cold mold where it is compressed into the desired size of the final component [89]. The polymer only passes through a single melt history. This minimizes thermal degradation and improves mechanical properties [90]. Additionally, this process can be used to produce both SFTs and LFTs [91]. Another LFT manufacturing technique is referred to as the direct strand deposition [92]. The direct strand deposition was developed to produce LFT charges that are placed into the mold for compression molding but using a single-screw extruder. However, this process completely depends on the single-screw plasticisation for both fiber dispersion and impregnation. Ren et al. [93] faced impregnation challenges when they directly mixed the dry fibers with PP in a single screw-extruder. They tested the effect of changing the fiber weight fraction from 10 to 40% on impregnation and dispersion levels. They observed that fiber length and dispersion decreased as fiber content increased. Fiber-to-fiber interactions were thought to increase with adding fiber content. Low impregnation was also observed at higher fiber content, and it was recommended to reduce the fiber weight fraction.

The adoption of the D-LFT process is costly. It was estimated that the adoption cost can be offset once the annual production volume is increased to 30,000 units and above [94]. In addition, the D-LFT process can be complicated to implement since it forces the part manufacturer to handle purchasing the dry fibers and the polymer at the same time. Offering ready-to-use LFT pellets gives part manufacturers the flexibility to choose the process that they wish to implement. It simply allows them to place the LFT pellets in the hopper for injection or bulk molding compound.

The second intermediate form, pellets, can be used to make SFTs and LFTs. SFT pellets are usually produced by extrusion compounding using short chopped fibers that are introduced into the extruder together along with the polymer. Commonly, 4 mm-long chopped fibers are used, and the fiber length is subsequently shortened to less than 0.5 mm in the pellet while passing through the extrusion screw [95]. Thus, due to the limitation of short fibers, SFT pellets add inadequate reinforcing capabilities to the final composite material. On the other hand, using LFT pellets was

proven to improve impact/stiffness as well as creep, fatigue and high temperature properties [96]. LFT pellets are often produced using the thermoplastic composites (TPC) pultrusion process. During the TPC pultrusion process, yarn precursors which contain the polymer and reinforcement fibers are wound into bobbins that are placed in a creel. The polymer and reinforcement fibers are then pulled together through a number of dies that are heated to liquefy the polymer fibers. In order to fully impregnate the reinforcement fibers, the yarns that enter the dies contain an excess of polymer fibers. This excess polymer, consequently, creates a backflow which helps raise the impregnation pressure [37, 54, 97, 98]. This technique does not damage the reinforcing fibers and the fibers typically remain quasi-continuous after they have been processed. The pultrudates are then set to cool off and are cut in pellets of desired length. The LFT fiber length is determined by the cut length of the pellets.

Vaidya et al. [99] produced 12 mm Glass/PP LFT pellets using a TPC pultrusion process. These pellets were blended with inorganic pigment-colored compound pellets in order to study the processing and performance of inorganic-pigmented colored LFTs in comparison with unpigmented LFTs. Their work proved that LFTs can be colored with inorganic pigments and still retain good mechanical properties. Batrus et al. [100] designed and fabricated E-glass/PP LFT bus seat using extrusion-compression molding. The LFT pellets were produced using a TPC pultrusion process. The LFT seat design acheived 43% weight savings and 18% total production cost savings over typical seats that contain a circumferential steel frame. Yet, these two research papers did not specify the pellets' void contents nor analyze the impact of LFT pellets' void contents on the mechanical properties of the final injected part. The TPC pultrusion conditions such as pulling speeds, die geometry and set temperatures were not reported. Furthermore, inorganic reinforcement fibers were used in both studies.

Hartness et al. [101] produced glass/PP LFT pellets using a TPC pultrusion process. The glass contents in the LFT pellets were varied between 10 and 70% by weight. It was observed that the TPC pultrusion process led to a high level of impregnation although the LFT pellets' void contents were not specified in their research. Several other researchers have implemented TPC pultrusion to produce LFT pellets as well. It was observed that the fibers attained high levels of impregnation with PP polymer using TPC pultrusion [102-104]. Additionally, LFT pellets can also be produced

by similar processes such as wire coating [105], solid state polymerization [106] and commingling [107].

Achieving low void contents in the pultrudates at relatively high pulling speeds using TPC pultrusion can be challenging as there seems to be a trade-off between increasing the pulling speed and decreasing the void contents due to the high molten viscosities of the thermoplastic polymers [28]. In fact, Lapointe et al. [108] observed a significant increase in void contents in C/PEEK pultrudates when the TPC pultrusion speed was increased from 50 to 100 mm/min. The void contents increased by over 85%. Wiedmer et al. [65] pultruded Carbon/Polymide-12 (C/PA-12) hybrid yarn using different pulling speeds. The void content tripled when the pulling speed increased from 100 to 400 mm/minute. Ghaedsharaf *el al.* [109] pultruded Carbon/Polyetherimide (C/PEI) biaxial braid which was made of commingled yarns. The void content significantly increased when the pulling speed was raised from 50 to 150 mm/minute. They hinted that the reason for the void increase was possibly due to the polymer flow time which became too short to fully penetrate the carbon fiber bundles when the pulling speed was raised to 150 mm/minute. Thus, all these findings indicated that increasing pulling speed, while keeping the same pultrusion tooling geometry, could lead to a significant increase in the void content.

There are very few published papers that studied the effect of intermediate forms on the performance of the end part of the Flax/PP composites [15, 110, 111]. Barkoula et al. [15] studied Flax/PP SFT and LFT pellets to be used for injection molding. They compared the reinforcing capabilities for both the SFT and LFT pellets using impact and tensile tests. Producing the Flax/PP pellets was done by an extruder for SFT pellets and by TPC pultrusion for the LFT pellets. They observed that the LFT pellets resulted in a significantly higher impact strength in the injection-molded parts. Yet, Barkoula et al. [15] did not discuss the influence of the LFT pellets' void contents on the manufacturability of injection molded parts.

Having a low void content requirement in LFT pellets may restrict the pulling speed of TPC pultrusion which may lead to limiting the use of LFT pellets in industrial applications. Thus, it is crucial to quantify the LFT pellets' void content that does not jeopardize the mechanical properties of the injected final parts. On the other hand, low void contents in the pultrudates may result in LFT pellets being structurally intact. In a previous study, Flax/PP LFT pellets having low void

contents using TPC pultrusion were produced [81]. The low-void LFT pellets were able to remain structurally intact during the pelletizing process and experienced a smooth injection molding process. However, the investigation was limited to well impregnated LFT pellets. To better understand the influence of the LFT pellets' void contents in injected molded parts, we produced pultrudates using four different void contents. These pultrudates were pelletized into two different lengths, 6 mm and 15 mm. The LFT pellets were then added, with pure PP pellets, into a master mixture before being added to the injection molding hopper to produce injection molded parts. Finally, the injected molded parts were characterized by tensile and Charpy impact tests to evaluate the mechanical strength. In the injection molded specimens, the fiber/polymer impregnation was characterized using scanning electron microscopy (SEM).

5.2 Experimental

5.2.1 Materials

Pure PP (Guangzhou Chemical Fiber Co.) in the fiber form (finess of 100 tex) and in the pellets form were used for the pultrusion and injection molding. The melting point of the PP was 166.5 ℃ as obtained by DSC at heating rate of 10 $℃/min$. Flax yarns (Safilin) having a size of 200 tex and a solid density of 1.53 g/cm^2 were used.

5.2.2 Flax thermal characterization

Thermogravimetric analyses (TGA) of Flax fibers were conducted (Q50, TA Instruments) with a temperature ramp-up of 2°C/min until 300°C under air atmosphere (40 mL/minute). However, during the TPC experiments, the total residence time at processing temperature of 220 °C is dependent of pultrusion speed. At low speed (50 mm/minute), Flax fibers spent 3.2 minutes inside the heating dies. While at the 250, 500 and 1000 mm/minute pultrusion experiments, Flax fibers spent 0.64, 0.32 and 0.16 minutes respectively. To better quantify the Flax degradation during the TPC pultrusion at different pultrusion speeds, TGA of Flax fibers was conducted by reproducing the thermal conditions during the pultrusion experiments. Three Flax samples of approximately 1g were dried for 48 hours at 60℃ before the TGA tests. All TGA experiments featured 40 mL/minute air flow. First, the Flax fibers were exposed to 100°C to reproduce the preheating stage, followed

by a thermal ramp at a 20 °C/minute to 220°C to reach the pultrusion dies' temperature. Finally, the Flax sample was exposed to an isothermal environment for 3.2 minutes, the same duration as the travel time in the pultrusion dies at 50 mm/min.

5.2.3 Pultrusion apparatus

Figure 5.1 (a) presents the schematic for the pultrusion system used in this study. The pultrusion apparatus contained a creel, a guide, a preheater, four heating dies, a cooling die, and a pulling system. The creel allowed for individual tension adjustment for each of the bobbins. The tension was set at 1 N per bobbin holding the reinforcement fibers. No tension was applied to the bobbins that were holding the polymer fibers. The preheater was a metallic tube, 300 mm-long and 16.2 mm in diameter, wrapped with a strip heater. (b) & (c) presents detailed dimensional description of the system. The final diameter decreases from die 1 to 4. All four heating dies had a 31.75 mm conical cavity tapered at 5° relative to the horizontal axis followed by a straight 6.35 mm (0.25 inch) cylindrical cavity. The diameter of each die's cylindrical exit was 5.13, 5.00, 4.90 and 4.76 mm respectively. The white triangles in Figure 5.1 denote the location of thermocouples in the heating dies. All heated dies (Die 1 to 4) were heated to 220°C. Additionally, the red circles represent the location of the heating cartridges whereas the blue circles represent the location of the air-cooling channels. A thin-walled tube was protruding from the last heated pultrusion die toward the cooling die. The tube length exposed to the air was 27.6 mm. The tube was inserted into a 3 mm-deep hole at the cooling die's inlet. The thickness of the thin wall was 1.59 mm in order to reduce the thermal interference between the fourth heating die and the cooling die. The cooling die was set to 60°C. The pultrusion speed was controlled by a puller throughout the process. The Flax fiber volume content was 50% by using 68 Flax yarns. The speeds and filling ratios (R_f) were varied to produce the LFT pellets at various void contents. The R_f is calculated as:

$$R_f = \frac{A_{in}}{A_{Die}}, \text{Eq. 1}$$

Where A_{in} is the material area entering the die and A_{Die} is the die exit area. The nominal R_f in the first die uses the Flax and PP material areas pulled from the creel. These areas are obtained by dividing the Flax and PP yarn finenesses (in Tex, or g/1000m) by their corresponding densities (in g/cc). The other dies nominal R_f are calculated using the same Flax area as in the first die. For the

PP area, in case of under filling ($R_f < 100\%$), all the PP is assumed to follow the pultrudate. In case of over filling ($R_f > 100\%$), the PP area was considered to be the non-Flax area from the previous die exit area. Table 5.1 shows the used filling ratios, pultrusion speeds and set temperatures to produce LFT pellets having target void contents of 4%, 8%, 15% and 22%. To obtain void contents of 4% and 8% at pultrusion speeds of 50 mm/min and 250 mm/min, all four dies had $R_f > 100\%$ by using 99 PP yarns. To obtain void contents of 15% and 22% at higher speeds of 500 mm/min and 1000 mm/min, only 74 PP yarns were mounted on the creel. This led to the first three dies having a $R_f < 100\%$. Only the last die was in an overfilling situation at $R_f = 105\%$.

Table 5.1: Filling ratios, pultrusion speeds and set temperatures used to produce pultrudates with different void contents.

Target Void Content	**Pultrusion Speed (mm/min)**	**Die Filling Ratios**			
		Die 1	**Die 2**	**Die 3**	**Die 4**
4	50	106%	105%	104%	106%
8	250	106%	105%	104%	106%
15	500	90%	95%	99%	105%
22	1000	90%	95%	99%	105%

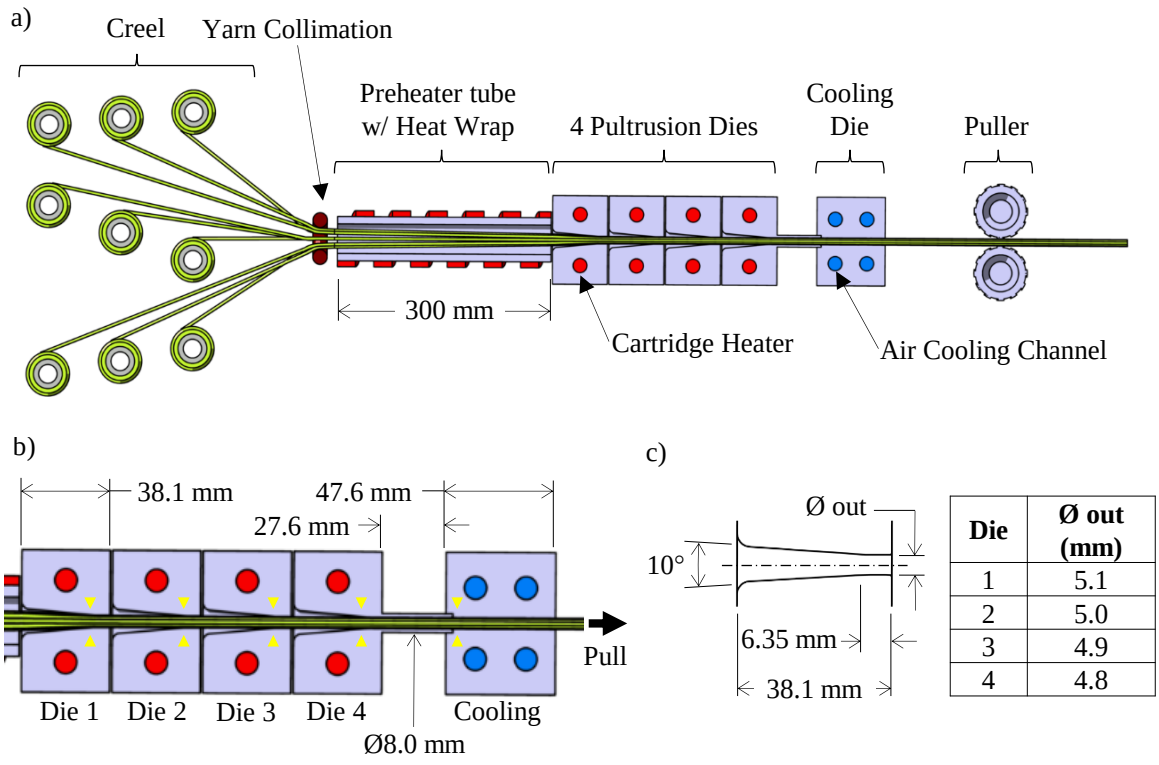

Die	Ø out (mm)
1	5.1
2	5.0
3	4.9
4	4.8

Figure 5.1: Schematic of the multi-die pultrusion system used in this study. The pultrusion system includes a creel, a pre-heater, four pultrusion dies, a thin-walled tube, a cooling die, a puller and a cutting saw (not shown). (b) & (c) dimensions of the system. The final diamter decreases from die 1 to 4 while the tapered angle of the die was constant in all dies at 10°.

5.2.4 Morphological characterization

The pultruded rods impregnation morphology was characterized by a microscopic observation of the cross-section. An injected coupon was polished and then analyzed using a digital microscope; (Keyence, VHX 7000). Full ring was selected for lighting type. Photos of 150 and 300 X magnification were taken of the injected coupon. Void content was measured according to ASTM2734-09 Method C. The fracture surfaces of specimens were examined in a SEM (TM300, Hitachi).

5.2.5 Injection molding

After production, Flax/PP pultrudates were cut into 6 and 15 mm long pellets using a manual

paper trimmer (Model #118, Dahle). The LFT pellets were dried oven-dried for 24 h at 60 ℃ right before the injection molding process. The Flax/PP LFT pellets were then blended with pure PP pellets in order to lower the fiber weight fraction. The mixture contained 60 wt. % PP pellets and 40 wt. % PP Flax PP LFT pellets. According to this mix, the Flax weight content in the injected coupons was 25%. The mixture was then added directly to the hopper of the injection molding machine (SE50S, Sumitomo).

Table 5.2 displays the process set points for compounding Flax/PP in the injection molding machine. The maximum temperature in the injection molding process was kept around 200 ℃ in order to minimize the degradation of the Flax fibers. The injection velocity used for testing was 65 mm/s. The naming format follows the order: void content-LFT length.

Table 5.3 displays the void contents, set points, and LFT pellets length for the injection molding experiments. Each injection was repeated three times. One coupon was randomly selected from each injection for mechanical testing.

Table 5.2: Injection molding machine process set points for compounding Flax/PP.

Zone	**1**	**2**	**3**	**4**	**Cooling**
Temperature	200 ℃	200 ℃	200 ℃	200 ℃	25 ℃
Inject. velocity	65 mm/s				
Cooling time	30 s				

Table 5.3: Void contents set points, LFT pellets' length and injection speed for the injection molding experiments.

Experiment	**Void content (%)**	**LFT length (mm)**
4%-6 mm	4	6
4%-15 mm	4	15
8%-6 mm	8	6
8%-15 mm	8	15
15%-6 mm	15	6
15%-15 mm	15	15
22%-6 mm	22	6
22%-15 mm	22	15

5.2.6 Mechanical Characterization

Tensile tests were performed according to ASTM D638-44 in a universal testing machine (Model, Brand). The size of the tensile specimen was 165 x 13 x 19 mm according to ASTM D638. The Charpy impact test specimens were tested according to ASTM D6100.

5.3 Results and discussions

5.3.1 Thermogravimetric analysis (TGA) of the Flax fiber

Table 5.2 shows a typical TGA plot of Flax fibres during a temperature ramp-up at 2°C/min under air atmosphere. This figure shows the Flax mass loss and mass rate of change with respect to temperature. As the temperature rises, and before reaching 200°C, the Flax mass decreases slightly due to water evaporation. Beyond 200°C, the Flax weight continues to decrease at a much higher rate. Results from this test are consistent with previous TGA of Flax fibre found in literature [112, 113]: as thermal degradation is triggered above 200°C, mass loss starts to increase. This finding implies that the thermal degradation during the pultrusion experiments happens inside the heating die at which the Flax is exposed to a temperature above 200 °C. To verify if substantial degradation could occur in the time span of manufacturing, TGA experiments were conducted. The TGA experiments resembled the thermal conditions for all pultrusion experiments.

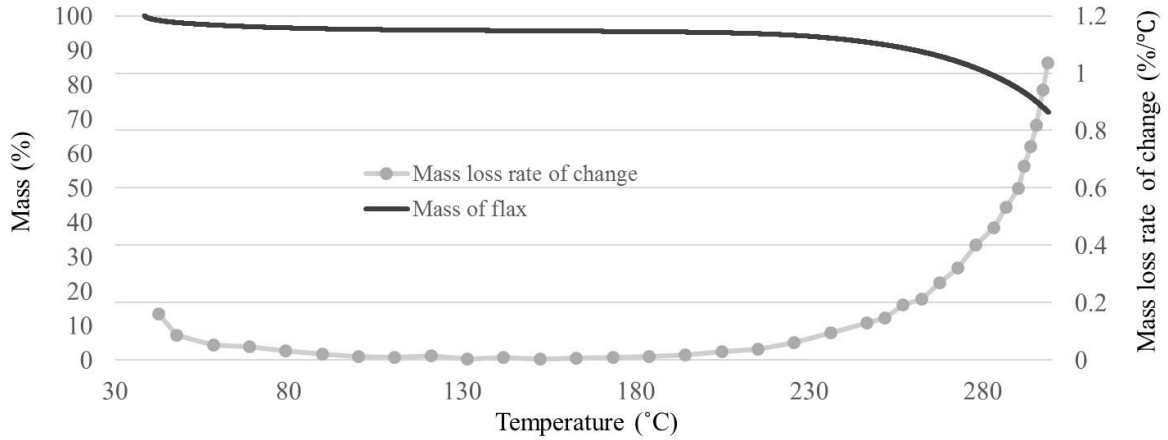

Figure 5.2: TGA of the Flax fiber at what rate and what air flow. The thermal degradation started at 200℃.

Figure 5.3 (a) shows the temperature evolution and mass loss monitored using Flax fibre weight percentage. Three samples were used to reproduce Flax thermal history in the pultrusion heating die. In the first 30 minutes, the temperature was set at 100 ℃ in order to remove mass associated to the humidity content. This drying was followed by a thermal ramp-up of 20 °C/minute to 220°C, and finally an isothermal environment for 3.2 minutes.

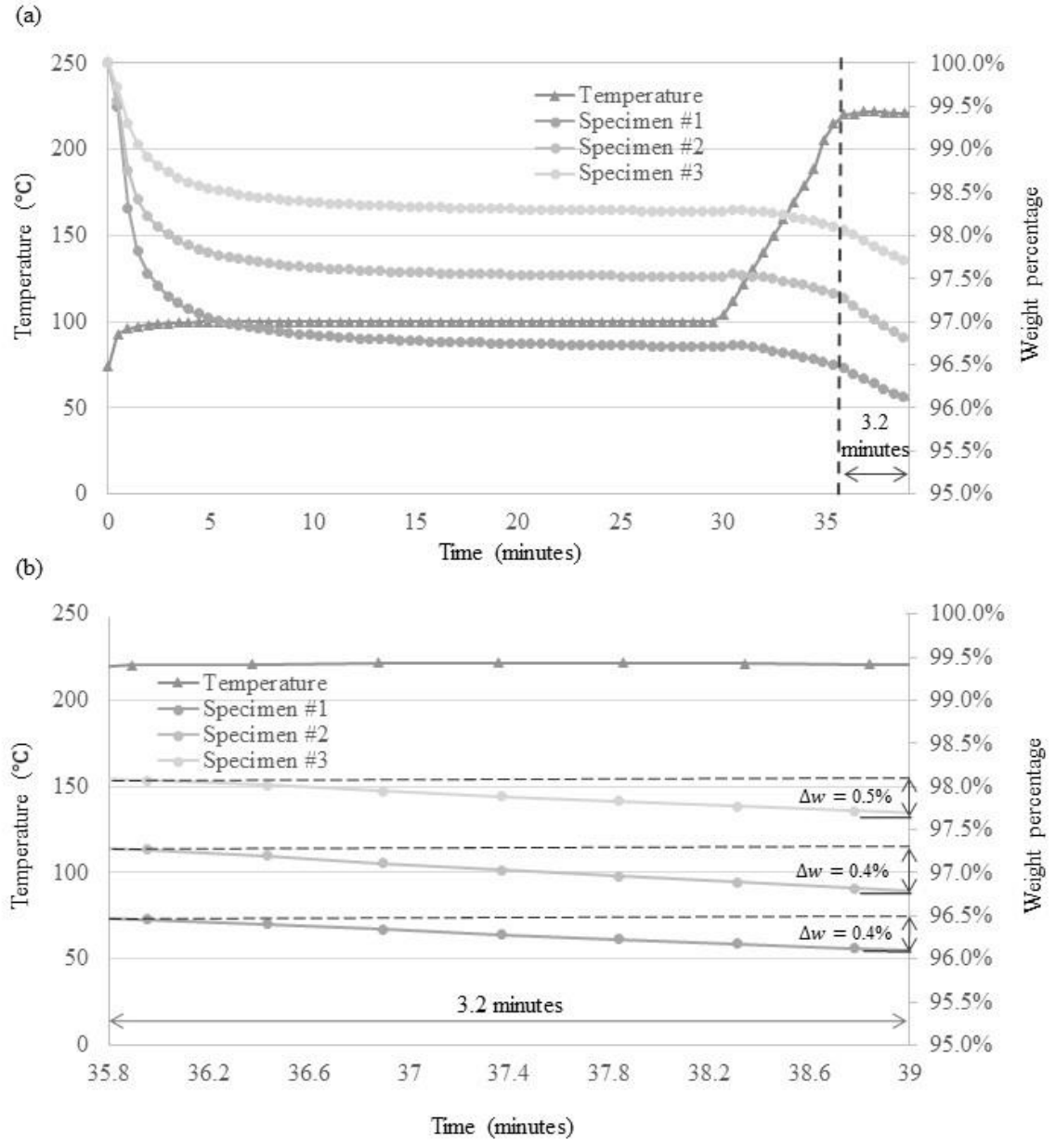

Figure 5.3 (b) shows the last 3.2 minutes of the TGA experiment. This time interval corresponds to the time that the Flax fiber spent inside the heating dies during pultrusion at 50 mm/minute. Table 5.4 and

Figure 5.3 (b) show the weight percentage change that occurred after exposing Flax fiber to 220℃ for a certain number of minutes. Pultrusion experiments that were done at low speeds resulted in a larger mass loss compared to the other higher speeds experiments. The LFT pellets produced at 50, 250, 500 and 1000 mm/minute experienced a weight loss of 0.42%±0.029%, 0.093%±0.006%, 0.036%±0.002% and 0.016%±0.001 %. The LFT pellets produced at the lowest pulling speed were significantly more degraded than the other speeds. The LFT pellets produced at 250, 500, 1000 mm/minute were only 22%, 9% and 4% degraded compared to the LFT pellets produced at 50 mm/minute. This calculation was done by dividing the resulting weight loss of the pellets produced at each pulling speed by weight loss of the pellets produced at 50 mm/minute. This finding indicates that Flax fibers in the LFT pellets that had the lowest void content were more degraded compared to the other LFT pellets.

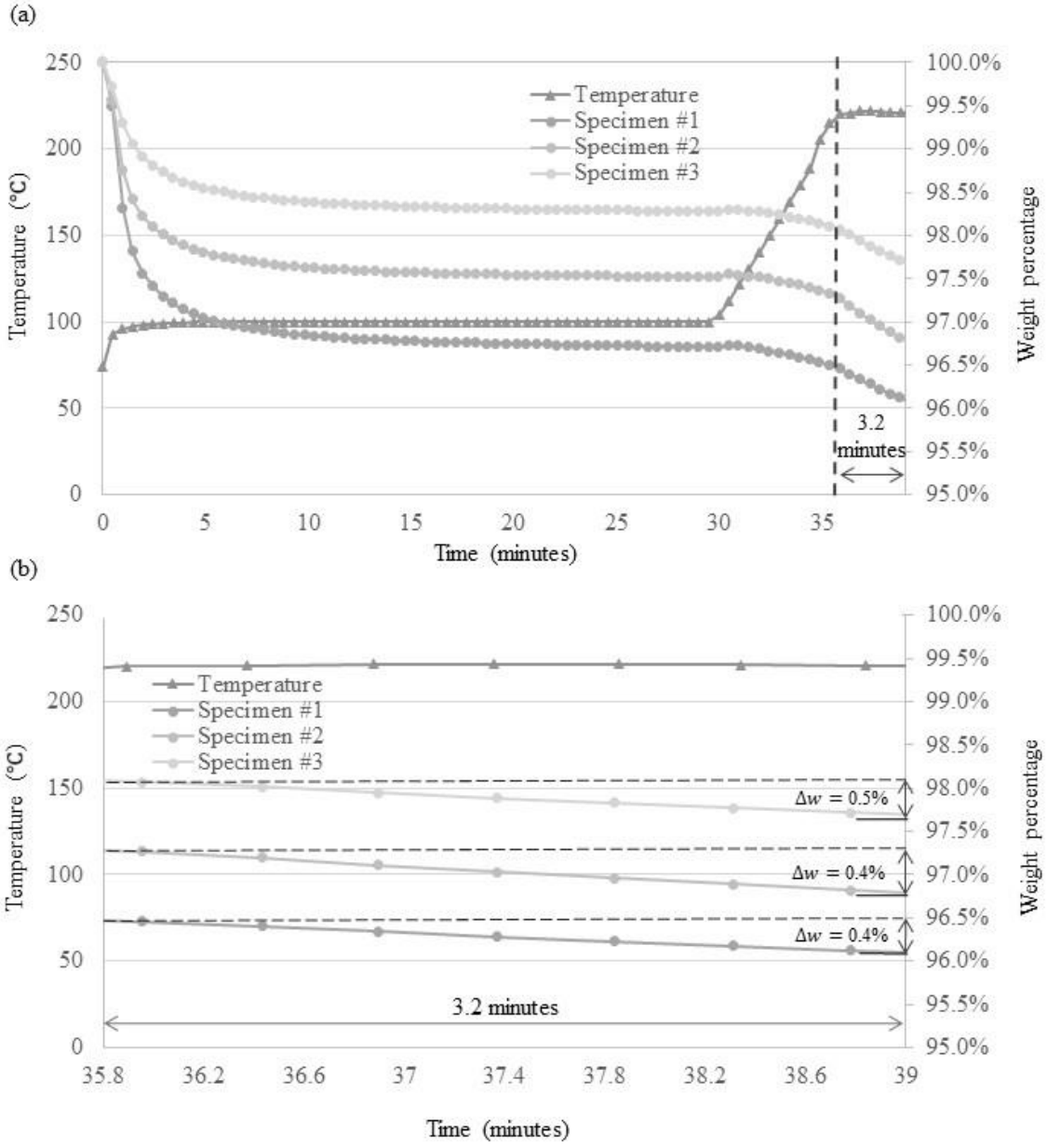

Figure 5.3: (a) TGA of Flax fiber. Three samples were used to reproduce Flax thermal history in the pultrusion heating die. (b) The last 3.2 minutes of the TGA expierment. This time interval corrosponds to the time that Flax fiber spent inside the heating dies during pultrusion at 50 mm/minute.

Table 5.4: Weight percentage change that occurred after exposing Flax fiber to 220℃.

Pult. Speed	**50 mm/min**	**250 mm/min**	**500 mm/min**	**1000 mm/m**
Exposure time (min)	3.2	0.64	0.32	0.16
Weight change	-0.420±**0.029**%	-0.093±**0.006**%	-0.036±**0.002**%	-0.016±0.001%

5.3.2 Pultrudate consolidation

The pultrusion of Flax/PP experiments were conducted without any fiber breakage event. Figure 5.4 shows cross sections with respect to the pultrusion process speed. Figure 5.4 (a) and (b) show cross-section images of LFT pellets produced at 50 and 250 mm/minute respectively. The cross-section images show round shapes with very few voids. The edges do not look damaged and the polymer had fully melted during the pultrusion process. Additionally, the two top insets show that the polymer fibers located at the center of the rod fully melted during the pultrusion process and impregnated the Flax fiber even at the centre, which is the last place in the pultrudate to melt.

Figure 5.4 (c) shows a cross-section image of LFT pellets produced at 500 mm/minute. The cross-section image shows less of a round shape with some voids. Additionally, the inset shows that the polymer fibers located at the center of the rod did not fully melt during the pultrusion process. However, the middle inset shows one Flax fiber inside an area which seems to be fully impregnated near the outer surface. This finding was expected since the outer surface is heated first during pultrusion. Figure 5.4 (d) shows a cross-section image of LFT pellets produced at 1000 mm/minute. The cross-section image shows an arbitrary shape with a significant amount of void. Additionally, the polymer did not fully melt during the pultrusion process. The arbitrary shape is attributed to the lack of Flax fiber wetting by the PP polymer. Poor load transfer between the two phases resulted in a deconsolidation state and difficulty to retain the circular shape. Moreover, similarly to the LFT pellets produced at 500 mm/minute, the middle-enlarged view close to the rod edge also shows a Flax fiber inside an area where there seems to be full impregnation near the outer surface. Obviously, increasing the pulling speed results in a reduction of the exposure duration at elevated temperatures. The cross-section images in Figure 4 clearly indicate that this short exposure duration reduces the time that the polymer is in a melted stated and able to flow. For 500 mm/min

and 1000 mm/min, that exposure was not long enough to melt the polymer at the center of the pultrudate.

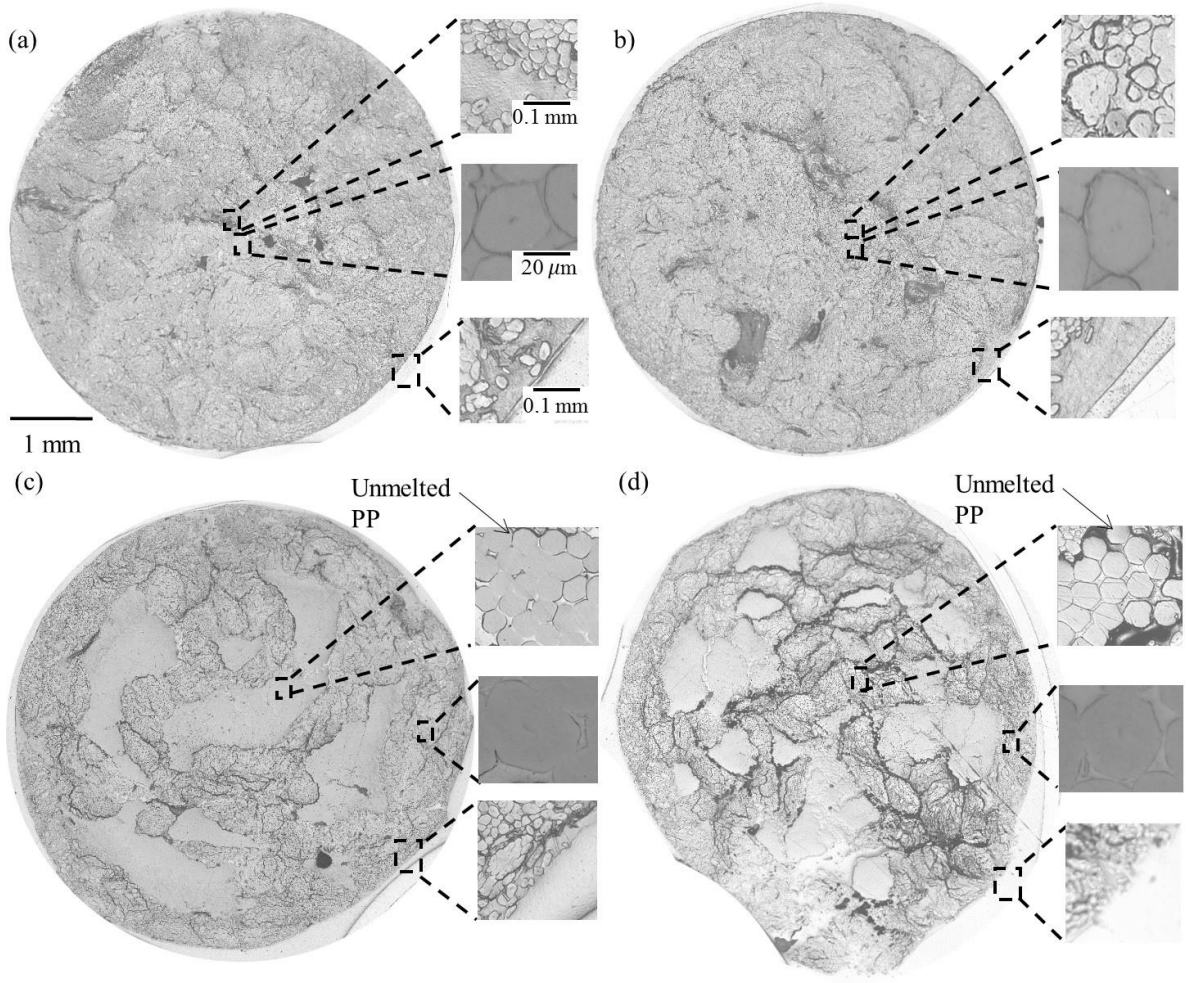

Figure 5.4: Microscopoc image for LFT pellets produced at: (a) 50 mm/minute. (b) 250 mm/minute. (c) 500 mm/minute. (d) 1000 mm/minute. LFT pellets produced at 500 mm/minute and above had un-melted PP fiber since the processing tempeture did not reach the core of the pultrudates at the heating dies. The scale bars in all images follow the same format as in (a).

Table 5.5 shows pultruded rods' measured porosities. The void content characterization indicated that 50 mm/min led to a 4% void content, 250 mm/min to an 8% void content, 500 mm/min to a 15% void, and 1000 mm/min led to the highest void content of 22%. As expected, higher pultrusion speed led to low impregnation quality. This is attributed to two factors. First, as seen in the microscopic images at high speed, the temperature within the pultrudate was not reached

leading to un-melted polymer regions. Second, at high speed, the time at which the polymer was under pressure in the conical regions of the dies was short, which led to a shorter impregnation time. LFT pellets produced at 500 mm/minute and above had un-melted PP fiber since the processing temperature did not reach the core of the pultrudates at the heating dies.

Table 5.5: Pultruded measured porosities.

Target Void Content	Pultrusion Speed (mm/min)	Measured Void content
4	50	4.3 $\pm$ 1.0%
8	250	8.4 $\pm$ 1.2%
15	500	15.1 $\pm$ 2.5%
22	1000	22.4 $\pm$ 2.8%

5.3.3 Pelletizing quality

These pultrudates were then cut into two different lengths; 6 and 15 mm. Figure 5.5 shows the appearance of LFT pellets cut at 6 and 15 mm for the four void contents, i.e. 4%, 8%, 15% and 22%. The top four images represent the 6 mm LFT pellets and the lower four images represent the 15 mm LFT pellets. Figure 5.5 (a) and (b) represent the LFT pellets with the lowest void content which was measured to be 4.3 $\pm$ 1.0%. The LFT pellets with the two lengths look structurally intact. The pelletizing process did not seem to significantly damage the LFT pellets. This is attributed to the impregnation quality of the rod indicated by low void content. Figure 5.5 (c) and (d) represent the LFT pellets which had a slightly higher void content, which was measured to be 8.4 $\pm$ 1.2%. Yet, the LFT pellets still look structurally intact. The increase in void content did not seem to cause any damage to the LFT pellets. Figure 5.5 (e) and (f) present the LFT pellets which had a higher void content and was measured to be 15.1 $\pm$ 2.5%. Here the LFT pellets seem to be damaged from the pelletizing process. In fact, some of the 6 mm LFT pellets have lost their cylindrical shape. Others cracked along their length and opened through their center. The 15 mm length LFT pellets at the same 15% void content have also lost their cylindrical shape. Very few were cracked and opened. This indicates that the 6 mm LFT pellets might be more prone to damage than the 15 mm LFT pellets at such void content. Figure 5.5 (g) and (h) represent the LFT pellets which had the highest void content, which was measured to be 22.4 $\pm$ 2.8%. Here most LFT pellets appeared damaged from the pelletizing process, for both LFT lengths. The damage is again a

rupture along the length of the pellet, opening it to expose its center. Moreover, un-melted PP fibers at the center of the cracked and opened pellets were observed. This confirms that high pultrusion speed prevented the core of the pultrudate to reach melting temperature. The damage during the pelletizing process is attributed to the high void content that reduces the transverse strength of the pultrudate. This is combined with the fact that un-melted fibers cannot provide transverse structural integrity to the pellet since they cannot bond the Flax fibers together. Finally, it must be noted that the pelletizing was done using a hand activated paper trimmer. The cutting action of the moving knife in such device is relatively gentle compared to industrialized pelletizers. Therefore, it is suspected that poorly impregnated pultrudate will not lead to repeatable pellet morphologies when using industrial pelletizers.

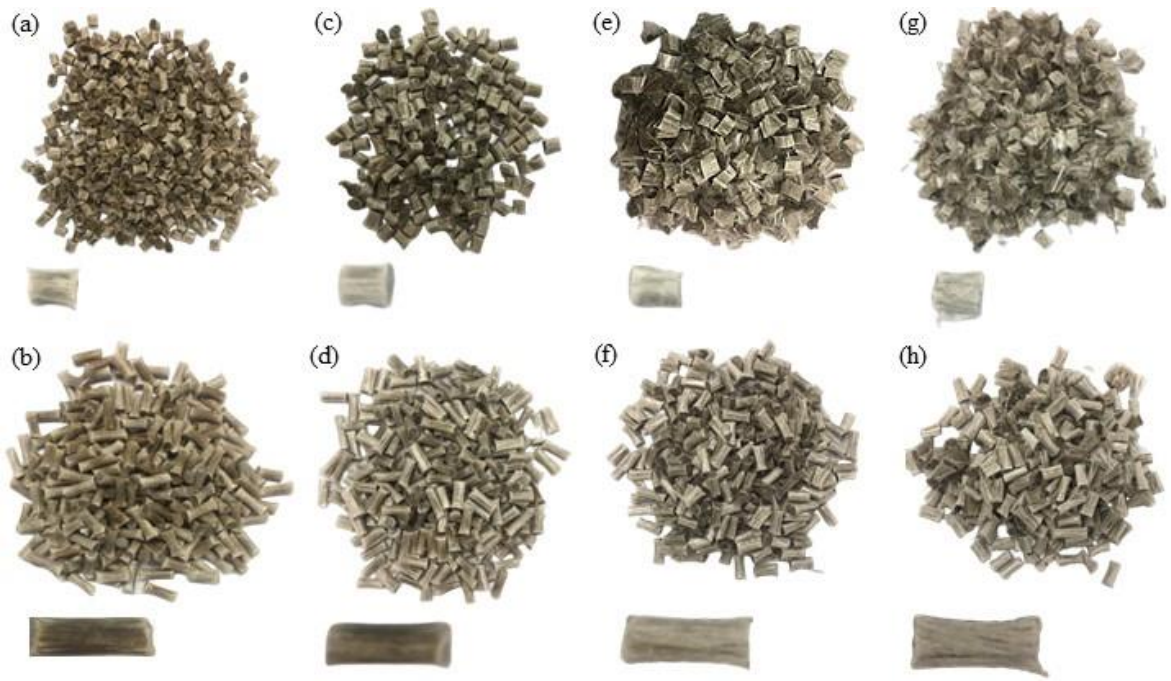

Figure 5.5: LFT pellets obtained with two different lengths (6 mm and 15 mm) and four different void contents. The top four images represent the 6 mm LFT pellets and the lower four images represent the 15m LFT Pellets. (a) & (b) 4%, (c) & (d) %8, (e) & (f) 15% and (g) & (h) 22% void content. Pelletizing pultrudates with void contents above 8% seems to result in cracked and opened pellets.

5.3.4 Observation of the manufacturability of the injection process

During injection molding, the LFT pellets with void content of 4% and 8% went smoothly through the hopper and the screw of the injection molding machine without any manual intervention as seen in a supplementary video, which can be viewed at https://youtu.be/0kOILBqbq0U. The remaining LFT pellets with higher void contents, 15% and 22%, required a manual intervention by using a plastic stick to push the mixture down toward the screw (see video above). Figure 5.6 shows images of the 15%-6mm master mixture. The broken LFT pellets resulted in a tangled fiber cluster which did not pass down smoothly though the hopper. The pure PP pellets went down smoothly carried by their own weight, but the tangled fiber cluster needed a manual intervention, using a pushing tool, to go down towards the screw of the injection molding machine. Without the manual intervention, the tangled fiber cluster would get larger and only the pure PP pellets would pass towards the screw. The high void LFT pellets were observed to bend and entangle with each other forming fiber clusters, obstructing uniform mixing. The diameter of the clusters became larger than the screw inlet, which blocked them from reaching the injection molding screw.

Figure 5.6 (a) shows the dog-bone coupons after the injection molding. Specimens made with pure PP and with Flax/PP LFT pellets . The pure PP dog-bone coupons were fully transparent. All Flax/PP dog-bone coupons had very similar appearances. The dog-bone coupons made out of the high void LFT pellets led to the same injected coupons' appearance, being opaque and a dark brown color. The fiber distribution in the dog-bone coupons appeared to be even and randomly oriented. However, there were some areas in the dog-bone coupons that were a light brown colour. These areas are attributed to bundles of less impregnated Flax fibers. Those bundles are not favoured since they indicate inefficient integration between the polymer and the fiber. Yet, this is a typical appearance for biocomposites produced using LFT pellets and injection molding. According to Chaitanya et al. [114] it is typical that the injection molding process causes the long fibers to bend and twist during processing, leading to the formation of fiber clusters within the produced biocomposites. Figure 5.6 (b) Microscopic images of the injected coupons produced using LFTs pellets having 22% void content; the highest void content. No void can be observed in the injected copouns. The white lines are traces of Flax fibers pullouts which was by the polishing process and

the low chemical interaction between Flax fibers and PP. This finding indicates that irrespective of the LFT void content, the injection molded coupons did not have any voids.

Figure 5.6: Images of the master mixture in the hopper. Master mixture of the 15%-6mm in the hopper as the mixture is going down some. Some LFT pellets broke on their way down.

Figure 5.7 (b) shows dog-bone coupons made with Flax/PP LFT pellets. All Flax/PP dog-bone coupons had very similar appearances. The dog-bone coupons made out of the high void LFT pellets led to the same injected coupons' appearance, being opaque and a dark brown color. The fiber distribution in the dog-bone coupons appeared to be even and randomly oriented. However, there were some areas in the dog-bone coupons that were a light brown colour. These areas are attributed to bundles of less impregnated Flax fibers. Those bundles are not favoured since they indicate inefficient integration between the polymer and the fiber. Yet, this is a typical appearance for biocomposites produced using LFT pellets and injection molding. According to Chaitanya et al. [114] it is typical that the injection molding process causes the long fibers to bend and twist during processing, leading to the formation of fiber clusters within the produced biocomposites.

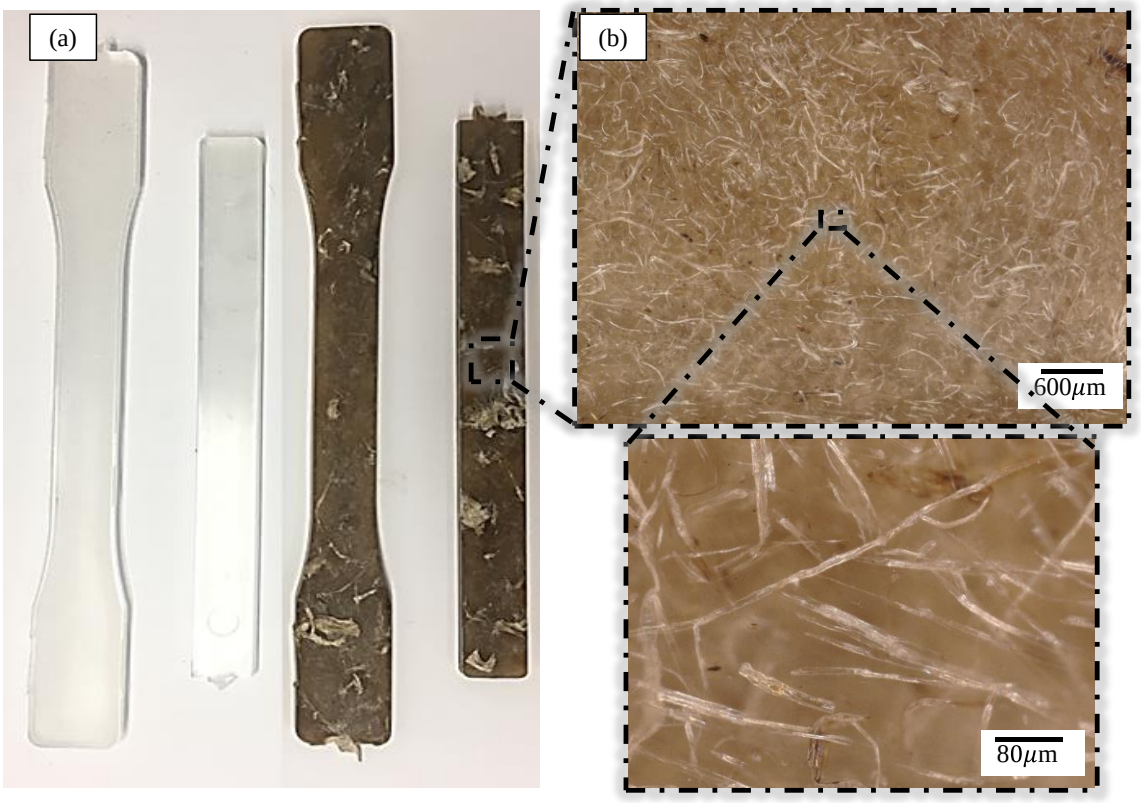

Figure 5.7: The dog bones post-injection. (a) Pure PP and Flax/PP. (b) Microscopic images of the injected coupons produced using LFT pellets having 22% void content. No void can be observed in the injected copouns. The white lines are traces of Flax fibers pullouts which was caused by the polishing process and the low chemical interaction between Flax fibers and PP.

5.3.5 Mechanical properties of the injected parts

Figure 5.8 presents the impact strength of the injection molded parts as function of void contents and LFT lengths. The specimens were made with (a) 6 mm and (b) 15 mm LFT pellets. The quasi-continuous LFT pellets resulted in an overall increase in impact strength. The pure PP injection molded parts had an impact of 2 kJ/m^2. All the other injection molded parts had higher impact strength than the pure PP. The LFT pellets with lowest void content, 4%-6 mm and 4%-15 mm, resulted in an impact strength of 5367 $\pm$ 218 and 7469 $\pm$ 551 J/m^2 respectively. Here, the 15 mm LFT size caused a 40% improvement in the impact strength. The LFT pellets with the second lowest void content, 8%-6 mm and 8%-15 mm, resulted in an impact strength of 6173 $\pm$ 213 and

10,515 $\pm$ 730 respectively. Here also, the 15 mm LFT size caused a significant improvement in the impact strength. In fact, specimen 8%-15 mm had the highest impact strength value compared to all other specimens. This value is almost five times (4.6x) as high as the pure PP impact strength. Considering only the 15 mm LFT pellets, those with around 8% void content resulted in coupons with higher impact strengths than the coupons made using the 4%-15mm. The LFT pellets with 4% void content were produced using a much lower pultrusion speed of 50 mm/minute. As mentioned above in section 3.1, the LFT pellets with 4% void content experienced higher levels of thermal degradation which possibly lowered the impact strength of the injection molded specimens. On the other hand, LFT pellets with around 8% void contents were produced at a significantly higher speed, 250 mm/min and thus had experienced less thermal degradation.

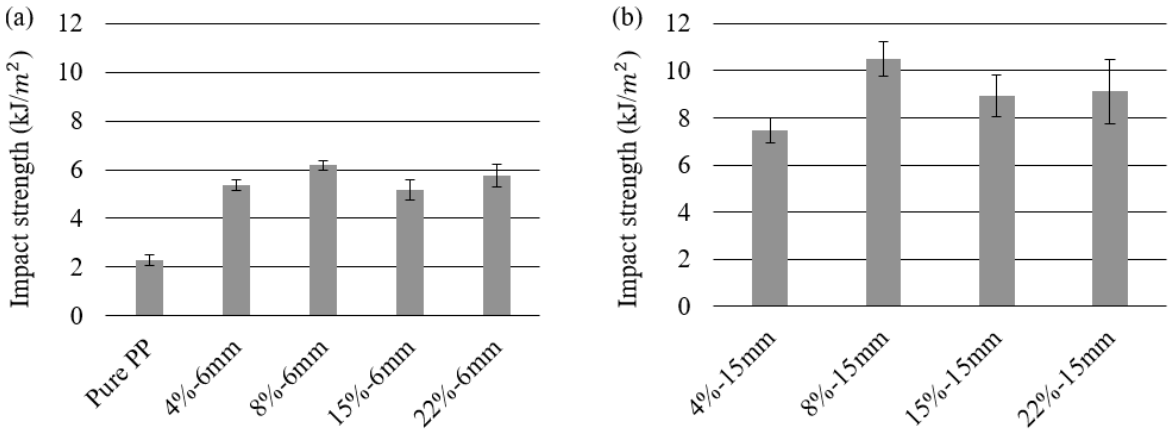

Figure 5.8: the impact strength of the injection molded parts as function of void content and LFT length. (a) specimens made with 6 mm LFT pellets and (b) specimens made with 15 mm LFT pellets.

Overall, the impact strengths for the 15% and 22% void contents were very comparable to the specimens produced with lower void content LFT pellets. However, the specimens produced using high void content LFT pellets required manual intervention during the injection molding process. Thus, the manual intervention was mostly responsible for improving the mixing quality in the hopper of the injection molding machine. In addition, the specimens produced using LFT pellets with having higher void content had wider standard deviations. This high standard deviation occurred possibly due to the inconsistent mixing during the injection molding experiments.

Figure 5.9 presents the tensile properties of injection molded parts as a function void content

and LFT length; (a) presents the modulus strength for 6 mm and (b) for the 15 mm LFT. It should be noted that in all cases the addition of Flax fibers led to an increase in stiffness compared to the pure PP sample. The 8%-15 mm specimens had the highest tensile modulus average of 4652 ± 113 MPa, a value which was more than twice as high as the pure PP tensile modulus of 1817 ± 106 MPa. For the specimens made using shorter pellets, shown in Figure 5.9 (a), the modulus slightly increases between specimen 4%-6mm to 8%-6mm, then slightly increases again to 15%-6mm and then stabilizing at approximately the same value. However, the difference in modulus values between 8%-6mm, 15%-6mm and 22%-6mm seems insignificant, and the pooled average modulus of the three conditions is 3764 ±192 MPa. This indicates that the fiber content and orientation is similar in all cases. Furthermore, the fiber degradation for specimen 4%-6mm was the highest and specimen 8%-6mm was the second highest. As seen in Table 5.4 , the 4% void content LFT pellets, which were produced at 50 mm/minute, experienced significantly higher thermal degradation. This explains the lowest modulus measured for 4% void content LFT pellet injected coupons.

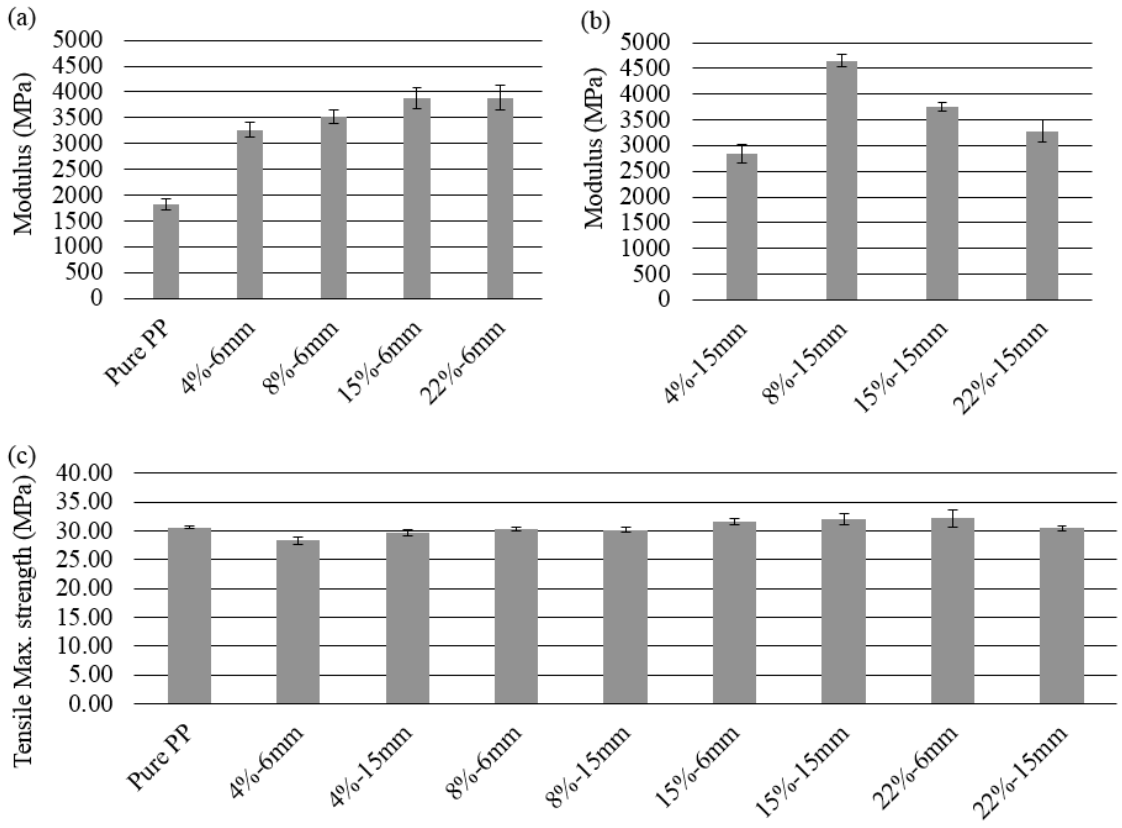

Figure 5.9: (a) and (b) The tensile modulus of injection molded parts as a function void content and LFT length. (c) the maximum tensile strength of the injection molded parts as a function void content and LFT length. No differnce can be observed. This finding indicates that poor bonding between the Flax fibers and the PP polymer.

For the longer pellets shown in Figure 5.9 (b), the 8%-15mm had the highest tensile modulus average of 4652 $\pm$ 113 MPa. The difference observed with the 4%-15 mm pellets is striking. The modulus value of the 4%-15mm pellets is 2837 $\pm$ 182 MPa, that is, 39% lower than the 8%-15 pellets. This difference is attributed to the thermal degradation due to longer thermal exposure during pultrusion. This may have weakened the Flax fibers and resulted in shortening during injection molding. Further studies are needed to verify this explanation. The lower modulus values for 15%-15mm and 22%-15mm are attributed to the lower load transfer caused by the bundling and improper mixing of dry Flax fibers during injection molding. Thus, the inadequate Flax fiber distribution was likely the cause behind the drop in modulus.

In comparing Figure 5.9 (a) and (b), it is observed that, except for the 8%-15 mm, the coupons made using shorter Flax fibers resulted in a higher tensile modulus than the longer Flax fiber reinforced biocomposites. This is counter-intuitive since longer fibers provide higher surface for stress transfer, which results in higher modulus. The 15%-15mm and 22%-15 mm modulus values, of 3744 $\pm$ 81 MPa and 3283 $\pm$ 221 MPa respectively, are equivalent or lower than the pooled average modulus of the 8%-6mm, 15%-6mm and the 22%-6mm coupons. In this case, the lower modulus values are attributed to fiber entanglement due to the fiber clustering during injection molding. An increase in the modulus can be generally attributed to an improved dispersion of the fibers within the biocomposites enabling better stress transfer between fibers and the polymer [115-117]. Chaitanya et al. [114] observed that long fibers in LFT biocomposites bend and entangle with each other forming fiber clusters, thus impeding uniform dispersion and orientation of fibers within the biocomposite. Therefore, it is likely that the manual intervention to mix the unimpregnated fibers in the injection machine hopper was insufficient to properly mix and detangle the fibers in the injected coupons.

Figure 5.9 (c) presents the maximum tensile strength of the injection molded parts as a function

of void content and length. As can be seen in the figure, there is no significant difference between specimens in the maximum tensile strength. All results are around the value of 30 MPa. Also, it is observed that the addition of Flax fibers in the PP did not improve the maximum tensile strength compared to the pure PP dog-bone coupons. This finding was expected since there is normally a very low chemical interaction between the hydrophilic fibers, such as Flax fibers, and hydrophobic matrices, such as PP, resulting in a low interfacial strength [58]. Adhesion between the polymer and the reinforcement fiber is an important characteristic to improve the mechanical strength of a composite part [118]. Yet, it is worth mentioning that the dog-bone coupons did not contain any coupling agent to improve adhesion which could improve the tensile properties of these samples. This result confirms similar findings by Barkoula et al. [15]. Typically, maleic anhydride polypropylene (MAPP) can be used as the coupling agent to improve wettability for natural fiber/PP composites [119-122].

5.3.6 Morphological analysis of the injection molded specimens

Figure 5.10 shows the SEM images of an impact fractured region. Typical SEM images are represented in (a) & (b), showing smooth surfaces at the Flax fibers as well as fiber pull-outs after the impact fracture. The smooth surfaces indicate that the Flax fibers had weak adhesion and chemical interaction with the PP polymer. The low chemical interaction between the Flax fibers and PP was the cause behind making the maximum tensile strengths unchanged relative to pure PP as seen in Figure 5.9 (c). Figure 5.10 (c) 8%-6mm & (d) 8%-15mm show paired specimen which had the same void content but different LFT length. As can be seen in Figure 5.10 (d), the SEM image shows relatively longer fiber compared to 8%-6mm specimen, even after the impact fracture. The longer fibers could explain the improvement of the impact strength of the 15 mm LFT pellets compared to the 6 mm LFT pellets.

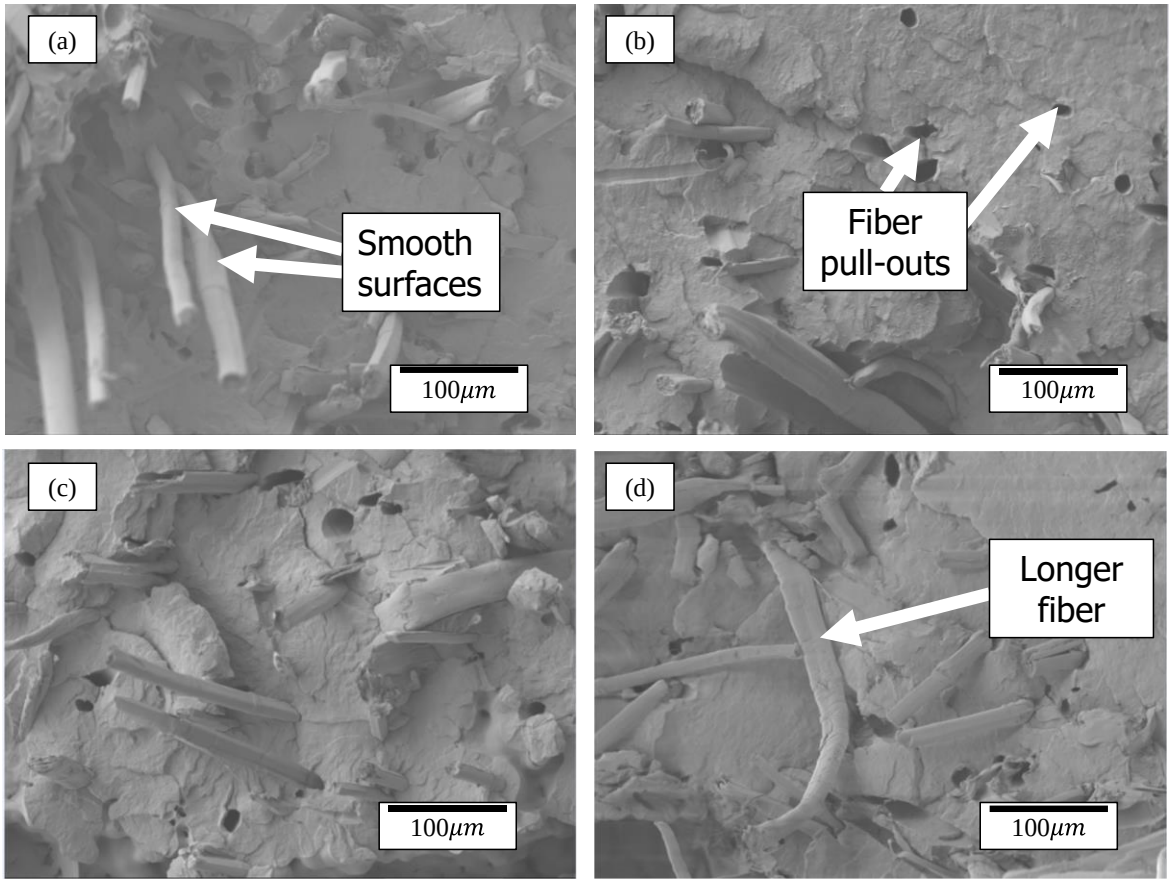

Figure 5.10: SEM images of impact fractured regions. (a) & (b) represent typical SEM images showing smooth surfaces at the Flax fibers as well as fiber pull outs after the impact fracture. The smooth surfaces indicates that the Flax fibers had weak adhesion and chemical interaction with the PP polymer. (c) 8%-6mm & (d) 8%-15mm are paired specimen which had the same void content but different LFT's length. As can be seen in (d), the SEM image is showing relatively longer fibers compared to 8%-6mm specimen even after the impact fracture.

5.4 Conclusion

This study investigated the effects of LFT pellets void contents during the pelletizing process and on the mechanical properties of the injection-molded parts. The fiber volume content of the pultrudates was 50% and four void content points were tested between 4% and 22%. The pultrudates were pelletized into two different lengths of 6 and 15 mm. Three sets of dog-bone coupons were injection-molded using a combination between the void contents and the LFT pellets

lengths. The LFT void content was found to have an influence on the LFT pelletizing quality as well as on the mechanical properties of the injection-molded parts. Flax/PP rods pultruded at 50 and 250 mm/min had void contents up to 8%. These rods were cut in well consolidated pellets. These structurally integral pellets were injection-molded without any issues. Flax/PP rods produced at 500 mm/min and 1000 mm/min led to void contents above 15%. The pelletizing process of these poorly impregnated rods was very damaging, resulting in broken pellets with exposed dry fibers. Manual intervention to allow the LFT pellets and dry Flax fibers to sink in the injection molding machine was required. The mechanical properties of the injection-molded parts using high void LFT pellets resulted in less consistent values attributed to inadequate Flax fiber distribution. The mechanical properties of the injection-molded parts using low void LFT pellets resulted in more consistent values. The highest recorded impact strength was 10,515 $\pm$730 J/m2, corresponding to an experiment that was done using 15 mm LFT pellets with around 8% void content. These pellets were cut from rods pultruded at 250 mm/min. The LFT void content and length did not have any influence on the maximum tensile strengths of the injection-molded parts. All SEM images showed that the exposed fibers had smooth surfaces, indicating very low chemical interaction between the Flax fibers and PP. Irrespective of the LFT void content, the injection molded coupons did not have any voids. Finally, further work will need to be conducted on the parameters of the injection molding machine such as using different injection speeds and pressures to confirm the effects of Flax/PP LFT pellets` morphology on the mechanical properties of injection-molded parts. This will help applicable industries, which make LFT components, to determine the void content threshold points and injection molding parameters. Also, future work will characterize, discuss and improve the seemingly poor interfacial properties between Flax and PP and thoroughly investigate the blending of Flax-PP compatibilizing agent with Flax/PP LFT pellets.

5.5 Acknowledgements

The authors would like to thank Danielle Szydlowski for her help with pelletizing pultrudates.
We would like also to thank Bombardier Aerospace, Pultrusion Technique, Saudi Arabia’s Saline Water Conversion Corporation and Ministry of Education (KSP12014087), NSERC (CRDPJ488387-15) and Prima Quebec (R10-009) for financing this research project.

CHAPTER 6 ARTICLE 3: EFFECT OF HIGH PULLING SPEEDS ON THE MORPHOLOGIES OF PULTRUDATES IN A THERMOPLASTIC PULTRUSION PROCESS

Nawaf Alsinani and Louis Laberge Lebel*

*LLL@polymtl.ca.

Advanced Composite and Fiber Structure laboratory (ACFSlab), Research Center for High Performance Polymer and Composite Systems (CREPEC), Department of Mechanical Engineering, Polytechnique Montréal, 2900 boul. Édouard-Montpetit, Campus of the University of Montreal, Montreal, H3T 1J4, Canada

This article was submitted to the Journal of Thermoplastic Composite Materials

Submission date: May 04, 2022

Abstract

During thermoplastic pultrusion, increasing the pulling speed generally leads to a melted polymer pressure rise in the pultrusion dies. Yet, it was not clear if the polymer pressure's increase would result in a faster impregnation flow that would compensate for the lower residency time inside the heating dies. Thus, the aim of this study was to verify if the speed-induced pressure can counterbalance the decrease in residency time that is required for impregnation quality and to analyze possible pultrudate morphology's reconfiguration. Three distant pulling speeds were selected: namely 50, 500 and 1000 mm/minute. Using a model, the polymer pressure in the pultrusion dies was computed to reach up to 1.0, 10.42, and 20.6 MPa for the respective pultrusion pulling speed. The morphology's characterization showed a reconfiguration of the pultrudate at a higher pulling speed leading to larger unimpregnated agglomerations and polymer rich areas. The highest tensile strength achieved was 233.4 ± 1.5 MPa at 50 mm/minute and dropped by around 20% when the pulling speed was raised to 1000 mm/minute. The pultrudate reconfiguration at higher speed, attributed to delayed melting of PP fibers in underfilled dies, is deemed responsible for the loss in impregnation and mechanical properties.

Keywords: Pultrusion, High-Speed Process, Natural fibers, Thermoplastic

6.1 Introduction

Talc, glass fibers and mica are all examples of inorganic fibers and fillers that are frequently used to reinforce the thermoplastic polymers in the in the automotive industry [1]. However, the manufacturing and discarding of these materials have a hostile impact on the environment. Due to growing environmental awareness, new environmental regulations were announced to help decrease the issue of excessive inorganic waste [2]. These new initiatives are putting pressure on the auto businesses to substitute inorganic fillers with biodegradable replacements. In addition, fuel consumption can be decreased by around 8% when a 10% weight reduction is achieved as lighter matters require less energy to get transported compared to heavier vehicles [73]. Thus, lighter materials offer improved vehicle fuel efficiency as well as lessening greenhouse gas (GHG) emissions. In response, several carmakers are using larger amounts of natural fiber-reinforced composite materials. Similarly, several other industries such as medical, pharmaceutical and food packaging are discovering more ways to use natural fiber reinforced composite materials for both structural and non-structural applications [123].

The use of Flax fibers is becoming popular in industrial applications as a result of their low environmental impact as well as their light weight. Compared to other natural fibers, Flax fibers can be processed at elevated temperatures due to its high cellulose content [10]. Natural fiber thermal degradation frequently happens when cellulose is exposed to temperatures above 200°C. Lignin, on the contrary, begins to degrade once the temperature is around 160°C. Flax fibers are composed of relatively high cellulose content (64%) and low lignin content (2%) [18]. The high cellulose content makes Flax more resistant to the thermal degradation relative to other natural fibers. Additionally, Flax is also favoured due to its higher tensile strength attributed to its high cellulose content. In fact, it is said that Flax fibers have the highest Young's modulus among all natural fibers [11]. Thus, the use of Flax-reinforced composite materials is beneficial for sustainable industrial applications.

In comparison to thermoset polymers, thermoplastic polymers have very high melt viscosity. This elevated viscosity makes it difficult to impregnate reinforcement fibers and mould the final product in one-step processes [79]. Consequently, an additional step such as bulk charge or pre-impregnated pellets is needed before the final production, which is usually done using compression

or injection molding process. Fibre-reinforced thermoplastic composite materials are frequently categorized based on their fiber reinforcement lengths. For example, long fibre-reinforced thermoplastic (LFT) are composite materials which have thermoplastic polymer and discontinuous reinforcement fibres having a length-to-diameter aspect ratio longer than the critical aspect ratio [79]. LFT pellets are frequently produced using a thermoplastic composites (TPC) pultrusion process[99, 100]. Pultrusion has drawn recent interests from academics after overcoming persistent impregnation and cooling problems [37, 54, 97, 98]. Through the TPC pultrusion process, strand precursors that contain the reinforcement and polymer fibers are wound into bobbins that are positioned in a creel. The reinforcement and polymer fibers are then dragged together via a cascade of dies that are heated in order to liquefy the polymer fibers. The yarns which enter the dies contain excess of polymer fibers relative to the die's volume. The excess polymer, therefore, creates a backflow that helps raise the impregnation pressure. During pultrusion, damage the reinforcement fibers can be avoided. As a result, the fibers stay continuous after they get processed.

When pultruding at high pulling speeds, attaining low void contents in the pultrudates can be challenging since there appears to be a trade-off between increasing the pulling speed and decreasing the void contents [28]. This also can be attributed the high viscosities of the thermoplastic polymers. Lapointe et al. [108] observed a significant rise in void contents in Carbon/Polyetheretherketone (C/PEEK) pultrudates after the TPC pultrusion's pulling speed was increased from 50 to 100 mm/min. In fact, the void contents increased by more than 85%. Wiedmer et al. [65] pultruded Carbon/Polymide-12 and tested the pultrusion process at different pulling speeds. The void content increased by around 300% after the pulling speed increased from 100 to 400 mm/minute. Ghaedsharaf et al. [109] pultruded Carbon/Polyetherimide (C/PEI) of commingled braided yarns. The void content surged after the pulling speed was raised from 50 to 150 mm/minute. They implied that the void rise was likely due to the polymer flow time which became too short to fully infiltrate through the carbon fiber agglomerations after the pulling speed was raised to 150 mm/minute. Therefore, all these findings indicate that rising pulling speed, while maintaining the same pultrusion tooling geometry, could lead to a significant rise in the void content.

Babeau et al. [17] modeled the heat transfer and polymer flow during a TPC pultrusion process.

Their model predicted that the time of residency required for impregnation is inversely proportional to the speed. In other words, when the pulling speed increases, a balance between the increase of pressure and the decrease of the residency time occurs; therefore, the impregnation quality would stay the same as long as the thermal conditions remain the same. Kim et al. [22] proposed a model to predict the pressure inside the heating die as well as impregnation quality in a TPC pultrusion process. This model was subdivided into two polymer flow sub-models, the axial backflow around yarns and the radial impregnation flow sub-models. They are both based on Darcy's law and each sub-model has a different permeability. The axial backflow sub-model was used to predict the pressure along the die longitudinal axis by modeling the polymer's backflow induced by the excess polymer. On the other hand, the radial impregnation sub-model was utilized to determine impregnation polymer flow through the fibers' agglomerations. The models were verified and tested experimentally, and they were proven to be accurate in determining the impregnation quality in TPC pultrusion. Babeau et al. [17] and Kim et al. [22] models both showed that the pressure-speed relationship was linear. Later, Lessard et al. [124] proposed a model, based on Kim *et al.*'s [22] approach, to predict the pulling force and degree of impregnation of a multi-die pultrusion system. They used Carbon/Polyetherimide (C/PEI) commingled fibers for their validation experiments. In their model, they assumed that backflow did not completely fill the die, thus creating an effective die length shorter than the actual die length. The accuracy of the model was proven to be adequate such that the predicted pulling forces and degree of impregnation agreed with experimental data for low pulling speeds. However, at higher pulling speeds and higher taper angles, their model did not match the experimental data due to non-isothermal conditions.

During a typical TPC process, the preheating stage and dies are heated according to a set process temperature. However, the actual temperature reached by the pultrudate depends on the apparatus' geometry and residency time. This can create significant discrepancies between the set and the actual material temperatures especially when the pulling speed is high. Alsinani et al. [125] pultruded (Flax/Polypropylene) Flax/PP rods at four distant speed between 50 to 1000 mm/minute. The pultruded rods were then cut into pellets for subsequent injection molding. The pulling speeds of 50 and 250 mm/minute led to void content increase up to 8% and the rods resulted in well consolidated pellets. Flax/PP rods produced at 500 mm/min and 1000 mm/min led to void contents above 15% as the polymer did not fully melt during the pultrusion process. While a follow-on

thermocouple was not used to confirm if the polymer had the same thermal history at all pulling speeds, the microscopic images showed that middle region of the pultrudates produced at 500 mm/min and above did not melt. Thus, at high pulling speeds, it was concluded that the polymer temperature did not reach the melting point and had a different thermal history compared to the low-pulling-speed experiments. Conversely, Babeau et al. [17] adjusted their pultrusion line set temperatures to obtain the same thermal conditions irrespective of the speed. They confirmed the consistency of the thermal conditions at different speeds; namely 100, 500 and 1000 mm/minute, using a follow-on thermocouple with the pultruded materials. They observed that an increase in pulling speed caused an increase in pressure that induced local compaction of the tows. This compaction decreased the tows` permeability since individual reinforcement fibers were closer to each other in the fiber agglomerations. These observations indicate that the reconfiguration of the fiber agglomerations during pultrusion must be considered to achieve proper consolidation.

The objective of this study is to verify if the speed-induced pressure can offset the decrease in residency time that is required for impregnation quality and observe possible pultrudate morphology's reconfiguration. Flax/PP precursors were pultruded at 50, 500 and 1000 mm/minute. To ensure consistency in the thermal conditions at different pulling speeds, the dies' temperatures were adjusted to obtain similar pultrusion thermal conditions at every pulling speed. The pressure in the pultrusion dies was estimated using an approach developed by Lessard et al. [124]. The pressure estimations were used to support the pultrudates' cross-section morphology, tensile and shear strength variations for different pultrusion pulling speeds.

6.2 Experimental

6.2.1 Materials

Pure PP (Normal tenacity PP multifilament yarn, Guangzhou Chemical Fiber Co.) in the 100-tex fiber form were used for the pultrusion. The melting point of the PP was 166.5 ℃ as obtained by DSC at heating rate of 10 ℃/min. The PP fiber's density was considered to be 0.910 g/cm^3 [126]. After melting, the PP density was considered to decrease to 0.750 g/cm^3[127]. Flax yarns (Flax Low Twist Roving, Safilin) having 200 tex size and a solid density of 1.53 g/cm^3 were used.

6.2.2 Pultrusion experiments

Figure 6.1 presents the schematic for the pultrusion system used in this study. The pultrusion apparatus contained a creel, a guide, a preheater, seven heating dies, a cooling die, a load-cell and a pulling system. The creel allowed for individual adjustment for each of the bobbins' tensions. One Newton tension was applied to each bobbin that contained Flax while no tension was applied to the bobbins that contained the PP fibers. The 1 m-long preheater had a square cross-section of 300 mm in width and was equipped with 3 hot-air blowers (VT-752C, Varitemp Heat Gun). The hot-air blowers were all manually controlled and their temperature was measured using thermocouples. All seven heating dies had a 31.75 mm-long conical cavity tapered at 5° relative to the global axis followed by a straight 6.35 mm cylindrical cavity. The diameter of each die's cylindrical exit was 7.91, 7.01, 6.40, 5.13, 5.00, 4.90 and 4.76 mm respectively. The white triangles in Figure 6.1 denote the thermocouple's locations in the heating dies. Additionally, the dark grey circles represent the location of the heating cartridges whereas the light grey circles represent the location of the air-cooling channels. A thin-walled tube protruded from the last pultrusion die toward the cooling die. Details about the cooling system can be found in [128]. The pultrusion pulling speed was controlled by a puller throughout the process. The precursor included 97 PP yarns and 68 Flax yarns distributed into several bobbins: 24 bobbins contained 4 PP yarns, one bobbin contained one PP yarn and 17 contained 4 Flax yarns. To ensure proper mixing in the creel, every Flax bobbin was placed beside a PP bobbin. The filling ratios (R_f) is calculated as:

$$R_f = \frac{A_{in}}{A_{Die}}, \quad (1)$$

Where A_{in} is the material area entering the die and A_{Die} is the die exit area. The nominal R_f in the first die uses the Flax and PP material areas pulled from the creel. These areas are obtained by dividing the Flax and PP yarn finenesses (in Tex, or g/1000m) by their corresponding densities (in g/cc). The melt density was considered for the PP material area. The other dies nominal R_f were calculated using the same Flax area as in the first die. For the PP area, in case of under filling ($R_f < 100\%$), all the PP is assumed to follow the pultrudate. In case of over filling ($R_f > 100\%$), the PP area was considered to be the non-Flax area from the previous die exit area. There were three experiments in total. The pultrudate's final Flax fiber volume content was 50%, while the pulling

speeds and set temperatures varied. Table 6.1 shows the used filling ratios, pulling speeds and set temperatures that were used to produce the Flax/PP pultrudates. The samples name follows the following format: Flax-<Puling speed>. For example, Flax-50 referrers to the pultrudates produced at 50 mm/min. In order to avoid premature melting which causes polymer dripping inside the preheater, the preheater's temperatures were adjusted such that the temperature would less than melting temperature of PP before entering the first heating die [29]. In addition, both preheater's and heating die's temperatures were adjusted so the pultrudates reached and maintained 200°C from the fourth die to the seventh die.

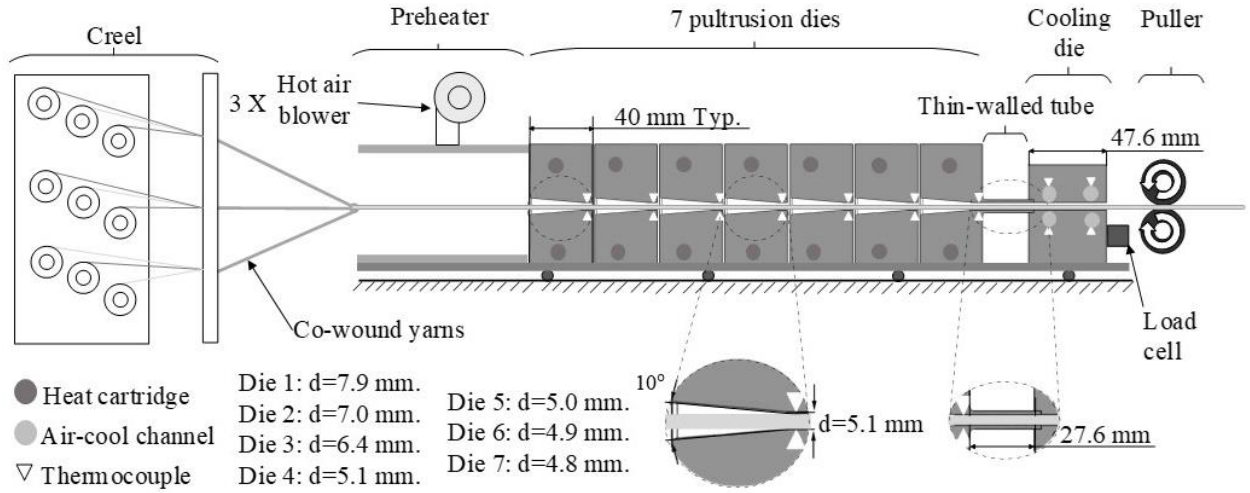

Figure 6.1: A schematic of the multi-die pultrusion system used in this study. The pultrusion system includes a creel, a pre-heater, seven pultrusion dies with 5° tapered angle and reducing exit diametere, a thin-walled tube, a cooling die, a load-cell and a pulling system.

Table 6.1: Die filling ratios and set temperatures of the dies and preheaters for the three pultrusion speed experiments

HAB/Die number		**HAB 1**	**HAB 2**	**HAB 3**	**Die 1**	**Die 2**	**Die 3**	**Die 4**	**Die 5**	**Die 6**	**Die 7**
Filling ratio		N/A	N/A	N/A	44%	57%	68%	106%	105%	104%	106%
Set temp. (℃)	**Flax-50**	50	100	100	200	200	200	200	200	200	200
	Flax-500	100	120	120	240	240	240	240	240	240	240
	Flax-1000	100	150	250	265	265	265	265	265	265	265

6.2.3 Characterization

Cylindrical samples were made using a precision saw. The cylindrical samples were polished and analyzed under a microscope (Metallovert, Leitz). Photos of 200 X magnification were taken and then stitched to form the whole cross-section of pultrudate. The void content was measured according to ASTM2734-09 Method C. The shear tests were conducted according to ASTM D3914-02. The tensile tests were conducted according to ASTM D3916-08.

6.3 Modelling

The model to determine the overfill-induced pressure and forces is similar to the approach presented in Lessard et al. [124] and can be found in Appendix A. This model is an implementation of Kim *et al.*'s pultrusion model for a multi-die pultrusion. The model is structured so that in each die, the axial backflow and the radial impregnation flow were solved by two separate sub-models. The model starts by taking the inputs of material properties. Then, the first die geometry is defined by its length and cross-sectional area in function of length. The modelling work is based on Darcy's law which describes the flow of a single phase fluid in a porous media. This law has been widely used by academics for composite material impregnation for many decades [129]. Both flows are solved using Darcy's equation of flow in a porous media with a specific media permeability. The permeability is modeled using Kozeny-Carman's equation with specific Kozeny constant for the axial backflow and the radial impregnation flow. Euler's method was employed to determine the pressure profile from the axial backflow sub-model. In this study, only the last four heated dies, i.e., Die 4 to Die 7, were considered since the first three dies were underfilled with the pultrudate (see Table 6.1). Similar to Lessard et al. [124], the backflow polymer was assumed to partly occupy

the die and thus creating an effective die length. Table 6.2 shows the table constant and parameters used to obtain the pressure distribution in the last four dies. The initial fiber volume fraction ($v_{f,i}$) value of 0.45 corresponds to the initial fiber volume fraction at the fourth heating dies' inlet. The final fiber volume fraction ($v_{f,\infty}$) of 0.5 corresponds to the pultrdate's final volume fraction at the 7th die's outlet. The radial impregnation Kozney (K_r) and axial backflow Kozney (K_z) constants are 12 and 1.2 respectively. They are fitting constants and were taken from Kim et al. [22] since the model in this study is similar to theirs.

Table 6.2: Models' constants and parameters

Property	**Value**			
Die number	**Die 4**	**Die 5**	**Die 6**	**Die 7**
Intial fiber volume fraction, $v_{f,i}$	0.28	0.43	0.45	0.47
Final fiber volume fraction, $v_{f,\infty}$	0.43	0.45	0.47	0.50
Radial impregnation Kozney constant, K_r [22]	12			
Backflow Kozney constant, K_z [22]	1.2			
Agglomeration radius, R_0 (μm)	527			
Flax fiber radius (μm) [130]	7			
Polymer viscosity (Pa.s) [22]	637			

The model assumes that the Flax yarn radius at die inlet, R_0, is calculated according to:

$$R_0 = \frac{\sqrt{\frac{N_Y f}{\rho}}}{\pi\, \alpha}, \tag{2}$$

Where ρ is the Flax density and α is the yarn compaction factor. In this study, α is assumed to be 60%. The values of Flax density ρ and the Flax yarn fineness f can be found in Section 2.1. N_Y is the number of yarns bobbined together. Using (Eq. 2), R_0 is set at 527 µm since the Flax bobbins contained 4 yarns. The radius of the Flax fiber for radial permeability was 7 µm. It is important note that melted PP exhibits a non-Newtonian fluid [131], and thus the behavior of non-Newtonian behaviour has an impact on the flow through the fiber. This also indicates that the melted viscosity is greatly affected by the pulling speed changes. It is possible to estimate the shear rate between the die surface and the pultrudate if the pulling speed and micro-flow shear rate are known. However, the micro-flow shear rate remains unknow and is expected be much lower than the shear

rate near the die surface. Thus, the viscosity value would be underestimated if only pulling speed was considered as the only factor affecting shear rate. Thus, the polymer's viscosity was assumed to be Newtonian, i.e., constant irrespective of the pulling speed and was calculated to be 637 Pa.s according to Kim et al. [22]. More details about the pultrusion modeling approach used herein can be found in Lessard et al. [124]. The effective die length ($L_{eff,i}$) at each die was calculated as follows:

$$L_{eff,i} = \frac{\phi_{Die,i-1} - \phi_{Die,i}}{2\tan\left(\frac{\theta_{Die,i}}{2}\right)}, \tag{3}$$

Figure 6.2 shows the computed pressure evolution in the tapered region of the last four dies, which are the only dies that had overfill for the three pultrusion speeds. As seen in Figure 6.2, the effective die length was calculated to be 7.26, 0.74, 0.57 mm and 0.80 for Die 4 to Die 7 respectively. Despite having a larger exit diameter, the pressure in Die 4 reached higher pressures compared to Die 5 and 6, for each pulling speed. This can be attributed to the longer effective die length of Die 4 compared to Die 5 and 6. Die 7 resulted in the highest pressure. From Die 5 to 7, the effective die length values are similar when compared to the effective die length of Die 4. For a given pultrusion speed, it is seen that progressive outlet diameter reduction from Die 5 to 7 resulted in progressive maximal pressure increase.

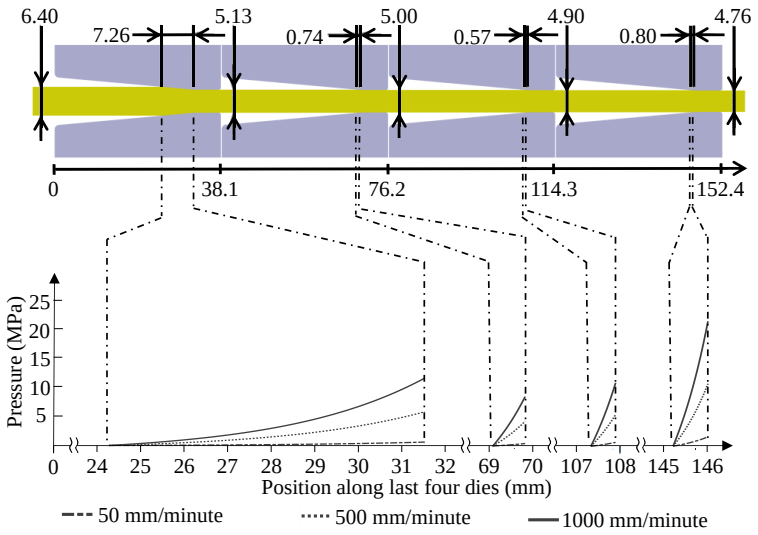

Figure 6.2: Pressure evolution in the tapered region of the dies 4 to 7. Higher effective die length and smaller exist diameters made the pressure go higher.

Finally, it is seen that faster pulling speeds made the computed maximal pressure in the seventh die to increase. The polymer pressure in the pultrusion dies was computed to reach only 1.0 MPa when the pulling speed was 50 mm/min. This pressure raised to 10.4 and 20.6 MPa when the speed was increased to 500 and 1000 mm/minute, respectively. The pulling force was considered here to be the force opposite to the polymer pressure application onto the filled dies' surface, projected onto the dies' axisymmetric axis. Thus, the pulling forces generated in the last four dies were summed according to,

$$F = \sum_{Die\ 4}^{Die\ 7} \int_{A_{Die,i}} P\ dA \cdot \sin\left(\frac{\theta_{Die,i}}{2}\right), \tag{4}$$

The solid line in Figure 6.3 shows the computed force using (Eq.3). The computed pultrusion force values are 2.4, 23.6, and 47.2 N for 50 mm/min, 500 mm/min, and 1000 mm/min, respectively. Moreover, the pulling force shows a linear increase with respect to pulling speed.

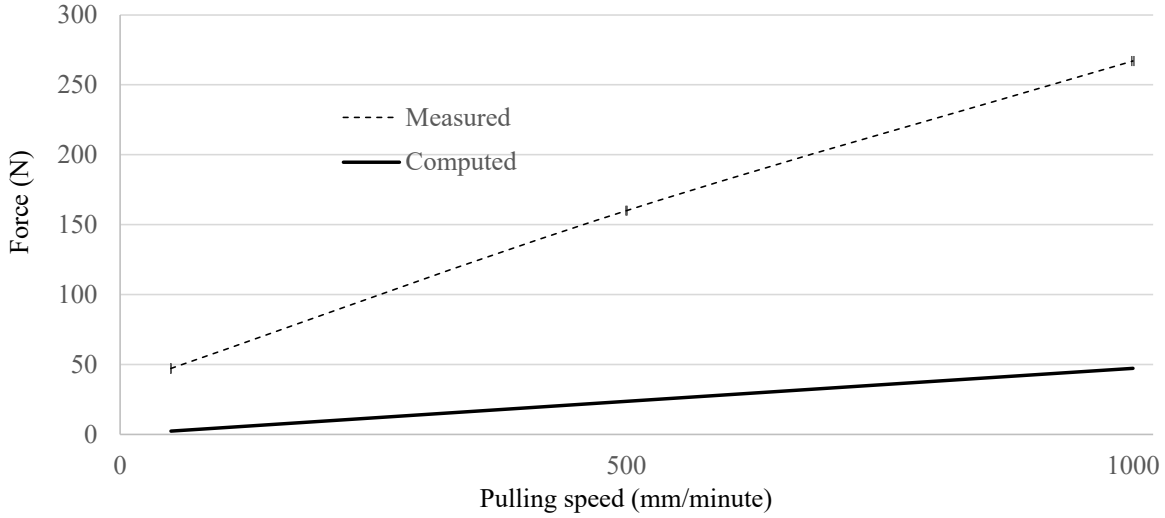

Figure 6.3: A comparison between measured pultrusion force and computed pultrusion force in dies four to seven according to model.

6.4 Results and discussions

6.4.1 Observation of the pultrusion experiments

During all the three experiments, there was no incident of fiber breakage. It is also important to note that the pulling speed was gradually raised especially during the high pulling speeds experiments. This reduced the probability of having fiber breakage. Figure 6.4 (a), (b) and (c) show the temperature measurements taken during Flax-50, Flax-500 and Flax-1000 experiments respectively. Before entering Die 1, the temperatures in all cases were well below the melting point. The highest temperature reached was 133, 108 and 96 ℃ for Flax-50, Flax-500, Flax-1000 respectively. This implies that the polymer did not melt before entering Die 1. Furthermore, the curves demonstrate that the pultrudates reached the processing temperature, i.e. 200 ℃, by the fourth die, for all speeds. The average temperatures in the last four dies were 201.3±1.3, 199.8±2.1, 201.2±2.6 ℃ for Flax-50, Flax-500, and Flax-1000 respectively. At the higher pulling speed experiments, the set temperatures were 245 for Flax-500, and 265 ℃ for Flax-1000 (see Table 6.1). The temperature stopped raising towards the set temperatures once the precursor entered the fourth die. The temperature stabilization is attributed to the overfilled state of the pultrudate beginning at the fourth die. The thermocouples were placed in the middle of precursors.

Once it entered the last four dies, it became encapsulated in the low thermally conductive Flax/PP composite. The first three dies worked as preheaters with filling ratios below 100%. Since the pultrudate was unconsolidated, it is supposed that heating could reach the separated fibers. Flax-50 pultrudate spent 3.2 minutes in the last four dies while Flax-500 spent 0.32 minute and Flax-1000 spent 0.16 minute. Figure 6.3 also shows the measured pultrusion force for all experiments compared to the computed force using Eq.3. Flax-50 resulted in 47.1±0.1 N pulling forces while Flax-500 and Flax-1000 resulted in 160.2±0.5 and 266.5±1.1 N respectively. The measured forces are one order of magnitude higher than the computed forces at their corresponding speed. The primary explanation is related to the fact that the model neglected the fiber-to-die-wall friction forces in all pultrusion and cooling dies. Friction forces are independent of relative speed between friction surfaces. However, in Figure 6.3, the measured pulling force differences with the computed force is seen to increase with increasing pulling speed. At 45 mm/min, the measured pulling force is 44 N higher than computed pulling force, while at 1000 mm/minute, it was 217 N higher than the computed forces. According to Figure 6.4, the polymer temperature rise was steeper at 50 mm/min than the other speeds. It is suspected that the polymer melted earlier at 50 mm/min than at the faster experiments. Therefore, the polymer acted as a lubricant that lowered the friction forces. Moreover, at higher speed, the unmelted polymer fibers in the first dies exerted higher pressure on the die surfaces upon compaction. Finally, it suspected that the cooling section also contributed to the increasing measured-to-computed difference in pulling force with respect to speed. As seen in Alsinani et al. [128], the polymer adheres to the die surface when cooling from the processing temperatures until it shrinks and separates. The adhesion length is directly related to the distance on which the polymer cools. At higher speed, the pultrudate adhesion length with cooling die's surface became higher. This likely added more frictional forces opposing the pulling action. The significantly higher actual pultrusion force at 1000 mm/min is an indication that the model cannot capture all phenomena occurring during pultrusion.

The increase in pultrusion force indicates higher impregnation pressure with increasing pulling speed. However, contrary to the computed pultrusion forces, the increase in measured force does not follow a linear relationship with speed. The apparent force increase rate was 0.25 N/(mm/min) from 50 mm/min to 500 mm/min, and 0.21 N/(mm/min) from 500 mm/min to 1000 mm/min. In comparison, the computed force in dies 4 to 7 was linear at an increase rate of 0. 06 N/(mm/min).

The non-linear increase observed experimentally is contradictory with behaviors predicted by Kim *et al.*[22], Babeau *et al* [17] as well as the modeling done in this study.

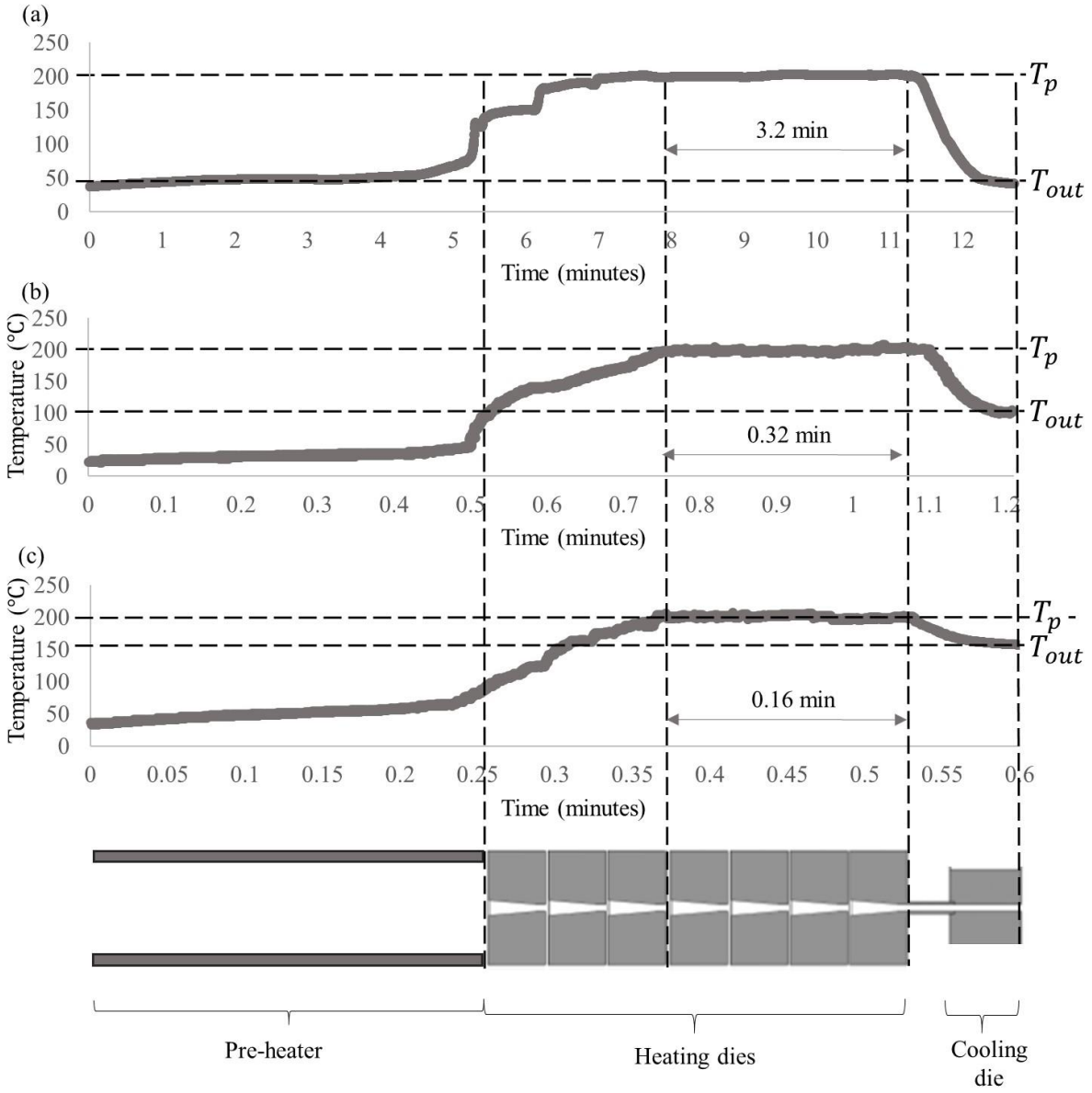

Figure 6.4: The temperature measurement during a typical: (a) Flax-50. (b) Flax-500. (c) Flax-1000. Before entering Die 1, the temperature in all cases was well below the melting point. The highest temperature reached was 133, 108 and 96 ℃ for Flax-50, Flax-500, Flax-1000 respectively. This implies that the polymer did not melt after entering Die 1.

Table 6.3: Measured temperatures during the pultrusion experiments

Sample denomination	Temperature (℃)
Flax-50	201.3±1.3
Flax-500	199.8±2.1
Flax-1000	201.2±2.6

6.4.2 Morphological analysis of the pultrudates

Table 6.4 shows pultruded rods` measured porosities. The void content characterization indicated that the 50 mm/min pultrusion speed led to a 2.5±0.9 % void content, the 500 mm/min to a 2.6±0.7 % void content and that 1000 mm/min led to the highest void content of 5.4±0.4 %. Figure 6.5 presents the typical cross-section microscopic photos of Flax/PP pultrudates with respect to the pulling speeds. Contrary to Alsinani *et al.*[125], the polymer in all cases had fully melted. Flax-50 microscopic image shows well distributed and well impregnated fibers. Figure 6.5 b) and c) shows pultrudates produced at higher pulling speeds. Large polymer rich areas are seen there. It seems that the increase in pulling forces, induced by higher pulling speeds, led to an increase in the fiber agglomeration compaction. Also, the pultrudates produced at high pulling speed experiments were reconfigured in large groups of yarns. Therefore, the effective agglomeration radius to be impregnated was larger at higher speed than at lower speed. A plausible explanation for this rearrangement can be deduced by analysing the temperature reading of the follow-on thermocouple in Figure 6.4. The temperature rise in the first three dies show that the maximum temperature is reached much faster in Flax-50 than the Flax-1000 experiment. This created a delay in polymer melting at higher speed. Moreover, as observed in Nawaf et al. [125] the PP polymer melts progressively from the die surface to the center of the pultrudate. Therefore, since un-melted polymer fibers cannot flow around Flax agglomerations, the area they occupied effectively compressed and pushed the Flax yarns into the melted PP in contact with the die. Then, the PP fiber rich areas finally melted before entering the fourth die leading to polymer rich regions seen in Figure 6.5 (b) and (c). The above explanation behind the fiber reconfiguration will be investigated thoroughly in future studies. In any case, it can be affirmed that a co-wound yarn precursor structure is more likely to result in such an rearrangement since the unimpregnated fiber agglomeration movement relative to each other is not secured by any mechanical feature once the

polymer is melted. Future work must develop a precursor structure for high speed pultrusion that is structured in a way that prevents polymer rich creation. Another possible solution would be to use preheating dies with low or no taper angle. These preheating dies would bring the polymer fibers to melt without compression, while securing them to prevent their separation from the pultrudate at die entrance.

Table 6.4: Tensile and shear tests results

Sample denomination	Void content (%)	Shear strength (MPa)	Tensile strength (MPa)	Young`s Modulus (GPa)
Flax-50	2.5±0.9	12.7±1.4	233.4±1.5	37.8±4.5
Flax-500	2.6±0.7	3.7±0.7	193.2±1.3	34.3±2.2
Flax-1000	5.4±0.4	3.15±1.2	189.3±4.5	25.6±2.7

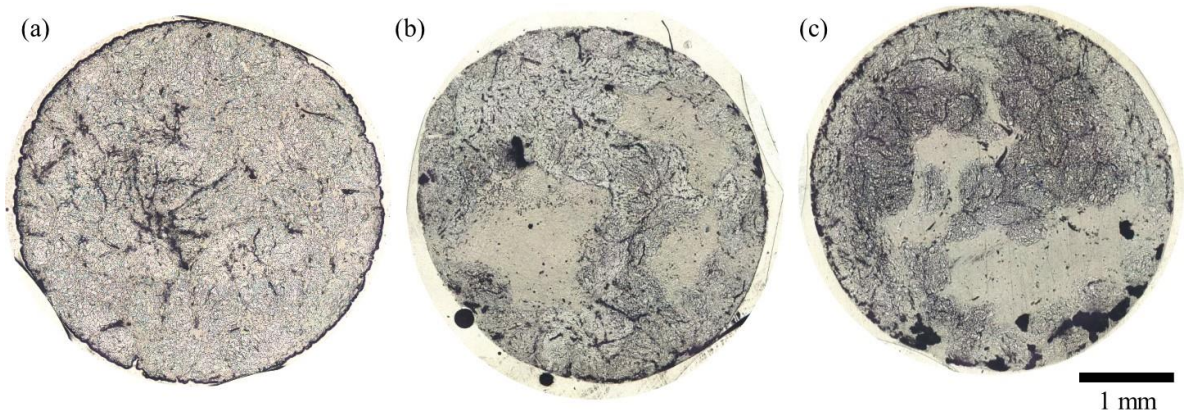

Figure 6.5: The microscopic photos of Flax/PP pultrudates. (a) Flax-50. (b) Flax-500. (c) Flax-1000. Flax-500 & Flax-1000 are showing enlarged polymer rich areas.

6.4.3 Mechanical properties of pultrudates

Figure 6.6 (a) presents a pultruded sample prepared for shear test; (b) presents a typical shear stress versus displacement result for pultrudates produced at 50, 500, 1000 mm/minute. The 50 mm/min curve exhibited the highest peak value which was 12.7±1.4 MPa. The pultrudates, produced at higher speeds, achieved much lower shear strengths of 3.7±0.7 and 3.15±1.2 for Flax-500 and Flax-1000 respectively. These values are 75% less than the Flax-50 shear strength. This large shear strength variation is more indicative of the impregnation state of the pultrudates studied here than the void content. Moreover, the 1000 mm/minute curve peaked sooner than the 500

mm/minute curve. This peak at lower displacement indicates that 1000 mm/minute specimen had the worst impregnation state. Figure 6.6 presents the tensile and shear strength values. Following the same trend, the highest tensile strength value was achieved for Flax-50 and was 233.4±1.5 MPa. The higher speed pultrudates achieved much lower tensile strengths: 193.2±1.3 and 189.3±4.5 MPa for 500 and 1000 mm/minute respectively. These values are significantly lower than the Flax-50. The lower tensile and shear strengths can be attributed the polymer rich regions and bad impregnation quality as reported in section 4.2. The tensile modulus slightly decreases between specimen Flax-50 and Flax-500, from 37.8 to 34.3 GPa. However, the difference in modulus values seems insignificant when considering the standard deviation on the measurements of 4.5 and 2.2 GPa, respectively. In comparison, the decrease in modulus values between Flax-500 and Flax-1000 is significant; it decreased by 8.7 GPa compared to the Flax-500 modulus. The decrease is caused by the significant rise in void content and fiber clustering. Both factors made it difficult for some fibers to share the tensile load and contribute to the sample stiffness.

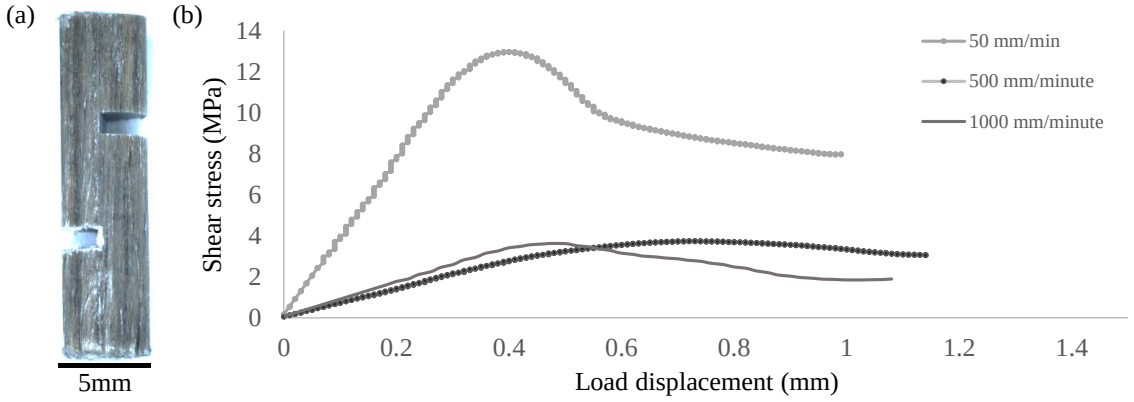

Figure 6.6: (a) Pultruded sample prepared for shear test. (b) A typical Shear stress-displacement result of shear test for 50, 500, 100 mm/minute. The 50 mm/minute sample is showing a higher shear strength value compared to the other samples.

6.5 Conclusions

Three different pulling speeds were selected to study the effect of high pulling speeds on the morphologies of pultrudates in a TPC pultrusion process. To ensure consistency in the thermal conditions at different pulling speeds, the dies' temperatures were adjusted to obtain similar

pultrusion thermal conditions at every pulling speed. The cross-section morphology characterization showed well-distributed reinforcement fibers for the low pulling speed experiment of 50 mm/min. On the contrary, the pultrudates that were produced at high pulling speed had compacted and clustered fibers, which resulted in polymer rich areas and more voids. Also, during Flax-500 and Flax-1000 experiments and when the polymer fibers melted, the melted polymer was not able impregnate the reinforcement fibers since they were more compacted when compared to Flax-50. It is important to note that the pulling forces during Flax-500 and Flax-1000 experiments were significantly higher than Flax-50. At every speed, the measured pulling forces were higher than the computed value. The significantly higher actual pultrusion force at every speed is an indication that the model cannot capture all phenomena occurring during pultrusion; it is also indicative that more realistic modeling approaches must be developed. The microscopic images showed well distrusted yarns for pultrudates produced at 50 mm/minute. While at higher pulling speeds, reconfiguration of the reinforcement fibers occurred. The pultrudate reconfiguration at higher speed, attributed to delayed melting of PP fibers in underfilled dies, is deemed responsible for the loss in impregnation. The reconfiguration was confirmed by mechanical property characterization. Tensile properties deteriorated when a faster pulling speed was used. The highest tensile strength achieved was 233.4±1.5 MPa at 50 mm/minute and dropped by around 20% when the pulling speed was raised to 1000 mm/minute. The shear strength also dropped by 75% when the pulling speed was raised from 50 to 1000 mm/minute. Future work should investigate this phenomenon and find mitigation strategies to counter the reconfiguration mechanism. For example, using low-angle Flax/PP braids might help secure the position of the Flax yarns in the pultrudate, while still allowing fiber separation in the processing of LFT pellets during injection molding.

6.6 Acknowledgements

The authors would like to thank Danielle Szydlowski for her experimental help. We would like also to thank Bombardier Aerospace, Pultrusion Technique, Saudi Arabia’s Saline Water Conversion Corporation and Ministry of Education (KSP12014087), NSERC (CRDPJ488387-15) and Prima Quebec (R10-009) for financing this research project.

CHAPTER 7 GENERAL DISCUSSION

7.1 General discussion

This study opens the door for the utilization of pultruded thermoplastics in many fields including high quality Flax-reinforced LFT pellets production, additive manufacturing and composite riveting. Due to the novelty of this objective and its vast potential industrial applications, notably in the aerospace and automotive industries, a patent for one of our cooling designs is pending approval by the US patent office entitiled “Pultrusion system with cooling stage and method therefor” (WO patent number: WO2020237381A1). [132]. This will allow the idea of this research to be transferred to industry. From a research point of view, the cooling die was further used at Polytechnique Montreal in two other impactful published research papers related to composite riveting and braid-trusion and were published in Composite Structures and Composites Part A, respectively [97, 133]. First, the proposed cooling system was capable of producing C/PEEK pultrudates having low void contents. Those C/PEEK pultrudates were cut to be used for subsequent riveting. The pultrudates’ diameters were very close to the desired diameters and they exhibited perfectly circular shapes, as desired. The diameters of produced rods were within 0.02 mm. This can be credited to the prevention of thermal deconsolidation after using the cooling technology developed in this thesis [133]. Figure 7.1 shows comparison between a standard metallic fastener and a C/PEEK rivet. Results showed that the specific shear strength of the C/PEEK rivets was almost twice as high as the titanium fasteners submitted. This promising result may likely attract aerospace manufacturers to replace metallic fasteners with composite rivets.

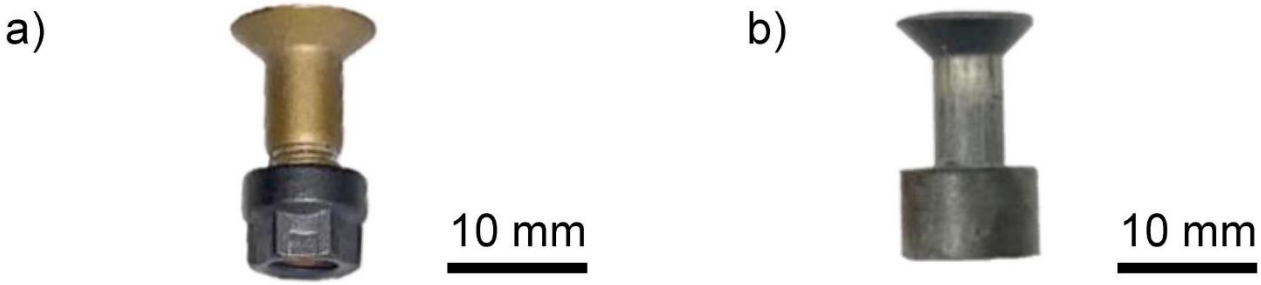

Figure 7.1: Comparison between standard metallic fasteners and C/PEEK rivet: a) Titanium Fastener; b) C/PEEK rivet [133].

Second, the proposed cooling system in this study was also capable of producing void-free braid-truded rods [97]. Thermoplastic braid-trusion is a composite manufacturing process that combines braided yarns that get processed by TPC pultrusion. The braided yarns contain reinforcement and polymer fibers. Figure 7.2 shows the cross-section of the braid-truded rod after processing, captured by a microscope. No void can be observed. The pultrudate's shape is almost perfectly circular. This can be credited to the newly developed cooling die in this thesis. The prevention of deconsolidation helped made the pultrudates become void-free also to achieve desired final diameters.

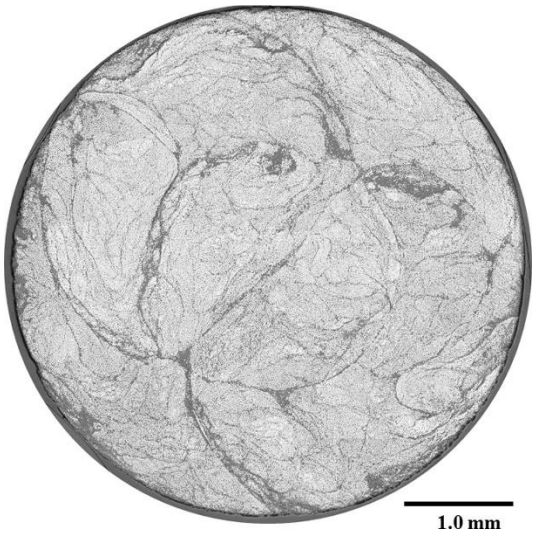

Figure 7.2: Cross-section image of the carbon fiber/PEI braid-truded pultrudate [97].

Internationally, the thin-walled-tube concept of the cooling die attracted interests from many other academics. Volk *et. al* used a similar thin-walled-tube concept to produce pultrudates having up to 40 mm diameters [134] and to produce thermoplastic pultrudates for high voltage insulator applications [135]. The pultrudates exhibited perfectly circular shapes having low void contents; below 2%. The thin-walled-tube concept resulted in the prevention of deconsolidation which helped achieved perfectly circular shapes having low void contents.

Moreover, we further used developed cooling system to make Flax reinforced LFT pellets which resulted in Flax/PP injected parts having modulus increase of 2.5 times the modulus of Pure PP, and impact strengths above 10.5 kJ/m^2 for coupons injected with 25 wt% Flax content. Those results are unmatched in the literature reviewed. Additionally, we were able to increase the pulling speed to 1 m/minute in order to make the production of LFT using TPC pultrusion suitable for industrial applications. Therefore, this research also demonstrates a practical solution towards adopting environmental-friendly material alternatives.

7.2 General discussion on unpublished achievements

The multi-die system is capable of producing well impregnated pultrudates [8, 34, 50, 52, 55]. A multi-die pultrusion system was implemented into additive manufacturing technology and was

able to bring down the void content in the printed extrudates by over 80% [53]. These results suggest the high potential of multi-die pultrusion technology to overcome impregnation challenges. However, the science behind the multi-die system and its impact on impregnation quality was never thoroughly studied. It is not clear yet why a multi-die pultrusion would give better impregnation quality than a longer single-die system. In TPC pultrusion, the backflow polymer in the die is assumed to partly occupy the die and thus creating an effective die length where polymer is exerting pressure on the hot precursor at the tapered region of the heating die. The modelling approach was taken from the PhD thesis of Lessard [124] and used in Chapter 6 consider the effective die length based on the outlet v_f of the previous die. For the sake of this discussion, the extract from Lessard's thesis is available at Appendix A. This assumption is not realistic as, as discussed in Chapter 4, deconsolidation is expected to occur between dies since the pultrudate exits an intermediary pultrusion die at a temperature higher than T_m .

Figure 7.3 shows an example of deconsolidation in PEI pultrudates. In this example, the pultrusion die exit diameter was 4.65 mm, for an exit area of 16.97 mm^2. However, the rod cross-section seen in Figure 7.3 have an area of 20.58 mm^2 that is 21% larger than the die exit diameter.

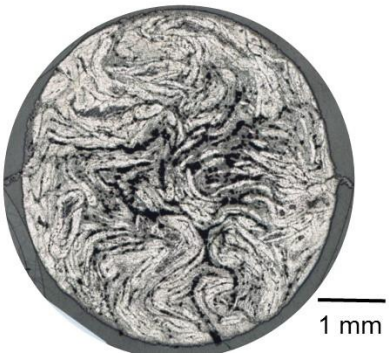

Figure 7.3: Example of deconsolidation in PEI pultrudates. Void areas are represented by the black areas. The surface finish looks rough. Deconsolidation occurred since the pultruded exited the pultrusion line at a temperature above T_g .

One could pose the hypothesis that the higher pultrudate diameter, due to deconsolidation at an

intermediary die exit, will cause an increase in the effective contact length of the pultrudate in the next die and lower inlet v_f . The effective die length, Eq. 3. of Chapter 6, can be expressed as:

$$L_{eff,i} = \frac{\phi_{Decons,i-1} - \phi_{Die,i}}{2\tan\left(\frac{\theta_{Die,i}}{2}\right)}, \quad (1)$$

Where the diameter of the previous die ($\phi_{Die,i-1}$) was replaced by the deconsolidated diameter of the pultrudate ($\phi_{Decons,i-1}$). To find $\phi_{Decons,i-1}$, we can express the diameter of the previous die ($\phi_{Die,i-1}$) as,

$$\phi_{Die,i-1} = \frac{v_{f\infty,i-1}}{\left[\frac{\overline{N_Y}f}{\rho}\right]}, \quad (2)$$

Where $v_{f\infty,i-1}$ is the Flax fiber volume content at the previous $(i-1)$ die exit, $\overline{N_Y}$ is the total number of Flax yarns in the pultrudate, f is the yarn fineness in Tex, and ρ is the Flax density. A deconsolidation fiber volume content variation, $\Delta v_{f,i-1}$, can be removed from $v_{f\infty,i-1}$ to obtain the deconsolidated pultrudate diameter after die $(i-1)$ exit, as:

$$\phi_{Decons,i-1} = \frac{v_{f\infty,i-1} - \Delta v_{f,i-1}}{\left[\frac{\overline{N_Y}f}{\rho}\right]}, \quad (3)$$

To verify this hypothesis, three scenarios were computed using the model using a model developed in the PhD thesis of Lessard [124]. The three scenarios are shown in in Table 7.1. A tapered angle of 5° and a pulling speed of 50 mm/min is assumed in all scenarios.

Table 7.1: Models' constants and parameters for the three scenarios.

Senario	**Property**	**Value**			
No-Deconsolidation	Die number	**Die 1**	**Die 2**	**Die 3**	**Die 4**
	Intial fiber volume fraction, $v_{f,in,\mathrm{i}}$	0.28	0.43	0.45	0.47
	Die Exit Diameter, $\phi_{Die,i}$ (mm)	5.1	5.0	4.9	4.8
	Effective Length, $L_{eff,i}$ (mm)	7.26	0.74	0.57	0.8
	Final fiber volume fraction, $v_{f,\infty,\mathrm{i}}$	0.43	0.45	0.47	0.50
5%-Deconsolidation		**Die 1**	**Die 2**	**Die 3**	**Die 4**
	Intial fiber volume fraction, $v_{f,in,\mathrm{i}}$	0.23	0.38	0.4	0.42
	Die Exit Diameter, $\phi_{Die,i}$ (mm)	5.1	5.0	4.9	4.8
	Effective Length, $L_{eff,i}$ (mm)	11.10	2.61	2.29	2.41
	Final fiber volume fraction, $v_{f,\infty,\mathrm{i}}$	0.43	0.45	0.47	0.50
Single-Die	Die Number	Single Die			
	Intial fiber volume fraction, $v_{f,in}$	0.28			
	Die Exit Diameter, ϕ_{Die} (mm)	4.8			
	Effective Length, $L_{eff,i}$ (mm)	9.37			
	Final fiber volume fraction, $v_{f,\infty}$	0.50			

The first scenario, the No-Deconsolidation scenario, is the same as the one presented in Chapter 6. The inlet fiber volume fractions $v_{f,in}$ from Die 1 to 4 were 0.28, 0.43, 0.45 and 0.47 respectively. This results in effective die length to be 7.26, 0.74, 0.57 and 0.80 mm for Die 1 to 4 respectively. The sum of the effective length is equal to 9.37 mm.

The second scenario is the 5%-Deconsolidation. The deconsolidation lowered the $v_{f,in}$ from Die 1 to 4 by 5% to 0.23, 0.38, 0.4 and 0.42 respectively. The effective die lengths were calculated to be 11.10, 2.61, 2.29 and 2.41 mm and for Die 1 to 4 respectively resulting in a sum of the effective length equals to 18.42 mm. This value is twice as high as the first case. It should be also noted that the final volume fraction at each die ($v_{f,\infty,\mathrm{i}}$), is the same as the No-Deconsolidation case.

The third scenario is the Single-Die. The $v_{f,in}$ is 0.28, the same as the first die of the No-Consolidation scenario. The $v_{f,\infty}$ is 0.5, the same as the other scenarios. The effective length is equal to 9.37 mm. This is the equal to the sum of all dies effective length of the No-Deconsolidation

scenario.

Figure 7.4 shows impregnation quality and pressure evolution in the tapered region of the dies 1 to 4. The No-Deconsolidation scenario assumes that no deconsolidation occurs between dies such that $v_{f,\mathrm{i}}$ is equal to $v_{f,\infty}$ of the previous die, as a reminder of Chapter 6. Figure 7.4 shows that the no deconsolidation scenario was 59% impregnated by the time it reaches the end of Die 4 and the highest pressure recorded was 1.02 MPa and it was at Die 4. For the 5%-Deconsolidation scenario, the impregnation is the highest compared to all other cases. By the end of Die 1, the 5%-Deconsolidation scenario was 94% impregnated and it went up to 100% by the time it reaches the Die 3 outlet. The highest pressure recorded pressure for the 5%-Deconsolidation scenario was 1.1 MPa and it was also at Die 4. As seen in Figure 7.4, the Single-Die scenario was 63% impregnated by the time it reaches the end of its length. This impregnation value is comparable to the No-Deconsolidation scenario of 59%. The highest pressure recorded for the Single-Die scenario was 0.91 MPa.

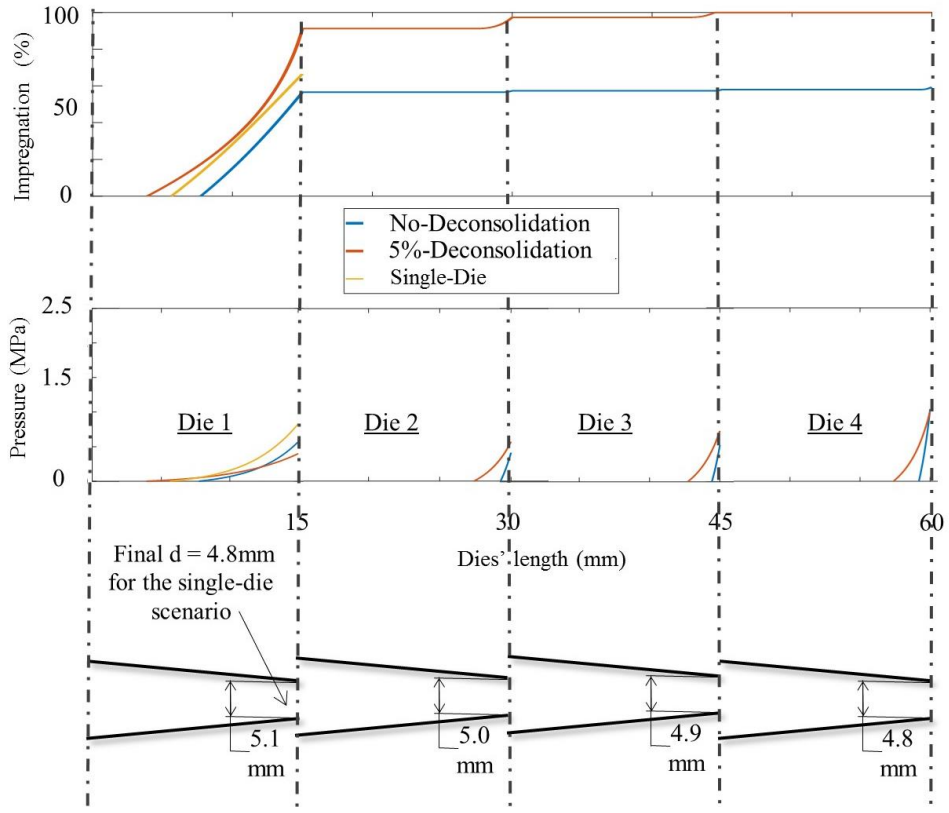

Figure 7.4: Impregnation quality and pressure evolution in the tapered region of the dies 1 to 4. Pulling speed was selected to be 50 mm/minute.

The 5%-Deconsolidation scenario, achieved the highest impregnation of 100% despite being subjected to similar pressure as the other two cases. The highest recorded pressure was 0.98, 1.01 and 0.91 MPa for the No-deconsolidation, 5%-Deconsolidation and Single-die scenario respectively. Yet 5%-Deconsolidation, the multi-die, achieved the highest impregnation. The multi-die system seems to allow the hot precursors to deconsolidate between dies. This deconsolidation causes increase in the pultrudate diameter at each die inlet; thus creating a larger effective contact length and increasing the impregnation quality. This finding indicates that with the same pressure, it is possible to achieve higher impregnation using the multi-die pultrusion system due to deconsolidation occurring between the dies. Yet, these promising modelling results need to be confirmed experimentally.

CHAPTER 8 CONCLUSION AND RECOMMENDATIONS

This dissertation's main objective is to produce Flax/PP LFT pellets using TPC pultrusion. The main objective was achieved by dividing the main objective into three objectives.

The first objective was to develop a cooling system which is able to accurately control the pultrudate's cooling temperature profile. In Chapter 4, we introduced an efficient technique to conduct cooling in TPC pultrusion. The average void contents in the pultrudate were below 2%. The newly developed cooling system was then utilized to investigate the effect of varying the cooling temperatures on the thermal profile of the pultrudates. Microscopic images exhibited a direct correlation between the cooling temperature, void content value and thermal deconsolidation. For C/PEI pultrusion, thermal deconsolidation, a higher void content and a significant increase in pulling forces were detected when the cooling temperature was increased above T_g. In addition, Ra testing results showed that pultrudates with lengthier SCD had inferior surface finish quality. Cooling temperature of $T_g/2$ resulted in pultrudates with Ra value of 0.72 $\pm$ 0.09 μm For C/PEEK pultrusion, temperature of $(T_g + T_m)/2$ resulted in the longest SCD while still resulted in the best surface finish quality (Ra = 0.56 $\pm$ 0.06 μm). This is can be attributed to the selected cooling temperature of 243°C, which induced fast crystallization of the PEEK polymer. To confirm the findings from reprocessing experiments, two experiments were conducted in steady-state conditions using commingled yarns. Pultrudates produced in steady-state conditions, resulted in equally low Ra values and attained the same shape and consolidation quality as the reprocessed samples. The newly developed cooling system was able control the temperature and pultrudates and also resulting in outstanding surface-finish quality. This, the system will surely generate significant new application for the utilizing of pultrudates in many fields. Thus, we achieved the first objective in Chapter 4.

The second objective was to present to the effect of high pulling speeds on the morphologies of pultrudates in a TPC pultrusion process. The second objective was to apply our recently developed multi-die thermoplastic pultrusion process with cooling stage to produce Flax fiber-reinforced (LFT) pellets. In Chapter 5, we studied the effects of LFT pellets' consolidation quality during the pelletizing process and on the mechanical properties of the injection-molded parts. The pultrudates' fiber volume fraction was 50% and four void fraction points were tried between 4%

and 22%. The pultrudates were cut into two different sizes. Three sets of dog-bone coupons were injection-molded using a blend of the void contents and LFT pellets sizes. The LFT void fraction was found to have an impact on the LFT pelletizing quality and on the mechanical properties of the injection-molded components. Flax/PP pultrudates produced at 50 and 250 mm/min had void fractions up to 8%. These pultrudates were cut into well consolidated pellets. These pellets were injection-molded without any problem. Flax/PP pultrudates produced at 500 and 1000 mm/min resulted in void fractions above 15%. The pelletizing process of these high-void pultrudates was very damaging, resulting in shattered pellets with detached dry fibers. Manual intervention was required to make the LFT pellets and dry Flax fibers sink in the injection molding machine. The injection-molded components using high-void LFT pellets resulted in less consistent values of mechanical properties due improper Flax fiber distribution. The injection molded coupons void content did not have any void regardless of the LFT void content. The highest impact strength value was 10,515 $\pm 730\ J/m^2$, belonged to an experiment was conducted using 15 mm LFT pellets having around 8% void fraction. This impact strengths with 25 wt% Flax content is unmatched in literature. With that, we achieved the second objective in Chapter 5.

The third objective was to present to analyze the effect of high pulling speeds on the morphologies of pultrudates in a thermoplastic pultrusion process. In Chapter 6, we studied the impact of pulling speed on the morphologies of pultrudates in a thermoplastic pultrusion process by selecting three different pulling speeds. To guarantee consistency, the dies' temperatures were adjusted to attain analogous thermal conditions at each pulling speed. The microscopic images showed well-distributed yarns for Flax-50. While at higher pulling speeds, reconfiguration was exhibited. The delayed melting of PP fibers in underfilled dies is also responsible for the loss in impregnation. At every pulling, the measured pulling forces were significantly higher than the computed value. This indicates that the model cannot capture all phenomena occurring during pultrusion. Tensile strength worsened when a faster pulling speed was used. The highest tensile strength achieved was at 50 mm/minute plunged by around 20% when the pulling speed was elevated to 1000 mm/minute. The shear strength too plummeted by 75% when the pulling speed was increased from 50 to 1000 mm/minute. We were able to increase out pulling speeds to 1 m/minute to make the process more suitable for high-volume industrial applications. With that, we achieved the third objective in Chapter 6.

This study opens the door for the usage of pultruded thermoplastic composites in many fields including producing high quality Flax-reinforced LFT pellets production. Our results demonstrate a practical solution towards adopting environmental-friendly material alternatives.

8.1 Limitations and future research direction

This research will create significant new opportunities for the usage of pultruded thermoplastic composites in many fields including LFT pellets manufacturing, additive manufacturing and composite joining. The following opportunities for future researches are proposed to address the limitations of this dissertation:

- **Injection molding machine' parameters, such as using different injection speeds and pressures, were kept constant in this thesis. Further work will need to be conducted on different parameters to analyze the effect of changing the parameters of the injection molding machine.**

By conducting a sensitivity study on effect of changing the parameters of the injection molding machine

- **Future studies should conduct visual analysis on the fiber distribution inside the injected to confirm the findings of this thesis particularly the void content induced fiber distribution. Fiber length Distribution was it shorten by the injection.**

By analysing the fiber distribution inside the injected parts

- **Improving the Flax/PP interphase Flax/PP compatibilizing agent**

By adding Falx/PP LFT pellets to pure polypropylene did not improve the tensile properties. All SEM images showed that the exposed fibers had smooth surfaces, indicating low chemical bond between the Flax fibers and PP. We recommend investigating the addition of Flax/PP compatibilizing agent to master mixture.

- **In this research, only co-wound Flax/PP yarns. The co-wound yarns allowed the polymers to escape easily. Having a low Flax/PP braid may help secure the position of the Flax yarns in the pultrudate.**

By analysing the effects of high pulling speeds using co-wound precursors but without having any tapered angle which normally causes backflow pressure.

REFERENCES

[1] M. Fogorasi and I. Barbu, "The potential of natural fibres for automotive sector-review," in *IOP Conference Series: Materials Science and Engineering*, 2017, vol. 252, no. 1: IOP Publishing, p. 012044.

[2] J. Zhu, H. Zhu, J. Njuguna, and H. Abhyankar, "Recent development of flax fibres and their reinforced composites based on different polymeric matrices," *Materials*, vol. 6, no. 11, pp. 5171-5198, 2013.

[3] M. Pervaiz, S. Panthapulakkal, K. Birat, M. Sain, and J. Tjong, "Emerging trends in automotive lightweighting through novel composite materials," *Materials sciences and Applications*, vol. 7, no. 01, p. 26, 2016.

[4] N. Alsinani and L. Laberge Lebel, "Effect of Flax/PP pellets' morphology on the mechanical properties of injection-molded parts," *Journal of Thermoplastic Composite Materials*, 2021.

[5] G. L. M. Batch, C.W., "Analysis of pressure, pulling force and sloughing in pultrusion," *American Society of Mechanical Engineers, Heat Transfer Division, (Publication) HTD*, vol. 132, pp. 109-112, 1990.

[6] S. Moschiar, M. Reboredo, J. Kenny, and A. Vazquez, "Analysis of pultrusion processing of composites of unsaturated polyester resin with glass fibers," *Polymer Composites*, vol. 17, no. 3, pp. 478-485, 1996.

[7] G. L. Batch and C. W. Macosko, "Heat transfer and cure in pultrusion: model and experimental verification," *AIChE journal*, vol. 39, no. 7, pp. 1228-1241, 1993.

[8] N. Alsinani and L. Lebel Laberge, "Effect of length variation of flax/polypropylene pellets produced by multi-die pultrusion on the quality of injection molded product.," presented at the Automotive Composites Conference & Exhibition (ACCE 2018), 2018. [Online]. Available: http://speautomotive.com/acce-2017-sustainable-composites.

[9] A. Oswald, "Multi-die vacuum assisted pultrusion of Flax/PLA thermoplastic composite," master`s degree, Departement de genie mecanique, Universite de Montreal, 2016.

[10] I. Angelov, S. Wiedmer, M. Evstatiev, K. Friedrich, and G. Mennig, "Pultrusion of a flax/polypropylene yarn," *Composites Part A: Applied Science and Manufacturing*, vol. 38, no. 5, pp. 1431-1438, 2007.

[11] K. Van de Velde and P. Kiekens, "Thermoplastic pultrusion of natural fibre reinforced composites," *Composite structures*, vol. 54, no. 2-3, pp. 355-360, 2001.

[12] S. Moritomi, T. Watanabe, and S. Kanzaki, "Polypropylene compounds for automotive applications," *Sumitomo Kagaku*, vol. 1, no. 1, pp. 1-16, 2010.

[13] S. M. Lee, "Handbook of Composite Reinforcements," ed: John Wiley & Sons.

[14] J. George, E. Klompen, and T. Peijs, "Thermal degradation of green and upgraded flax fibres," *Advanced Composites Letters(UK)*, vol. 10, no. 2, p. 81, 2001.

[15] N. Barkoula, S. Garkhail, and T. Peijs, "Effect of compounding and injection molding on the mechanical properties of flax fiber polypropylene composites," *Journal of reinforced plastics and composites,* vol. 29, no. 9, pp. 1366-1385, 2010.

[16] A. Luisier, P.-E. Bourban, and J.-A. Månson, "Reaction injection pultrusion of PA12 composites: process and modelling," *Composites Part A: applied science and manufacturing,* vol. 34, no. 7, pp. 583-595, 2003.

[17] A. Babeau, S. Comas-Cardona, C. Binetruy, and G. Orange, "Modeling of heat transfer and unsaturated flow in woven fiber reinforcements during direct injection-pultrusion process of thermoplastic composites," *Composites Part A: Applied Science and Manufacturing,* vol. 77, pp. 310-318, 2015.

[18] C. Baley *et al.*, "Flax/PP manufacture by automated fibre placement (AFP)," *Materials & Design,* vol. 94, pp. 207-213, 2016.

[19] G. Sala and D. Cutolo, "The pultrusion of powder-impregnated thermoplastic composites," *Composites Part A: Applied Science and Manufacturing,* vol. 28, no. 7, pp. 637-646, 1997.

[20] K. Van de Velde, Kiekens, Paul. , "Thermoplastic pultrusion of natural fiber reinforced composites," *Composite Structures,* vol. 54, pp. 355-360, 2001.

[21] A. Memon and A. Nakai, "Mechanical properties of jute spun yarn/PLA tubular braided composite by pultrusion molding," *Energy Procedia,* vol. 34, pp. 818-829, 2013.

[22] D. Kim, W. Lee, and F. Friedrich, "A model for a thermoplastic pultrusion process using commingled yarns " *Composites Science and Technology,* vol. 61, no. 8, pp. 106-1077, 2001.

[23] M. Ueda, N. Ui, and A. Ohtani, "Lightweight and anti-corrosive fiber reinforced thermoplastic rivet," *Composite Structures,* vol. 188, pp. 356-362, 2018.

[24] B. Ali, B. Bouiadjera, E. Chikh, and M. Elmeguenni, "The effect of the plastic instability on the behavior of an amorphous polymer," *Mathematical Modelling of Engineering Problems,* vol. 4, no. 1, pp. 53-58, 2017.

[25] K.-S. Kim, J.-C. Heo, and K.-W. Kim, "Effects of temperature on the microscale adhesion behavior of thermoplastic polymer film," *Tribology letters,* vol. 38, no. 2, pp. 97-106, 2010.

[26] D. Srinivasagupta, S. Potaraju, J. L. Kardos, and B. Joseph, "Steady state and dynamic analysis of a bench-scale injected pultrusion process," *Composites Part A: applied science and manufacturing,* vol. 34, no. 9, pp. 835-846, 2003.

[27] B. J. Devlin, Williams, M.D., Quinn, J.A. Gibson, A.G., "Pultrusion of unidirectional composites with thermoplastic matrices," *Composites Manufacturing,* vol. 2/3-4, pp. 203-207, 1991.

[28] V. D. Kamble, "Optimization of thermoplastic pultrusion process using commingled fibers," University of Alabama at Birmingham, 2008.

[29] P. J. Novo, J. P. Nunes, J. F. Silva, V. Tinoco, and A. T. Marques, "Production of thermoplastics matrix preimpregnated materials to manufacture composite pultruded profiles," *Ciência & Tecnologia dos Materiais,* vol. 25, no. 2, pp. 85-91, 2013.

[30] A. Carlsson, Astrom, B. T.,, "Experimental investigation of pultrusion of glass fibre reinforced polypropylene composites," *Composites Part A*, vol. 29, pp. 585-593, 1998.

[31] G. Bechtold, Wiedmer, S., Friedrich, K., "Pultrusion of Thermoplastic Composites – New Developments and Modelling Studies," *Journal of Thermoplastic* vol. 15, no. 5, 2002.

[32] P. Bates and I. Ekhator, "Continuous Consolidation of Commingled Glass and Polypropylene Roving," *Journal of Reinforced Plastics and Composites,* vol. 23, no. 13, pp. 1409-1424, 2004.

[33] F. Lapointe, A. Oswald, A. Nakai, and L. Laberge Lebel, "Manufacturing of carbon/polyamide beam by vacuum assisted pultrusion," in *Proceedings of the ECCM*, 2016.

[34] F. Lapointe and L. Laberge Lebel, "Fiber damage and impregnation during multi-die vacuum assisted pultrusion of carbon/PEEK hybrid yarns," *Polymer Composites*, 2018.

[35] H. Lee and D. Cho, "Effects of A, B, and S components on fiber length distribution, mechanical, and impact properties of carbon fiber/ABS composites produced by different processing methods," *Journal of Applied Polymer Science*, vol. 138, no. 28, p. 50674, 2021.

[36] D. Hwang and D. Cho, "Fiber aspect ratio effect on mechanical and thermal properties of carbon fiber/ABS composites via extrusion and long fiber thermoplastic processes," *Journal of Industrial and Engineering Chemistry,* vol. 80, pp. 335-344, 2019.

[37] N. Alsinani, M. Ghaedsharaf, and L. L. Lebel, "Effect of cooling temperature on deconsolidation and pulling forces in a thermoplastic pultrusion process," *Composites Part B: Engineering,* vol. 219, p. 108889, 2021.

[38] N. Alsinani and L. Laberge Lebel, "Thermoplastic pultrusion's cooling temperature effects on pulling forces and deconsolidation," presented at the Automotive Composites Conference & Expo (ACCE 2019), Novi, MI, 2019.

[39] N. Alsinani and L. Laberge Lebel, "Effect of high pulling speeds on the morphologies of pultrudates in a thermoplastic pultrusion process," *Journal of Thermoplastic Composite Materials,* 2022.

[40] B. T. Astrom, P. Larsson, and R. Pipes, "Experimental investigation of a thermoplastic pultrusion process," presented at the 36th International SAMPE Symposium, 1991.

[41] B. T. Astrom, "Development and application of a process model for thermoplastic pultrusion," *Composites manufacturing,* vol. 3/3, pp. 189-197, 1992.

[42] B. T. Astrom, Pipes, R.B., "A modeling approach to thermoplastic pultrusion. II: Verification of models," *Polymer Composites,* vol. 14/3, pp. 184-194, 1993.

[43] B. T. Astrom, Pipes, R.B., "A modeling approach to thermoplastic pultrusion. I: Formulation of Models," *Polymer Composites,* vol. 14/3, pp. 173-183, 1993.

[44] W. Michaeli, Jurss, D., "Thermoplastic pull-braiding: pultrusion of profiles with braided fibre lay-up and thermoplastic matrix system (PP)," *CompositeS Part A,* vol. 27, pp. 3-7, 1996.

[45] A. H. Miller, Dodds, N., Hale, J. M., Gibson, A. G.,, "High speed pultrusion of thermoplastic matrix composites," *Composites Part A,* pp. 773–782, 1998.

[46] C. Gensewich and U. Riedel, "Pultrusion von Konstruktionswerkstoffen aus nachwachsenden Rohstoffen," *Die Angewandte Makromolekulare Chemie,* vol. 272, no. 1, pp. 11-16, 1999.

[47] L. Z. Linganiso, R. Bezerra, S. Bhat, M. John, R. Braeuning, and R. D. Anandjiwala, "Pultrusion of flax/poly(lactic acid) commingled yarns and nonwoven fabrics," *Journal of Thermoplastic Composite Materials,* vol. 27, no. 11, pp. 1553-1572, 2013.

[48] J. P. Nunes, J. F. Silva, and P. J. Novo, "Processing Thermoplastic Matrix Towpregs by Pultrusion," *Advances in Polymer Technology,* vol. 32, no. S1, pp. E306-E312, 2013.

[49] K. Jamiyanaa, "Thermoplastic pultrusion development and characterization of residual in pultruded composites with modeling and experiments," Dissertation/Thesis p. 73, 2014 2014.

[50] F. Lapointe, A. Oswald, A. Nakai, and L. L. Lebel, "Manufacturing of Carbon/Polyamide Beam by Vacuum Assisted Pultrusion," in *ECCM17-17th European Conference on Composite Materials, Munich*, 2016, pp. 1-9.

[51] P. J. Novo, J. F. Silva, J. P. Nunes, and A. T. Marques, "Pultrusion of fibre reinforced thermoplastic pre-impregnated materials," *Composites Part B: Engineering*, vol. 89, pp. 328-339, 2016.

[52] A. Oswald, F. Lapointe, and L. Laberge Lebel, "Multi-die, Vacuum Assisted Pultrusion of Flax/PLA Thermoplastic Biocomposite Rods," in *ECCM17-17th European Conference on Composite Materials*, 2016, pp. 1-8.

[53] M. Eichenhofer, J. C. Wong, and P. Ermanni, "Exploiting cyclic softening in continuous lattice fabrication for the additive manufacturing of high performance fibre-reinforced thermoplastic composite materials," *Composites Science and Technology,* vol. 164, pp. 248-259, 2018.

[54] A. Carlsson and B. T. Åström, "Experimental investigation of pultrusion of glass fibre reinforced polypropylene composites," *Composites Part A: Applied Science and Manufacturing,* vol. 29, no. 5-6, pp. 585-593, 1998.

[55] M. Ghaedsharaf, J. Brunel, and L. L. Lebel, "Thermoplastic composite rod manufacturing using biaxial braid-trusion," presented at the ECCM18 - 18th European Conference on Composite Materials, Athens, Greece., 2018.

[56] S.-L. Gao and J.-K. Kim, "Cooling rate influences in carbon fibre/PEEK composites. Part 1. Crystallinity and interface adhesion," *Composites Part A: Applied science and manufacturing*, vol. 31, no. 6, pp. 517-530, 2000.

[57] A. M. Harris and E. C. Lee, "Improving mechanical performance of injection molded PLA by controlling crystallinity," *Journal of applied polymer science*, vol. 107, no. 4, pp. 2246-2255, 2008.

[58] S. V. Hoa, *Principles of the manufacturing of composite materials*. DEStech Publications, Inc, 2009.

[59] K.-S. Kim, Y. Ando, and K.-W. Kim, "The effect of temperature on the nanoscale adhesion and friction behaviors of thermoplastic polymer films," *Nanotechnology*, vol. 19, no. 10, p. 105701, 2008.

[60] Y. Hirai *et al.*, "High aspect pattern fabrication by nano imprint lithography using fine diamond mold," *Japanese journal of applied physics*, vol. 42, no. 6S, p. 3863, 2003.

[61] L. Heyderman, H. Schift, C. David, J. Gobrecht, and T. Schweizer, "Flow behaviour of thin polymer films used for hot embossing lithography," *Microelectronic Engineering*, vol. 54, no. 3-4, pp. 229-245, 2000.

[62] C. Yan, Y. Shi, and L. Hao, "Investigation into the differences in the selective laser sintering between amorphous and semi-crystalline polymers," *International polymer processing*, vol. 26, no. 4, pp. 416-423, 2011.

[63] A. Brack, S. Senger, G. Fischer, H. Janssen, J. Oertel, and C. Brecher, "Development of an artifact-free aneurysm clip," *Current Directions in Biomedical Engineering*, vol. 2, no. 1, pp. 543-546, 2016.

[64] L. L. Lebel and A. Nakai, "Design and manufacturing of an L-shaped thermoplastic composite beam by braid-trusion," *Composites Part A: Applied Science and Manufacturing*, vol. 43, no. 10, pp. 1717-1729, 2012.

[65] S. Wiedmer and M. Manolesos, "An experimental study of the pultrusion of carbon fiber-polyamide 12 yarn," *Journal of thermoplastic composite materials*, vol. 19, no. 1, pp. 97-112, 2006.

[66] T. Lee, F. Boey, and K. Khor, "On the determination of polymer crystallinity for a thermoplastic PPS composite by thermal analysis," *Composites Science and Technology*, vol. 53, no. 3, pp. 259-274, 1995.

[67] A. Mehmet-Alkan and J. Hay, "The crystallinity of poly (ether ether ketone)," *Polymer*, vol. 33, no. 16, pp. 3527-3530, 1992.

[68] J. J. Tierney and J. Gillespie Jr, "Crystallization kinetics behavior of PEEK based composites exposed to high heating and cooling rates," *Composites Part A: Applied science and manufacturing*, vol. 35, no. 5, pp. 547-558, 2004.

[69] W. E. Lawrence, J. C. Seferis, and J. W. Gillespie Jr, "Material response of a semicrystalline thermoplastic polymer and composite in relation to process cooling history," *Polymer composites*, vol. 13, no. 2, pp. 86-96, 1992.

[70] P. P. Parlevliet, H. E. Bersee, and A. Beukers, "Residual stresses in thermoplastic composites—A study of the literature—Part I: Formation of residual stresses," *Composites Part A: Applied Science and Manufacturing*, vol. 37, no. 11, pp. 1847-1857, 2006.

[71] R. S.P.A. (2018). *Roughness Conversion Chart* [Online]. Available: http://rampinelli.eu/wp-content/uploads/2018/01/Roughness-Conversion-Chart-Rampinelli.pdf.

[72] M. Pervaiz, S. Panthapulakkal, M. Sain, and J. Tjong, "Emerging trends in automotive lightweighting through novel composite materials," *Materials sciences and Applications,* vol. 7, no. 01, p. 26, 2016.

[73] L. W. Cheah, "Cars on a diet: the material and energy impacts of passenger vehicle weight reduction in the US," Massachusetts Institute of Technology, 2010.

[74] T.-D. Ngo, "Natural fibers for sustainable bio-composites," *Natural and artificial fiber-reinforced composites as renewable sources,* pp. 107-126, 2018.

[75] S. J. L. Bispo, R. C. S. Freire, and E. M. F. d. Aquino, "Mechanical properties analysis of polypropylene biocomposites reinforced with curaua fiber," *Materials Research,* vol. 18, pp. 833-837, 2015.

[76] Q. Bénard, M. Fois, and M. Grisel, "Roughness and fibre reinforcement effect onto wettability of composite surfaces," *Applied Surface Science,* vol. 253, no. 10, pp. 4753-4758, 2007/03/15/ 2007.

[77] E. Sinha and S. Panigrahi, "Effect of Plasma Treatment on Structure, Wettability of Jute Fiber and Flexural Strength of its Composite," *Journal of Composite Materials,* vol. 43, no. 17, pp. 1791-1802, 2009.

[78] M. Bera, R. Alagirusamy, and A. Das, "A study on interfacial properties of jute-PP composites," *Journal of Reinforced Plastics and Composites,* vol. 29, no. 20, pp. 3155-3161, 2010.

[79] H. Ning, N. Lu, A. A. Hassen, K. Chawla, M. Selim, and S. Pillay, "A review of Long fibre thermoplastic (LFT) composites," *International Materials Reviews,* vol. 65, no. 3, pp. 164-188, 2020.

[80] S. R. Gottgetreu, "Injection compression molding of long glass fiber reinforced polypropylene," *SAE transactions,* pp. 611-618, 1998.

[81] N. Alsinani and L. L. Laberge, "Effect of length variation of flax/polypropylene pellets produced by multi-die pultrusion on the quality of injection molded product," in *Automotive Composites Conference & Exhibition (ACCE 2018)*, 2018.

[82] K. Rohan, T. McDonough, V. Ugresic, E. Potyra, and F. Henning, "Mechanical study of direct long fiber thermoplastic carbon/polyamide 6 and its relations to processing parameters," in *Proc. 14th-Annual SPE Automotive Composites Conference & Exhibition*, 2015.

[83] C. Wang, P. Uawongsuwan, Y. Yang, and H. Hamada, "Effect of molding condition and pellets material on the weld property of injection molded jute/polylactic acid," *Polymer Engineering & Science,* vol. 53, no. 8, pp. 1657-1666, 2013.

[84] T. Xie and G. Yang, "Interface and mechanical properties of poly (methyl methacrylate)–fiber composites," *Journal of applied polymer science,* vol. 93, no. 5, pp. 2478-2483, 2004.

[85] A. Garcia-Rejon, A. Meddad, E. Turcott, and M. Carmel, "Extrusion blow molding of long fiber reinforced polyolefins," *Polymer Engineering & Science,* vol. 42, no. 2, pp. 346-364, 2002.

[86] Y. Fan, Y. Liu, T. Whitfield, T. Kuboki, J. Wood, and V. Ugresic, "Effects of processing parameters on the thermal and mechanical properties of LFT-D-ECM glass fiber/polyamide 6 composites," *SPE Automotive*, 2016.

[87] M. Bondy and W. Altenhof, "Low velocity impact testing of direct/inline compounded carbon fibre/polyamide-6 long fibre thermoplastic," *International Journal of Impact Engineering*, vol. 111, pp. 66-76, 2018.

[88] K. Weidenmann, M. Grigo, B. Brylka, P. Elsner, and T. Böhlke, "Time temperature dependence of long fiber reinforced polypropylene manufactured by direct long fiber thermoplastic process," *International Journal of Materials and Metallurgical Engineering*, vol. 11, no. 1, pp. 13-18, 2016.

[89] C. Perez, T. A. Osswald, and S. Goris, "Study on the fiber properties of a LFT strand," *SPE ACCE*, vol. 2, pp. 1115-1126, 2013.

[90] R. C. Hawley and R. F. Jones, "In-line compounding of long-fiber thermoplastics for injection molding," *Journal of Thermoplastic Composite Materials*, vol. 18, no. 5, pp. 459-464, 2005.

[91] V. Kumar *et al.*, "High-performance molded composites using additively manufactured preforms with controlled fiber and pore morphology," *Additive Manufacturing*, vol. 37, p. 101733, 2021.

[92] K. Brast and W. Michaeli, "Processing of long-fibre reinforced thermoplastics using the direct strand-deposition process," *Plastics, Additives and Compounding*, vol. 3, no. 6, pp. 22-29, 2001.

[93] P. Ren and G. Dai, "Fiber dispersion and breakage in deep screw channel during processing of long fiber-reinforced polypropylene," *Fibers and Polymers*, vol. 15, no. 7, pp. 1507-1516, 2014.

[94] R. Leaversuch, "In-Line compounding of long-glass/PP gains strength in automotive molding," *Plastics Technology*, vol. 9, pp. 39-40, 2001.

[95] Y. Kim and O. O. Park, "Effect of fiber length on mechanical properties of injection molded long-fiber-reinforced thermoplastics," *Macromolecular Research*, vol. 28, no. 5, pp. 433-444, 2020.

[96] S. M. Lee, *Handbook of composite reinforcements*. John Wiley & Sons, 1996.

[97] M. Ghaedsharaf, J.-E. Brunel, and L. L. Lebel, "Multiscale numerical simulation of the forming process of biaxial braids during thermoplastic braid-trusion: Predicting 3D and internal geometry and fiber orientation distribution," *Composites Part A: Applied Science and Manufacturing*, vol. 150, p. 106637, 2021.

[98] C. Absi, N. Alsinani, and L. L. Lebel, "Carbon fiber reinforced poly (ether ether ketone) rivets for fastening composite structures," *Composite Structures*, p. 114877, 2021.

[99] U. K. Vaidya, K. B. Thattaiparthasarthy, S. Pillay, S. Vaidya, H. Ning, and D. Bansal, "Colored inorganic-pigmented long-fiber thermoplastics," *Journal of Thermoplastic Composite Materials*, vol. 28, no. 12, pp. 1627-1643, 2015.

[100] S. Bartus, U. Vaidya, and C. Ulven, "Design and development of a long fiber thermoplastic bus seat," *Journal of Thermoplastic Composite Materials,* vol. 19, no. 2, pp. 131-154, 2006.

[101] T. Hartness, G. Husman, J. Koenig, and J. Dyksterhouse, "The characterization of low cost fiber reinforced thermoplastic composites produced by the DRIFT™ process," *Composites Part A: Applied Science and Manufacturing,* vol. 32, no. 8, pp. 1155-1160, 2001.

[102] Y. Tan, X. Wang, and D. Wu, "Preparation, microstructures, and properties of long-glass-fiber-reinforced thermoplastic composites based on polycarbonate/poly (butylene terephthalate) alloys," *Journal of Reinforced Plastics and Composites,* vol. 34, no. 21, pp. 1804-1820, 2015.

[103] K. Friedrich, "Carbon fiber reinforced thermoplastic composites for future automotive applications," in *AIP Conference Proceedings,* 2016, vol. 1736, no. 1: AIP Publishing LLC, p. 020001.

[104] K. Friedrich and A. A. Almajid, "Manufacturing aspects of advanced polymer composites for automotive applications," *Applied Composite Materials,* vol. 20, no. 2, pp. 107-128, 2013.

[105] R. J. Bockstedt and R. J. Skarlupka, "An overview of long fiber reinforced thermoplastics," 1995.

[106] K. q. Han, Z. j. Liu, and M. h. Yu, "Preparation and mechanical properties of long glass fiber reinforced PA6 composites prepared by a novel process," *Macromolecular Materials and Engineering,* vol. 290, no. 7, pp. 688-694, 2005.

[107] T. Bayerl and P. Mitschang, "Rheological and mechanical behavior of long-polymer-fiber reinforced thermoplastic pellets," *Journal of Applied Polymer Science,* vol. 131, no. 1, 2014.

[108] F. Lapointe and L. Laberge Lebel, "Fiber damage and impregnation during multi-die vacuum assisted pultrusion of carbon/PEEK hybrid yarns," *Polymer Composites,* vol. 40, no. S2, pp. E1015-E1028, 2019.

[109] M. Ghaedsharaf, J.-E. Brunel, and L. Laberge Lebel, "Thermoplastic composite rod manufacturing using biaxial braid-trusion," in *Proceedings of the ECCM18–18th European Conference on Composite Materials, Athens, Greece,* 2018, pp. 24-28.

[110] H. L. Bos, J. Müssig, and M. J. van den Oever, "Mechanical properties of short-flax-fibre reinforced compounds," *Composites Part A: Applied Science and Manufacturing,* vol. 37, no. 10, pp. 1591-1604, 2006.

[111] B. Nyström, R. Joffe, and R. Långström, "Microstructure and strength of injection molded natural fiber composites," *Journal of reinforced plastics and composites,* vol. 26, no. 6, pp. 579-599, 2007.

[112] A. G. Barneto, C. Vila, J. Ariza, and T. Vidal, "Thermogravimetric measurement of amorphous cellulose content in flax fibre and flax pulp," *Cellulose,* vol. 18, no. 1, pp. 17-31, 2011.

[113] A. Arias, M.-C. Heuzey, and M. A. Huneault, "Thermomechanical and crystallization behavior of polylactide-based flax fiber biocomposites," *Cellulose,* vol. 20, no. 1, pp. 439-452, 2013.

[114] S. Chaitanya and I. Singh, "Processing of PLA/sisal fiber biocomposites using direct-and extrusion-injection molding," *Materials and Manufacturing Processes,* vol. 32, no. 5, pp. 468-474, 2017.

[115] A. Bourmaud and S. Pimbert, "Investigations on mechanical properties of poly (propylene) and poly (lactic acid) reinforced by miscanthus fibers," *Composites Part A: Applied Science and Manufacturing,* vol. 39, no. 9, pp. 1444-1454, 2008.

[116] A. K. Bledzki, A. Jaszkiewicz, and D. Scherzer, "Mechanical properties of PLA composites with man-made cellulose and abaca fibres," *Composites Part A: Applied science and manufacturing,* vol. 40, no. 4, pp. 404-412, 2009.

[117] Y. Du, T. Wu, N. Yan, M. T. Kortschot, and R. Farnood, "Fabrication and characterization of fully biodegradable natural fiber-reinforced poly (lactic acid) composites," *Composites Part B: Engineering,* vol. 56, pp. 717-723, 2014.

[118] X.-F. Wu and Y. A. Dzenis, "Droplet on a fiber: geometrical shape and contact angle," *Acta mechanica,* vol. 185, no. 3, pp. 215-225, 2006.

[119] A. Arbelaiz, B. Fernandez, J. Ramos, A. Retegi, R. Llano-Ponte, and I. Mondragon, "Mechanical properties of short flax fibre bundle/polypropylene composites: Influence of matrix/fibre modification, fibre content, water uptake and recycling," *Composites science and technology,* vol. 65, no. 10, pp. 1582-1592, 2005.

[120] A. Bledzki, H. P. Fink, and K. Specht, "Unidirectional hemp and flax EP-and PP-composites: Influence of defined fiber treatments," *Journal of Applied Polymer Science,* vol. 93, no. 5, pp. 2150-2156, 2004.

[121] J. Gassan, "A study of fibre and interface parameters affecting the fatigue behaviour of natural fibre composites," *Composites part A: applied science and manufacturing,* vol. 33, no. 3, pp. 369-374, 2002.

[122] T. G. Kannan, C. M. Wu, and K. B. Cheng, "Influence of laminate lay-up, hole size and coupling agent on the open hole tensile properties of flax yarn reinforced polypropylene laminates," *Composites Part B: Engineering,* vol. 57, pp. 80-85, 2014.

[123] T.-D. Ngo, "Natural Fibers for Sustainable Bio-Composites," in *Natural and Artificial Fiber-Reinforced Composites as Renewable Sources*: IntechOpen, 2017.

[124] F. Lessard, "Développement d'un système de pultrusion thermoplastique multi-filière pour production de pièces d'intérieur d'aéronef," Doctor of Philosophy, Génie mécanique Université de Montréal, Polytechnique Montréal, 2022.

[125] N. Alsinani and L. Laberge Lebel, "Effect of Flax/PP pellets' morphology on the mechanical properties of injection-molded parts," *Journal of Thermoplastic Composite Materials,* vol. 0, no. 0, p. 08927057221095394, 2022.

[126] T. Dai Lam, T. V. Hoang, D. T. Quang, and J. S. Kim, "Effect of nanosized and surface-modified precipitated calcium carbonate on properties of CaCO3/polypropylene nanocomposites," *Materials Science and Engineering: A*, vol. 501, no. 1-2, pp. 87-93, 2009.

[127] S. E. Barbosa and J. M. Kenny, "Processing of short-fiber reinforced polypropylene. I. Influence of processing conditions on the morphology of extruded filaments," *Polymer Engineering & Science*, vol. 40, no. 1, pp. 11-22, 2000.

[128] N. Alsinani, M. Ghaedsharaf, and L. L. Lebel, "Effect of cooling temperature on deconsolidation and pulling forces in a thermoplastic pultrusion process," *Composites Part B: Engineering*, p. 108889, 2021/04/27/ 2021.

[129] S. Sharma and D. A. Siginer, "Permeability measurement methods in porous media of fiber reinforced composites," *Applied Mechanics Reviews*, vol. 63, no. 2, 2010.

[130] L. Yan, N. Chouw, and K. Jayaraman, "Flax fibre and its composites–A review," *Composites Part B: Engineering*, vol. 56, pp. 296-317, 2014.

[131] H. Kobayashi, R. Kitamaru, and W. Tsuji, "The Viscous Flow of Molten Polypropylene (Special Issue on Polymer Chemistry, II)," *Bulletin of the Institute for Chemical Research, Kyoto University*, vol. 43, no. 2, pp. 179-192, 1965.

[132] L. Laberge Lebel and N. A. Alsinani, "Pultrusion system with cooling stage and method therefor," Patent WO2020237381 Patent Appl. PCT/CA2020/050728, 2020. [Online]. Available: https://patentscope.wipo.int/search/en/detail.jsf?docId=WO2020237381&tab=PCTBIBLIO.

[133] C. Absi, N. Alsinani, and L. L. Lebel, "Carbon fiber reinforced poly (ether ether ketone) rivets for fastening composite structures," *Composite Structures*, vol. 280, p. 114877, 2022.

[134] M. Volk, J. Wong, S. Arreguin, and P. Ermanni, "Pultrusion of large thermoplastic composite profiles up to Ø 40 mm from glass-fibre/PET commingled yarns," *Composites Part B: Engineering*, vol. 227, p. 109339, 2021.

[135] M. Volk, S. Arreguin, P. Ermanni, J. Wong, C. Bär, and F. Schmuck, "Pultruded thermoplastic composites for high voltage insulator applications," *IEEE Transactions on Dielectrics and Electrical Insulation*, vol. 27, no. 4, pp. 1280-1287, 2020.

[136] D.-H. Kim, W. I. Lee, and K. Friedrich, "A model for a thermoplastic pultrusion process using commingled yarns," *Composites science and technology*, vol. 61, no. 8, pp. 1065-1077, 2001.

[137] B. R. Gebart, "Permeability of unidirectional reinforcements for RTM," *Journal of composite materials*, vol. 26, no. 8, pp. 1100-1133, 1992.

[138] T. S. Lundström and B. R. Gebart, "Effect of perturbation of fibre architecture on permeability inside fibre tows," *Journal of composite materials*, vol. 29, no. 4, pp. 424-443, 1995.

[139] M. Sandberg *et al.*, "Permeability and compaction behaviour of air-texturised glass fibre rovings: A characterisation study," *Journal of Composite Materials,* vol. 54, no. 27, pp. 4241-4252, 2020.

[140] M. A. Kabachi, M. Danzi, S. Arreguin, and P. Ermanni, "Experimental study on the influence of cyclic compaction on the fiber-bed permeability, quasi-static and dynamic compaction responses," *Composites Part A: Applied Science and Manufacturing,* vol. 125, p. 105559, 2019.

[141] P. C. Carman, "Fluid flow through granular beds," *Trans. Inst. Chem. Eng.,* vol. 15, pp. 150-166, 1937.

[142] T. Sochi, "Non-Newtonian flow in porous media," *Polymer,* vol. 51, no. 22, pp. 5007-5023, 2010.

[143] S. Haffner, K. Friedrich, P. Hogg, and J. Busfield, "Finite-element-assisted modelling of a thermoplastic pultrusion process for powder-impregnated yarn," *Composites science and technology,* vol. 58, no. 8, pp. 1371-1380, 1998.

APPENDIX A AN EXTRACT OF THE PHD THESIS ENTITLED: DÉVELOPPEMENT D'UN SYSTÈME DE PULTRUSION THERMOPLASTIQUE MULTI-FILIÈRE POUR PRODUCTION DE PIÈCES D'INTÉRIEUR D'AÉRONEF

Author: Felix Lessard [a c]

Co-supervisor: Martine Dube [b c]

Supervisor: Louis Laberge Lebel [a c]

[a] Advanced Composite and Fiber Structure Laboratory, Department of Mechanical Engineering, Polytechnique Montréal, 2900 Édouard-Montpetit, University of Montréal Campus Montréal, H3T 1J4, Canada

[b] Department of Mechanical Engineering, École de Technologie Supérieure, 1100 Notre-Dame W, Montréal, QC Canada H3C 1K3

[c] Research Center for High Performance Polymer and Composite Systems (CREPEC)

2. Model Structure

In pultrusion of commingled fibre yarn, the polymer is mixed with the re inforcement fibre under its solid form and thus carried by the latter into the die, even when molten. This implies the yarns can be pre-heated close to their processing temperature even before entering the forming die. In the die, the pro- cessing temperature is thus quickly reached. In the modelling approach used, the polymer matrix is assumed at a constant temperature and fully liquid when entering the die while being carried by the reinforcement fibres.

Figure 2 illustrates the structure of the current model and highlights the use of Kim et al. original model [136]. The proposed model is based on a multi-scale approach where the macroscopic and microscopic flow behaviours are solved by a combination of two sub-models. The algorithm starts by defining the material properties such as fibre agglomeration initial sizes (Rj), size distribution (Nj), fibre radius (Rf), and processing conditions such as the processing velocity (U) and polymer viscosity (η) which is dependent on processing temperature. Then, the first die geometry is defined by its length (L) and cross-sectional area in function of length (A(z)) where z denotes the axial coordinate starting at the die entrance.

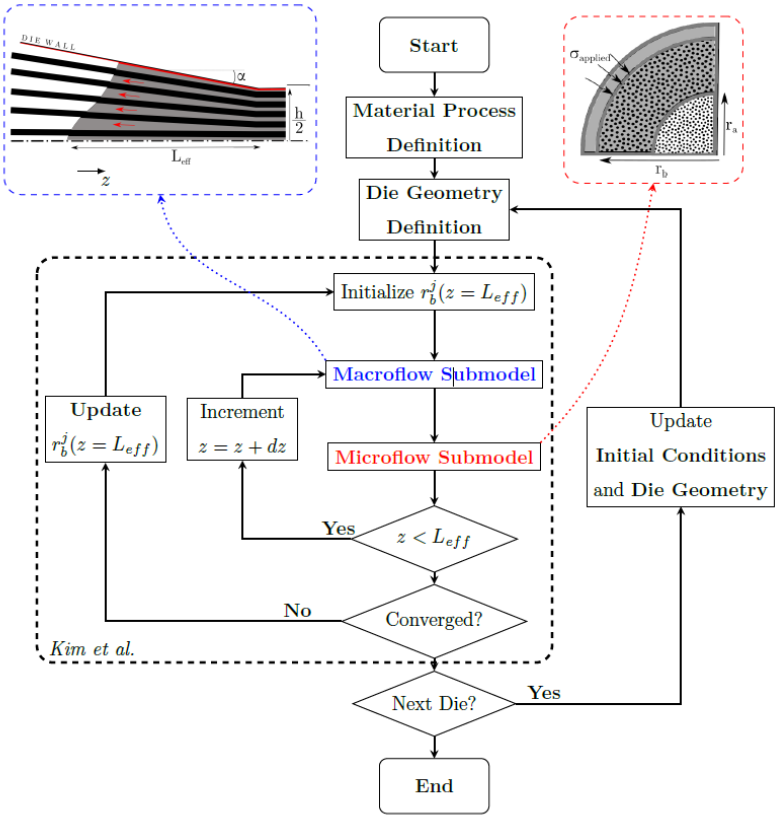

Figure 2: Structure of multi-die pultrusion algorithm based on Kim et al. model

The initial conditions of the first die are defined at the entrance of the die. For the first die, they consist of a fully unsaturated REV (r_b^j (z = 0) = r_a^j (z =0)=R_0^j while, for subsequent dies, initial conditions are taken from the outlet of the previous die. The outlet's r_b^j value also has to be initialized since it is required in the macroflow calculation. An arbitrary value is taken as the initial guess. The macroflow and microflow sub-models are then evaluated over the discretized domain into 100 dz increments. The macro flow sub-model is used to obtain the hydrostatic polymer pressure surrounding the agglomer-ations. The micro-flow sub-model is then used to compute the progression of impregnation (r_a^j reducing and r_b^j increasing) of the fibre agglomeration. Both sub-models are evaluated using Euler's method over the die's domain. The com- puted outlet's r_b^j value

is then compared to the original guess. The initial guess is updated and calculation restarted until the norm of change is under 10−5. At this point, the outlet conditions (r_a^j and r_b^j) are taken to the subsequent die geometry.

2.0 Macroscopic flow sub-model

The macroscopic flow of polymer moving towards the entrance of the die is modelled as a flow of polymer through porous media where the permeability is given by the cross-sectional area between the fibre agglomerations. Kim et al. originally used a uni-modal distribution of fibre agglomeration (R0). Because of the different nature of the commingled yarn used, it was replaced with a multi- modal distribution in this study (R_0^j). The macroscopic flow equation, derived from the mass balance, is then formulated as

$$\frac{d}{dz}[A(z)(\frac{\kappa_z(z)}{\eta}\frac{dp}{dz} - V_p) + U\pi\, {r_a}^j(z)^2\, N^j] \qquad (1)$$

Where κz the axial permeability, U the process velocity, r_a^j the dry area of the REV, and Nj the number of REV of size r_a^j . Integration of equation 1 provides a formulation of the pressure gradient ($\frac{dp}{dz}$), which can itself be used with Euler's method to evaluate the pressure profile from its first derivative. This pressure profile is then used to compute the microscopic flow. Since the pressure gradient formulation depends on the final bundle radius (r_b^jj(z = Leff)), an iterative solving process is used to converge on the solution (z = Leff). The macroflow submodel boxed image (top-left box in blue dashed lines) in Figure 2 illustrates a situation where the polymer backflow stops before the die entrance, or the flow is slow enough that the polymer pools at the bottom of the die due to gravity. Empirical evidence shows that this phenomenon primarily occurs at relatively slow process velocity (500 mm/min). Such a situation is especially likely to occur if not enough material enters the die. In such a case, the macroscopic flow has to be adjusted for the effective die length (Leff). Leff was calculated as the intersection between the die wall and

incoming material cross-section areas. Since the latter is constrained by the previous die's outlet area, Leff can be defined as

$$A_i(z = 0) = A_{i-1}(z = L_{eff}) \quad (2)$$

Where Ai refers to the ith die's exit cross-section area. In the case of the first die, its effective length is calculated as the point where material enters in contact with the die wall. This translates to the position where the die cross- sectional area equals the incoming material (fibre and polymer) cross-section area. In multi-die pultrusion, the pultrudate usually exits the forming die before being completely impregnated. This implies the REV conditions (r_a^j and r_b^j) at the end of the nth die become the initial conditions of the (n + 1)th die. No other material properties were changed from a die to the other. The microscopic flow model neglects hydrostatic compaction forces on the fibre agglomeration. It considers static dry and wetted vf therefore, inter-die deconsolidation is neglected.

2.1 Microscopic flow sub-model

The sub-model is based on a set of cylindrical REV as depicted in Figure 3. Equations are developed for a general case of multi-modal distribution of fibre agglomerations. The agglomerations have an initial radius Rj and are divided into two zones: a dry fibre center of radius r_a^j having a fibre volume fraction vf,i surrounded by a wetted fibre layer of radius r_b^j having a fibre volume fraction of $v_{f,\infty}$ where j denotes properties of the jth REV. The wetted fibre volume fraction ($v_{f,\infty}$) is always lower than the dry fibre volume fraction ($v_{f,i}$). During the impregnation of the REV, the value of r_a^j decreases while r_b^j Increases.

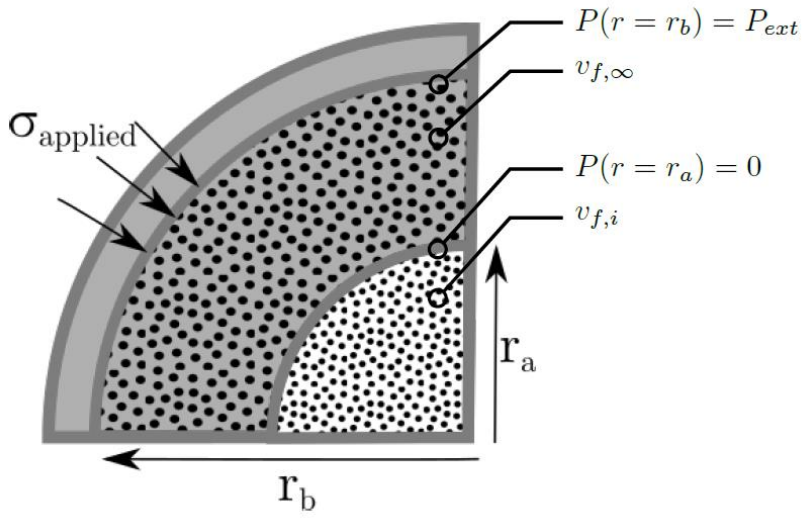

Figure 3 Illustration of a cylindrical REV as defined in the problem.

Microscopic flow therefore occurs as a converging flow of polymer through porous media. This sort of flow is well described by Darcy's law such that

$$(1 - {v_f}^j)(u_r - u_f) = -\frac{\kappa}{\eta}\frac{dp}{dr} \tag{3}$$

Where ${v_f}^j$ is the dry v_f , u_r the polymer velocity, u_f the fibre velocity, κ the transverse. The Permeability of the fibre structure, η the polymer viscosity, and $\frac{dp}{dr}$ the hydrostatic pressure gradient. The mass conservation equations for the polymer and fibres is then expressed as

$$(1 - {v_f}^j) = \frac{1}{r}\frac{\partial}{\partial r}\left[(1 - {v_f}^j) r u_r\right] = 0 \tag{4}$$

$$\frac{\partial}{\partial t}{v_f}^i = \frac{1}{r}\frac{\partial}{\partial r}\left({v_f}^j\, r u_r\right) = 0$$

Where the first equation represents the conservation of resin content and the second equation represents the conservation of fibre. Finally, the conservation of the initial fibre content in the REV is also ex- pressed as

$${v_f}^i\, {R_0}^2 = v_{f,i}\, {r_a^j}^2 + v_f\, ({r_b^j}^2 - {r_a^j}^2) \tag{5}$$

Equations 3, 4, and 5 can than be combined with the boundary conditions 6a 6b to obtain the first derivative of rj such that

$$p=0,\ u_r=\frac{dr_a^j}{dt}\ \text{at r=}\ r_a^j \qquad (6a)$$

$$p=P_{ext},\ u_r=\frac{dr_b^j}{dt}\ \text{at r=}\ r_b^j \qquad (6b)$$

Where P_{ext}, is the hydrostatic pressure provided by the macroscopic flow model. Integration of this equation is performed using Euler's method to solve for r_a^j which in turn is used to obtain r_b^j.

2.2 Permeability of fibrous structure

Appropriate representation of the preform permeability is essential to ad equately represent the polymer flow. Several models have been proposed to represent the permeability of porous media. Some formulations have been pro- posed for geometry-specific arrangement like Gebart [137] who proposed a model for flow parallel or transverse to aligned fibres. This specific model provides a relationship for permeability as a function of particle size and flow direction. Because permeability is affected by a myriad of factors such as fibre size [137], size distribution [138], fibre waviness [139], or compaction history [140] such a model may be too rigid to adequately represent experimental conditions. The original model proposed by Kim et al. used Kozeny-Carman's model [141] to represent both the intra-bundle transverse permeability and the inter-bundle axial permeabil- ity. The Kozeny-Carman model for instance presents as follow:

$$\kappa = -\frac{\hat{r}^{\,2}\,(\phi)^3}{4\,K_z\,(1-\phi)^2}, \qquad (7)$$

where the predicted permeability (κ) is a function of particle radius ($\hat{r}$) porosity (φ), and a fitting constant (K). This fitting constant provides flexibility of the model to better represent the effect on permeability of other phenomena such as fibre waviness, yarn twist, non-circularity of fibres, etc. In the case of microscopic flow, the particle radius is the fibre radius ($\hat{r}$ = (R_f)) and the porosity is defined using the REV fibre volume fraction $(v_f{}^j)_f$. In the case of macroscopic flow,

particle radius is taken as the smallest agglomeration size (min($r^j{}_b$)) and the porosity as the inter-agglomeration area defined as

$$\varphi(z) = A(z) - \sum \pi r^j(z)^2 N^j \qquad (8)$$

2.3 Polymer rheology

Thermoplastic polymers' viscosity is non-Newtonian and highly dependent on temperature. The use of a high pre-heating temperature ensures the poly- mer quickly attain its processing temperature when entering the die. Therefore, the represented polymer viscosity η is adjusted to reflect its dependant on the targeted processing temperature, assumed constant in the die. The dependence on the shear rate of the polymer was however neglected. Sochi et al. [142] high- lighted in their review that no general model yet exists to adequately represent non-newtonian flow in porous media. Moreover, Haffner et al. [143] concluded that the shear-dependant behaviour is rather negligeable in a pultrusion context